Ontwerpstrategieën voor hoogperformante textielantennes gericht op satellietnavigatie

Design Strategies for High Performance GNSS Textile Antennas

Arnaut Dierck

Promotoren: prof. dr. ir. H. Rogier, dr. ir. F. Declercq
Proefschrift ingediend tot het behalen van de graad van
Doctor in de Ingenieurswetenschappen: Elektrotechniek

Vakgroep Informatietechnologie
Voorzitter: prof. dr. ir. D. De Zutter
Faculteit Ingenieurswetenschappen en Architectuur
Academiejaar 2014 - 2015

UNIVERSITEIT GENT

ISBN 978-90-8578-745-7
NUR 959
Wettelijk depot: D/2014/10.500/91

Design Strategies for High Performance GNSS Textile Antennas

Arnaut Dierck

Dissertation submitted to obtain the academic degree of
Doctor of Electrical Engineering

Publicly defended at Ghent University on November 12th, 2014

Supervisor:
prof. dr. ir. H. Rogier
Electromagnetics group
Department of Information Technology
Faculty of Engineering and Architecture
Ghent University
St.-Pietersnieuwstraat 41
B-9000 Ghent, Belgium
http://emweb.intec.ugent.be

Supervisor:
dr. ir. F. Declercq
ON Semiconductor
Westerring 15
B-9700 Oudenaarde, Belgium
http://www.onsemi.com/

Members of the examining board:

prof. dr. ir. P. De Baets (chairman)	Ghent University, Belgium
prof. dr. ir. D. Vande Ginste (secretary)	Ghent University, Belgium
prof. dr. ir. H. Rogier (supervisor)	Ghent University, Belgium
dr. ir. F. Declercq (supervisor)	Ghent University, Belgium
prof. dr. ir. D. Zito	University College Cork & Tyndall National Institute, Ireland
prof. dr. ir. J. Vanfleteren	Ghent University, Belgium
prof. dr. ir. J. Bauwelinck	Ghent University, Belgium

Dankwoord

Bij de aanvang van mijn doctoraatsonderzoek had ik nooit gedacht dat deze vier jaren zo snel voorbij zouden vliegen. Ze vormden een onvergelijkbaar interessante periode, waarin ik zelfstandig, maar met deskundige begeleiding, mijn pad in de wondere wereld der antennes mocht uitstippelen. Langsheen dit pad waren er heel wat mensen die elk op hun eigen manier hebben bijgedragen tot het welslagen van deze onderneming. Hier maak ik met graagte gebruik van de gelegenheid deze mensen te bedanken.

In de eerste plaats wens mijn onmiskenbare dank uit te drukken voor mijn promotor, prof. Hendrik Rogier, die me niet enkel de kans gaf mijn doctoraatsstudie aan te vatten, maar ook immer paraat stond om me te begeleiden bij het analyseren van problemen, het schrijven van artikels en het voorbereiden van presentaties. Met zijn klare kijk en inzicht gaf hij steeds nuttige feedback over velerlei zaken, en dit steeds met de glimlach. Ook met mijn co-promotor dr. Frederick Declercq, nooit verlegen om zijn hulp aan te bieden, was het aangenaam werken. Tevens wil ik prof. Daniël De Zutter, hoofd van het het departement Informatietechnologie en de onderzoeksgroep Elektromagnetisme, bedanken om mij de mogelijkheid te geven onderzoek uit te voeren in deze leerrijke omgeving. Bedankt ook prof. Dries Vande Ginste, die, in zijn bureau of de koffiehoek, nooit aarzelde zijn interessante kijk op de dingen te geven. Ook richt ik een dankjewel aan Isabelle, die de administratieve rompslomp steeds vakkundig tot een minimum herleidde. Daarnaast wens ik ook de leden van de lees- en examencommissie die hierboven nog niet werden vernoemd te bedanken voor het beoordelen van mijn werk en het aanreiken van interessante opmerkingen: prof. Patrick De Baets, prof. Domenico Zito, prof. Jan Vanfleteren en prof. Johan Bauwelinck.

Verder heb ik tijdens de afgelopen jaren het bureau, de gang, en bij uitbreiding het Technicum gedeeld met zovelen die middels discussie of lach mijn verblijf aangenaam hebben beïnvloed. In een kantoor waarvan de samenstelling doorheen de jaren enkele malen is gewijzigd, was Thomas een constante compagnon, steeds een fijn klankbord aan het bureau tegenover het mijne. Met Sam was het niet enkel aangenaam werken, maar ook vermakelijk nu en dan smakelijk te tafelen, een vleugje cultuur op te snuiven of een agrarisch getinte race bij te wonen. Hem en Laura wens ik veel geluk met Bonaventure (en minstens evenveel geluk in het schier onmogelijke geval dit toch niet de uiteindelijke naam zou worden). Een iets jongere Sam vormde vervolgens een sympathieke aanwinst voor de ambiance op het bureau, en ook de andere bewoners van kantoor 1.13A, oud en nieuw, droegen hun steentje bij tot de leuke sfeer. Af en toe kruiste ik op -T of +2 nog eens mijn masterthesisgenoot Timothy, wat steevast in een leuke babbel resulteerde. Met Bart, Freek en Mykola herontdekte ik de geneuglijke spijzen van De Brug of

genoot ik van een pizza op giornata internazionale. Ook de vele andere collega's die van -T zo'n aangename werkomgeving maakten, bedankt!

All'angolo del caffè ho incontrato la gente Italiana del -T. Alessandro era un hombre molto sympatico, per discutere di lavoro e delle cose della vita. Anche Luigi, il Dottorissimo, benediceva noi tutti colla sua grazia incomparabile. Damiano, fotografo poetico, mi ha insegnato tutte le finezze della crusca. E non può mancare qui l'amatore di birre e cinefilo elitario Marco, un gentiluomo della Valtellina (apparentemente non lontano dal Tirolo), col cuore nella posizione giusta. Ook mensen van wat verder op de gang werden door de geur van de Moka Express naar de koffiehoek gelokt. Zo leerde Joachim, die Alessandro steevast te snel af was bij het karten, me klimmen met veel te kleine schoenen om vervolgens het wereldrecord pasta-pesto eten te verbreken.

Natuurlijk had ik 's avonds en in het weekend af en toe nog wat tijd over om me te amuseren in een niet-werkgerelateerde omgeving, gezellig thuis met mijn broer Robrecht en zijn vriendin Ana, out and about met soon to-be weds Lien en Nicolas, een whisky'tje degusterend met dr. Niels, een biertje brouwend met Lias, een trappistje drinkend met Marten of dolle fratsen belevend met Ben en Jasper. Ook de leuke feestjes en aangename tijden met de kernleden in het jeugdhuis, leerrijke avonden met de mensen van het fijnproeversverbond Ambrond, heerlijke vakanties, culinaire escapades en gezellige soirées zorgden voor het nodige vertier en welgekomen ontspanning, en dit in het goede gezelschap van fijne vrienden.

Ook wil ik mijn familie bedanken, en wel in het bijzonder mijn mama en papa, die me doorheen mijn hele studie- en doctoraatsloopbaan steeds ten volle hebben gesteund. En last but not least wil ik ook mijn liefste Liesa bedanken, die er de voorbije jaren steeds voor me was. Samen beleven we altijd prachtige momenten, en ik kijk uit naar de avonturen die ons nog te wachten staan.

Gent, oktober 2014
Arnaut Dierck

There ain't but one way.

Hugh Laurie

Inhoudsopgave

Samenvatting

Intelligent textiel biedt een veelbelovende manier om op comfortabele wijze geavanceerde functies te integreren in ons dagelijkse leven. Een intelligent textielsysteem verwezenlijkt deze functionaliteiten, zoals waarnemingen via sensoren, lokalisatie en communicatie, zonder hinderlijk te worden, door de verschillende sensoren, elektronica en antennes rechtstreeks in het textiel zelf te implementeren, en op die manier de anders ongebruikte oppervlakte optimaal te benutten. Niet alleen kan intelligent textiel de levenskwaliteit van gebruikers verhogen in hun dagdagelijkse bezigheden, het kan ook de veiligheid en efficiëntie van reddingswerkers op het veld significant verhogen. Functies zoals het opvolgen van vitale signalen, het scannen van de omgevingstoestand, betrouwbare communicatie en precieze lokalisatie kunnen worden toegevoegd aan professionele reddingswerkerskledij, zonder de reddingswerker te overbelasten met bijkomende uitrusting die moet meegedragen worden. Niet alleen kunnen nieuwe toepassingen worden toegevoegd aan professionele reddingswerkerskledij, ook kan bestaande apparatuur worden geïntegreerd in het intelligente textielsysteem, met als uiteindelijke doel het creëren van een kledingstuk dat in staat is de reddingswerker te voorzien van een reeks levensreddende functionaliteiten. Ondertussen verhoogt dit ook het comfort en de bewegingsvrijheid omdat toestellen die nu overbodig zijn, niet langer hoeven te worden meegedragen.

Dit werk concentreert zich op de draagbare textielantennes die deel uitmaken van zo'n intelligent textielsysteem. Deze draagbare antennes staan voor een uitdagende set van vereisten. Eerst en vooral vereist hun draagbaarheid dat ze comfortabel, niet hinderlijk en flexibel zijn. Vanuit een materiaalstandpunt creëert dit de nood aan geschikte flexibele schuim- en textielsubstraten en flexibele (textiel)geleiders, die de draagbare antenne toelaten flexibel en ademend te zijn, en ondertussen hoge prestaties garanderen. Vanuit het gezichtspunt van de antennetopologie, kan deze eis vervuld worden door gebruik te maken van planaire antennetopologieën. Deze hebben een laag profiel en een licht gewicht, en hun gelaagde structuur laat een eenvoudige fabricage toe aan de hand van textielmaterialen. De flexibiliteit van de antennes, noodzakelijk voor een comfortabele integratie, zorgt ervoor dat de antennes kunnen worden blootgesteld aan invloeden van buiging, wat in de ontwerpfase in rekening moet worden gebracht. Daarenboven vereist hun nabijheid tot het menselijk lichaam specifieke zorg, teneinde de antenneperformantie hierdoor niet aan te tasten. Wanneer meer specifiek het veld van reddingswerkers als doelgroep wordt beoogd, is robuustheid een essentiële vereiste, niet enkel voor de draagbare antennes, maar voor het gehele intelligente textielsysteem. Grote mogelijkheden bieden zich aan tijdens het antenneontwerp om de robuustheid van de antenne en het intelligente textielsysteem te vergroten.

Een geschikte keuze van antennetopologie, een doorgedreven materiaalselectie en een verreikende integratie van functionaliteiten in één enkele antennemodule laten draagbare textielantennes toe om uitmuntend te presteren in deze veeleisende omgeving, en te voldoen aan de zware ontwerpvereisten. In dit werk worden ontwerpstrategieën voor hoogperformante draagbare textielantennes, en specifieker, antennes voor globale satellietnavigatiesystemen, voorgesteld. Deze strategieën nemen de uitdagingen in rekening die worden gesteld in de context van draagbare textielantennes voor reddingswerkersystemen, en worden gevalideerd aan de hand van innovatieve draagbare textielantenneontwerpen.

Het eerste hoofdstuk reikt de lezer een overzicht aan van de concepten die verder in dit werk worden gebruikt. Daarna wordt in het tweede hoofdstuk een methode gepresenteerd waarop bijkomende functionaliteiten op een compacte manier kunnen worden geïntegreerd in een wearable antenne, door actieve elektronica toe te voegen op de achterzijde van de antenne. In dit hoofdstuk wordt het ontwerp van een actieve wearable dual-band GPS/Iridium antenne besproken, bedoeld voor integratie in brandweerpakken. Een on-chip lageruisversterker wordt geïntegreerd in een circulair gepolariseerde apertuurgekoppelde microstrip patch antenne. Prototypes worden gefabriceerd met behulp van textiel en flexibele materialen, en hun prestaties worden geëvalueerd door middel van uitgebreide metingen, inclusief metingen van de antenne in gebogen toestand en gedragen op het lichaam. Deze metingen tonen uitmuntende prestaties aan, in zowel off- als on-body omgevingen, zelfs in vergelijking met traditionele, rigide antennes, wat aantoont dat de voorgestelde antennetopologie en integratiemethode voor elektronica optimaal geschikte kandidaten zijn voor het ontwerp van hoogperformante textielantennes gericht op satellietnavigatie. Hoofdstuk 3 behandelt de kwestie van autonomie van textielantennes, en presenteert een nieuw, toepassingsspecifiek ontwerpparadigma voor autonome actieve textielantennes die kunnen dienen als platforms voor lichaamsgecentreerde sensing, lokalisatie en draadloze communicatie in professionele reddingswerkerstoepassingen. Langs de ene kant kan de grote hoeveelheid ruimte beschikbaar in professionele reddingswerkerskledij benut worden om meerdere antennes in te zetten. Langs de andere kant kunnen stralende elementen groot genoeg worden ontworpen, teneinde een hoge stralingsefficiëntie te garanderen wanneer de antenne op het lichaam wordt gebruikt. Deze antenneoppervlakte wordt dan hergebruikt door actieve elektronica rechtstreeks onder en energy harvesters rechtstreeks bovenop het antennevlak te plaatsen. Dit ontwerpparadigma wordt geïllustreerd aan de hand van recente prototypes van textielantennes geïntegreerd in professionele kledij om te voorzien in sensing-, lokalisatie- en communicatiemogelijkheden. In het bijzonder wordt een nieuwe Galileo E1-band antenne gepresenteerd en volledig gekarakteriseerd, inclusief de ruis- en lineariteitsprestaties. In het vierde hoofdstuk wordt de optimalisatie behandeld van de steeds complexere textielantenneontwerpen die worden vervaardigd met onconventionele materialen. Een toepassingsspecifieke ontwerpstrategie wordt voorgesteld die het mogelijk maakt antennes te produceren die geoptimaliseerd zijn over een grote bandbreedte voor vaak tegenstrijdige eigenschappen, zoals impedantieaan-

passing, axiale ratio, efficiëntie en antennewinst. Deze nieuwe aanpak is bovendien in staat om de toleranties in rekening te brengen die van toepassing zijn op de eigenschappen van de onconventionele materialen die worden gebruikt in intelligente textielsystemen. Deze strategie incorporeert een multi-objectieve begrensde Pareto-optimalisatie, en wordt toegepast op het ontwerp van een Galileo E6-band antenne met optimale impedantieaanpassing en circulaire polarisatie. Vervolgens worden verschillende prototypes van de geoptimaliseerde antenne gefabriceerd en opgemeten om de voorgestelde ontwerpstrategie te valideren. Hoofdstuk 5 bouwt verder op de in hoofdstuk 4 uiteengezette strategie, en presenteert een verbeterde versie die steunt op surrogaatmodellering om een hogere computationele efficiëntie te verkrijgen. Dit is van bijzonder belang wanneer geavanceerdere antennetopologieën worden ontwikkeld, die meer functionaliteiten kunnen integreren in één enkele antenne, maar vaak langere simulatietijden vereisen in vergelijking met eenvoudigere ontwerpen. Daarom wordt een strategie gepresenteerd die een multi-objectief constrained Pareto-optimalisatie uitvoert door middel van surrogaatmodellen, om de computationele kost te verkleinen die deze complexere antenneontwerpen met zich meebrengen. Deze strategie wordt toegepast op het ontwerp van een wearable stacked patch antenne, bedoeld voor GNSS-ontvangst in het onderste en bovenste deel van de L-band. In het zesde hoofdstuk wordt een nieuwe fabricagemethode voor actieve textielantennes voorgesteld. In een poging om de flexibiliteit van actieve wearable apertuurgekoppelde patchantennes gebruikt in smart textile systemen te verhogen, wordt een lasergebaseerde vormgevingstechniek gebruikt. Deze techniek omvat het verwijderen van het grootste deel van het voedingssubstraat van de antenne, tot zeer dicht bij de microstrip interconnecties en de aperturen in het grondvlak van de antenne. Langs de ene kant verandert dit de effectieve diëlektrische constante van het substraat, wat een invloed heeft op de prestaties van de impedantiegecontrolleerde RF-circuits, en op de apertuurkoppeling tussen de voedingslijnen en de stralende structuur. Langs de andere kant heeft het verwijderen van verlieshebbend textielsubstraat rondom de RF interconnecties het potentieel om de verliezen in het voedingssubstraat te verminderen. Door de invloed van dit veranderde voedingssubstraat in rekening te brengen, kunnen ontwerprichtlijnen worden opgesteld om hoogperformante, lichte en flexibele actieve draagbare antennes te ontwerpen.

Summary

Smart textiles provide a promising way to conveniently integrate advanced functions into our daily lives. A smart textile system realizes these functionalities, such as sensing, localization and communication, in an unobtrusive way, by implementing the different sensors, electronics and antennas into the textile itself, optimally exploiting the otherwise unused area. Not only can smart textiles increase the quality-of-life of users in their day-to-day activities, they can also significantly enhance the safety and efficiency for rescue workers on the field. Functions such as vital signs monitoring, scanning of environmental conditions, reliable communication and precise localization can be added to professional rescue worker garments, without overburdening the rescue worker with additional pieces of equipment that have to be carried around. Not only can new features be added to rescue worker systems, existing devices can also be integrated into the smart textile system, with the ultimate goal of creating a garment that is able to provide the rescue worker with an plethora of life-saving functionalities, while offering increased comfort and range of motion because the now redundant devices no longer have to be carried around.

This work focuses on the wearable textile antennas that are part of such a smart textile system. These wearable antennas face a challenging set of design requirements. First, and foremost, their wearability requires them to be comfortable, unobtrusive and flexible. From a material perspective, this specifies a need for suitable flexible foam/textile substrate materials and flexible (textile) conductors that allow the wearable antenna to be flexible and breathable, while maintaining high performance. From an antenna topology viewpoint, this requirement can be fulfilled by relying on planar antenna topologies. These are low-profile and lightweight, and their layered structure enables an easy fabrication with textile materials. The flexibility of the antennas, necessary for a comfortable integration, also makes them vulnerable to bending influences, which has to be taken into account in the design stage. Moreover, their vicinity to the body requires particular care to ensure that antenna performance is not affected. In particular, when targeting the field of rescue-workers, robustness is another key requirement of not only the wearable antennas, but of the complete smart textile system. Great opportunities present themselves in the antenna design to improve the robustness of the antenna and the smart textile system. A suitable choice of antenna topology, a thorough material selection and a far-stretching integration of functionalities into a single antenna module allow wearable textile antennas to perform excellently in this demanding environment, coping with the heavy design requirements. In this work, design strategies for high performance wearable textile antennas, and more specifically, antennas for localization using global navigation satellite systems, are

presented. These strategies tackle the challenges faced in the context of wearable textile antennas for rescue worker systems, and are validated by means of novel wearable antenna designs.

The first chapter presents the reader with an overview of the concepts used in the rest of the work. Next, in the second chapter of this work, a method to integrate additional functionalities into a wearable antenna in a compact way, by deploying active electronics on the antenna's backside, is presented. In this chapter, the design of an active wearable dual-band GPS/Iridium antenna, intended for integration into a firefighter garment, is discussed. A chip low-noise amplifier (LNA) is integrated onto a circularly polarized aperture-coupled microstrip patch antenna. Prototypes of this antenna are fabricated using textile/flexible materials, and their performance is evaluated by means of elaborate measurements, including measurements of the antenna in bent and on-body conditions. These measurements show excellent off- and on-body performance, even compared to traditional, rigid antennas, demonstrating that the presented antenna topology and electronics integration technique are excellent candidates for the design of high performance GNSS textile antennas. Chapter 3 addresses the issue of autonomy of textile antennas, presenting a novel dedicated design paradigm for autonomous active textile antenna systems that may serve as platforms for body-centric sensing, localization and wireless communication systems in professional rescue worker applications. On the one hand, the large amount of real estate available in professional rescue worker garments may be exploited to deploy multiple textile antennas. On the other hand, the size of each radiator may be designed large enough to ensure high radiation efficiency when deployed on the body. This antenna surface is then reused by placing active electronics directly underneath and energy harvesters directly on top of the antenna patch. This design paradigm is illustrated by means of recent textile antenna prototypes integrated into professional garments, providing sensing, positioning and communication capabilities. In particular, a novel wearable active Galileo E1-band antenna is presented and fully characterized, including noise figure and linearity performance. In the fourth chapter, the optimization of increasingly complex textile antenna designs, fabricated using unconventional materials, is addressed. A dedicated design strategy is presented that is able to produce antennas that are optimized over a wide bandwidth for often conflicting characteristics such as impedance matching, axial ratio, efficiency and gain, and, moreover, that is able to account for the tolerances that apply for the characteristics of the unconventional materials used in smart textile systems. This strategy incorporates a multi-objective constrained Pareto-optimization, and is applied to the design of a Galileo E6-band antenna with optimal return loss and axial ratio characteristics. Subsequently, different prototypes of the optimized antenna are fabricated and measured to validate the proposed design strategy. Chapter 5 builds further on the strategy presented in chapter 4, and proposes an improved version that relies on surrogate modeling to achieve a greater computational efficiency. This is of particular importance when using more advanced antenna topologies, which can be used to incorporate more functionalities into a

single wearable antenna, but often require longer simulation times compared to simpler designs. Therefore, a strategy is presented that performs a multi-objective constrained Pareto-optimization by means of surrogate models for reducing the computational cost caused by more complex antenna designs. This strategy is applied to the design of a wearable stacked patch antenna, intended for GNSS reception in the lower and upper L-bands. In the sixth chapter, a novel fabrication method for active wearable antennas is presented. In an effort to improve the flexibility of active wearable aperture coupled patch antennas applied in smart textile systems, a laser shaping technique for the antenna feed substrate is used. The technique consists of the removal of most of the antenna feed substrate, up to very close distances to the microstrip interconnects and in close vicinity of the coupling slots in the antenna ground plane. One the one hand, this changes the effective dielectric constant of the substrate, influencing the performance of the impedance-controlled RF circuitry, and the aperture coupling between the feed lines and the radiating structure. On the other hand, the removal of lossy, textile substrate material surrounding the RF interconnections has the potential to reduce losses in the feed circuit. By taking into account the effects of this altered substrate, design guidelines can be defined to produce high performance, light-weight and flexible wearable antenna designs.

List of Abbreviations

AC	Alternating Current
ADS	Advanced Design System
AR	Axial Ratio
BAW	Bulk Acoustic Wave
CAD	Computer-Aided Design
DC	Decent Current
FCB	Flexible Circuit Board
FDTD	Finite Difference Time Domain
FEM	Finite Element Method
FIT	Finite Integration Technique
GLONASS	GLObalnaja NAvigatsionnaja Spoetnikovaja Sistema
GNSS	Global Navigation Satellite System
GPS	Global Positioning System
IoT	Internet of Things
LHCP	Left-Handed Circularly Polarized
LHP	Left-Handed Polarized
LNA	Low-Noise Amplifier
MIMO	Multiple-Input and Multiple-Output
MoM	Method of Moments
MPIE	Mixed Potential Integral Equation
NF	Noise Figure
PI	Polyimide
PIFA	Planar Inverted-F Antenna
PoI	Probability of Improvement
RBF	Radial Basis Functions
RF	Radio Frequency
RHCP	Right-Handed Circularly Polarized
RHP	Right-Handed Polarized
SAR	Search And Rescue
SAW	Surface Acoustic Wave
SBO	Surrogate-Based Optimization
SFIT	Smart Fabric Interactive Textile
SGA	Standard Gain Antenna
SMA	SubMiniature version A
SNR	Signal-to-Noise Ratio
SUMO	SUrrogate MOdel
TPU	Thermoplastic Polyurethane
UHF	Ultra High Frequency
VNA	Vector Network Analyzer

List of Symbols

$\lvert\cdot\rvert$	Magnitude of a complex or real number
α	Tilt angle of polarization ellipse
Γ	Reflection coefficient
ϵ	Permittivity of a medium
ϵ_r	Relative permittivity
θ	Elevation angle
λ	Wavelength
μ	Permeability of a medium
τ	Eccentricity of polarization
ϕ	Azimuth angle
ω	Angular frequency
a_1	Incident power wave
AR	Axial ratio
b_1	Reflected power wave
e_{cd}	Conduction-dielectric efficiency
$e(r)$	Far-field of a transmitting antenna
f	Frequency
F	Antenna radiation vector
G	Antenna gain
I	Current
$IIP3$	Third order input intercept point
j	Imaginary unit
k	Wavenumber
L	Path loss
M	Mismatch factor
$OIP3$	Third order output intercept point
$P1dB$	1 dB compression point
P_{rad}	Radiated power
P_t	Power injected at antenna terminals
R_a	Radiation resistance
R_{cd}	Conduction-dielectric loss resistance
S_{11}	One-port S-parameter
$tan\ \delta$	Loss tangent
U	Radiation intensity
U_{iso}	Radiation intensity of isotropic antenna
V	Voltage

V^{th}	Thévenin-equivalent voltage
X_a	Radiation reactance
Z_0	Characteristic impedance of a transmission line
Z_a	Radiation impedance
Z_c	Free-space characteristic impedance
Z^{th}	Thévenin-equivalent impedance

List of Publications

Articles in International Journals

- A. Dierck, F. Declercq and H. Rogier, "A Wearable Active Antenna for Global Positioning System and Satellite Phone," *IEEE Trans. Antennas Propag.*, vol. 61, no. 2, pp. 532-538, 2013.
- A. Dierck, S. Agneessens, F. Declercq, B. Spinnewyn, G-J. Stockman, P. Van Torre, L. Vallozzi, D. Vande Ginste, J. Vanfleteren, T. Vervust and H. Rogier, "Active Textile Antennas in Professional Garments for Sensing, Localisation and Communication," *International Journal of Microwave and Wireless Technologies*, vol. 6, pp. 331-341, 2014.
- M. Rossi, A. Dierck, H. Rogier and D. Vande Ginste "A Stochastic Framework for the Variability Analysis of Textile Antennas ," *IEEE Trans. Antennas Propag.*, accepted for publication.
- A. Dierck, F. Declercq, T. Vervust and H. Rogier, "Dedicated Multi-objective Constrained Pareto-optimization for Design of Textile Antennas," *Submitted to International Journal of Antennas and Propagation*.

Articles in Conference Proceedings

- A. Dierck, T. De Keulenaer, F. Declercq, and H. Rogier, "A Wearable Active GPS Antenna for Application in Smart Textiles," in *Proceedings of the 32nd ESA Antenna Workshop on Antennas for Space Applications*, Oct. 2010, pp. 1-7.
- A. Dierck, F. Declercq, and H. Rogier, "Review of Active Textile Antenna Codesign and Optimization Strategies," in *2011 IEEE International Conference on RFID-Technologies and Applications (RFID-TA)*, Sept. 2011, pp. 194-201.
- P. Van Torre, L. Vallozzi, A. Dierck, H. Rogier and M. Moeneclaey, "Power-efficient Body-centric Communications," in *URSI Benelux Forum 2012, Proceedings*, 2012, pp. 8-10.
- A. Dierck, F. Declercq, H. Rogier, T. Vervust, and J. Vanfleteren "Highly Flexible, Low Loss Feed Structure for Active Wearable Aperture Coupled Antennas with Radically Trimmed Substrate," in *IC1004 Joint Workshop, Abstracts*, 2013.

- H. Rogier, S. Agneessens, A. Dierck, F. Declercq, P. Van Torre, L. Vallozzi, E. Tanghe, G. Vermeeren and W. Joseph, "Active Textile Multi-antenna Systems for Energy-efficient Body-centric Communication," in *Progress in Electromagnetics Research Symposium, Abstracts*, 2013, pp. 992.

- H. Rogier, S. Agneessens, F. Declercq, A. Dierck, W. Joseph, M. Moeneclaey, L. Vallozzi, P. Van Torre and J. Vanfleteren,"Textile Antenna Systems for Positioning and Off-body Communication," *IET Seminar on Body-Centric Wireless Communications*, 5 July 2013, pp.1-33.

- A. Dierck, F. Declercq, and H. Rogier, "An Active Wearable Dual-band Antenna for GPS and Iridium Satellite Phone Deployed in a Rescue Worker Garment," in *2013 IEEE International Conference on RFID-Technologies and Applications (RFID-TA)*, Sept. 2013, pp. 1-5.

- H. Rogier, S. Agneessens, A. Dierck, B. Spinnewyn, G.-J. Stockman, F. Declercq, P. Van Torre, L. Vallozzi and D. Vande Ginste, "Active Textile Antennas in Professional Garments for Sensing, Localisation and Communication," in *2013 European Microwave Conference (EuMC)*, 6-10 Oct. 2013, pp.850-853.

Design Strategies for High Performance GNSS Textile Antennas

1 Introduction

In this chapter, some general concepts are outlined to form a frame of reference for the work presented in this dissertation. Afterwards, an overview of the different chapters is given.

First, the general concept of smart textiles and their use in the field of rescue workers is described. Subsequently, additional attention is given to the topic of wearable textile microstrip patch antennas. An overview of these antennas is given, briefly covering the basic theory, design methods and performance characteristics. Following the presentation of the wearable antennas, some light is shed onto the main application area of the antennas discussed in this work, being satellite-based navigation.

1.1 Smart textiles

In today's reality, we are faced with an unmistakable ubiquitousness of *smart devices*. Aside from the more obvious examples, such as smartphones, television sets or cars, at this moment, even coffee makers and ovens have built-in computers and are able to communicate wirelessly, adding advanced functionalities and interactivity to everyday appliances, and, in this way, creating a *smart environment*. Such a smart environment not only offers opportunities in everyday situations, but also presents a great potential in military and public services. More and more functionalities can be implemented to enhance the safety of people putting their lives on the line to save others, not only reducing their own personal risk, but also directly being beneficial to the people in distress. A promising path to facilitate these enhanced capabilities, is offered by *smart textiles* [1]–[3]. The idea of smart textiles is to extend traditional garment functionalities to include advanced features. In the field of rescue workers, these features entail, for example, vital signs monitoring, environment scanning and precise localization. They have the potential to vastly

increase safety and efficiency in disaster situations. Notwithstanding the increasing miniaturization of electronic devices, adding these functionalities by means of traditional, often bulky equipment would diminish the comfort of the wearer, and potentially limit the range of motion. Smart textiles, however, offer a way to integrate these functionalities in the wearer's garments, exploiting as much as possible the space provided, without jeopardizing the safety and comfort of the wearer.

When breaking it down into parts, a smart textile system consists of some form of power supply, a selection of sensors and actuators, data processing units, interconnections, and, forming the focus of this work, one or more wearable antennas. In terms of power supply, smart textiles greatly benefit from lightweight, flexible technologies, not only depending on power stored in, for example, flexible batteries [4], [5], but also relying on power generation by means of harvesting, for example, solar power, kinetic energy, thermal energy and RF energy [6]–[16]. Smart textile sensors are able to provide a variety of data, and can be used for monitoring vital signs of the wearer or monitoring environmental conditions [17]–[20]. Wearable actuators are mostly used for, but not limited to, giving feedback to the user, by means of, for example, flexible/textile displays integrated into the garment [21], [22]. Other wearable actuator examples include protective systems, such as a wearable air-bag [23]. Data processing converts sensor data into usable information for steering actuators, or for transmission to a base station. It is often a part of the wearable sensors/actuators/antennas, instead of a separate unit. Interconnections in smart textiles are realized by means of conductive yarns, stretchable RF interconnects or wireless on-body links [24]–[27]. Finally, the wearable antennas form a vital element of the wearable system, providing communication to base stations, other users, satellites and other parts of the smart textile system. So-called *off-body* communication focuses on communicating away from the body, be it to a base station, another user or a satellite. Examples include short and long-range data links and satellite-based navigation [28]–[35]. *On-body* communication entails the communication between the different components of the smart textile system [26]. Finally, *In-body* communication deals with the communication between devices on or near the body, and body-implanted devices [36]–[38]. Wearable antennas have been extensively studied in the recent years, and provide an interesting and challenging research area. Wearable systems have already been studied and realized for different applications, such as medicine and health care, fire-fighting, military, sports and rescue worker applications [10], [39]–[42]. The context of rescue worker systems has been the key application area of this work, and more specifically, the integration of satellite based navigation capabilities. The field of rescue workers provides several opportunities for advantageous smart textile implementations, but of course poses specific challenges in terms of robustness. Moreover, the strict requirements of GNSS technology further increase the challenges faced by the designer.

1.2 Wearable textile antennas for rescue worker systems

Wearable antennas in the field of rescue workers systems are of high interest to the research community, and a lot of effort has been devoted to finding new and improved design methods, optimization strategies and antenna implementations. The first antenna designs, presented in this dissertation, build further onto the work that was carried out in the European FP6 ProeTex integrated project, in which Ghent University was a scientific partner. The aim of this project was to develop a wearable smart textile system for rescue workers, such as fire fighters or civil protection personnel, that allowed monitoring and coordination of interventions in disaster scenarios. Other research efforts presented in this dissertation were carried out within the context of the EC-FP7 Galileo.2011.3.1- 2: Collaborative Project, Grant agreement no.: 287166. The goal of this project was to create Galileo satellite navigation antennas and front-end solutions, focusing on ultra-small and wearable implementations. As a partner, UGent/IMEC contributed to the research, design, fabrication and validation of several active wearable antenna designs.

Wearable antennas for smart textile rescue worker systems have to meet a set of specific requirements. As it is the aim of smart textiles to provide advanced functionalities without deteriorating the form and function of the garment, the wearable antennas should be flexible and low-profile. Flexibility will guarantee that the range of motion of the wearer is not limited, which is of special importance in rescue worker applications. Moreover, flexibility will allow the antenna to move with the garment, instead of breaking under stress, increasing robustness. A low-profile antenna is necessary in order to seamlessly integrate the antenna into the garment. Again, this prevents the smart textile system from hindering the user. Additionally, low-profile, and in general, smaller, more compact devices, increase system robustness by reducing the footprint that is exposed to harsh conditions. This robustness is a requirement that is emphasised in rescue-worker applications. Not only does the antenna conformability add to the robustness, but also the specific topology on which the antenna design is based, as discussed further in 1.2.1. Depending on the usage scenario, additional application-specific requirements are imposed. For example, a smart textile system for patient monitoring will require a wearable antenna that is not only flexible and low-profile, but also breathable, in order to retain the full functionality of the patient's garments. On the other side, a wearable antenna implemented in the bladder of an inflating safety vest, does not specifically require breathability, or should even be guaranteed to be impenetrable by moisture.

1.2.1 Microstrip patch antennas

The microstrip patch antenna is a popular type of antenna for a wide variety of applications. Originally conceptualized in 1953 [43], development accelerated in

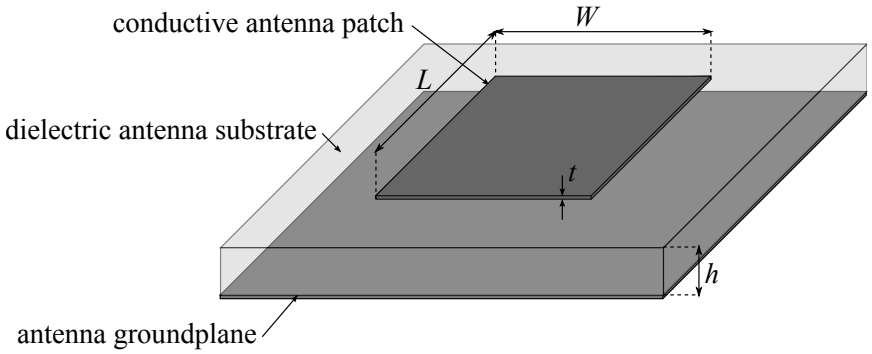

(a)

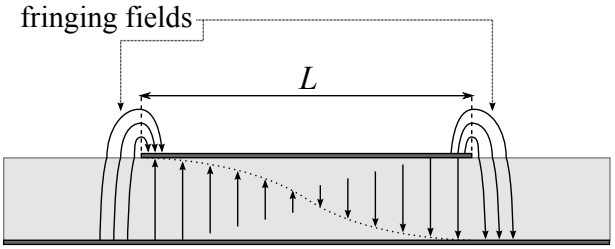

(b)

Figure 1.1: Microstrip patch antenna geometry (a) and radiation mechanism (b).

the 1970s and continued throughout the recent decades to make the microstrip patch antenna the popular antenna it is today. Microstrip patch antennas offer numerous advantages, such as a light weight, a low profile, the possibility to be integrated conformally onto curved surfaces, a low fabrication cost and an easy fabrication. Another benefit is the presence of a ground plane, which in case of wearable antennas shields the antenna from the body of the wearer. Drawbacks of this antenna topology are the rather low bandwidth and moderate gain and efficiency, although techniques exist to minimize the effects of these limitations [44].

As depicted in Fig. 1.1(a), a microstrip patch antenna consists of a conductive microstrip patch, often in a regular shape, such as a rectangle or circle, to simplify analysis, design and fabrication. The conductive patch, in this case a rectangle with dimensions $L \times W$, is located on an dielectric *antenna substrate* with height h, permittivity ϵ_r and loss tangent $tan\ \delta$. In turn, this antenna substrate sits on a conductive ground plane. The length of the patch L corresponds roughly to half the wavelength of the lowest order resonant mode of the cavity formed by the patch

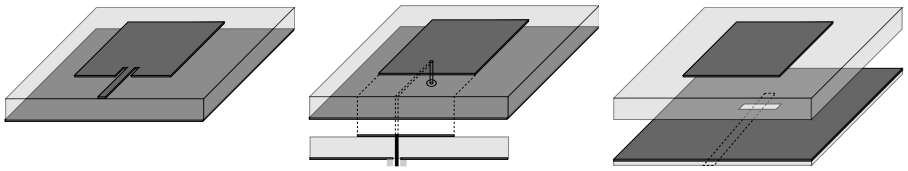

(a) (b) (c)

Figure 1.2: Schematic representation of inset feeding (a), probe feeding (b) and aperture-coupled feeding (c).

and the ground plane. This resonant mode exhibits a sinusoidally varying electric field along the length of the patch, as depicted in Fig. 1.1(b). This electric field is radiated through the apertures that are formed by the spacing between the patch and the ground plane. The two apertures along the width of the patch provide the main contribution to the radiation of the microstrip patch antenna, by means of the fringing fields depicted in Fig. 1.1(b).

Different feeding techniques exist for microstrip patch antennas. In Fig. 1.2, inset feeding, probe feeding, and aperture-coupled feeding are depicted. In this work, aperture-coupled feeding is the preferred topology for designing wearable antennas. This technique offers several benefits. First, in the aperture coupled topology, the feed structure is shielded from the radiating patch by a ground plane. As mentioned before, this ground plane shields the antenna from influences of the human body, such as antenna radiation pattern distortion, resonance frequency shifts and bandwidth changes [45], [46]. Moreover, by shielding the feed structure of the antenna, it becomes possible to integrate (active) electronics onto the antenna backside without these being affected by the antenna's radiated fields. In this way, amplifiers, power management circuits and transceivers can be integrated directly behind the groundplane, on the antenna feed circuit, producing *active antennas*. By implementing active electronic circuits on the antenna backside, interconnections to electronics in other parts of the smart textile system are eliminated, reducing potential weak links. Besides increasing the overall robustness of the smart textile system, by integrating electronics into the wearable antennas, the complete smart textile system is miniaturized. This allows an easier integration and can increase the comfort of the resulting smart garment. Unlike the probe feed, which also shields the feed circuit from the antenna patch, the aperture-coupled topology eliminates vias through the, often thick, antenna substrate. These vias form weak links in the wearable antenna design, and are prone to breaking when the antenna is exposed to stresses. Another benefit is that the aperture-coupled feeding technique allows higher bandwidths to be reached, compared to other feeding techniques [47].

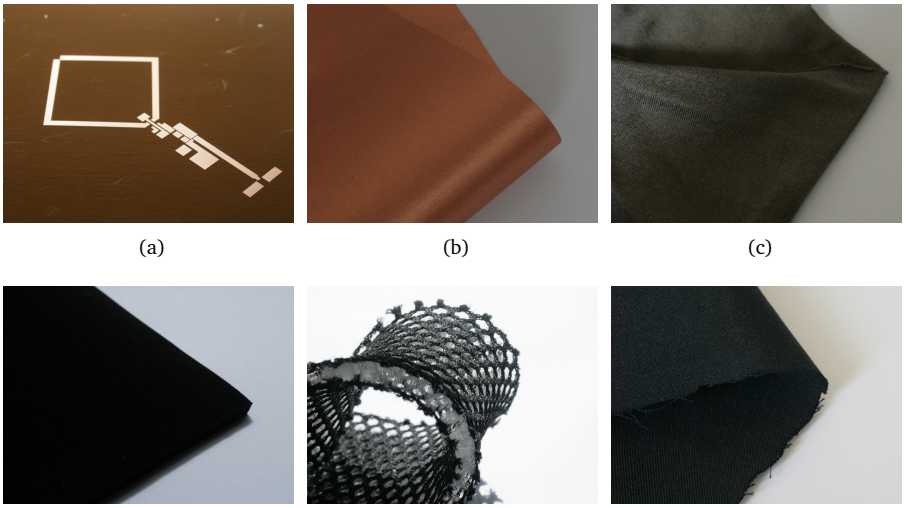

(a) (b) (c)

(d) (e) (f)

Figure 1.3: Examples of wearable antenna materials: polyimide (a); copper-plated nylon taffeta (b); silver-plated stretch fabric (c); closed-cell expanded rubber foam (d); 3D fabric (e); aramid (f).

1.2.2 Wearable microstrip patch antenna materials

In the design of wearable antennas, an important step consists of the material selection. To ensure a flexible antenna that can be comfortably integrated into a garment, flexible textile materials have to be selected.

Wearable antenna conductors can be realized by using conductive textiles, such as copper-plated nylon taffeta and silver plated stretchable fabric, by using laminations of metal films onto a polymer carrier, such as copper-on-polyimide, or by using conductive patterns defined by screen printing conductive ink or embroidering conductive yarns. In this work, conductive textiles and metal-on-polymer laminations were preferred. Conductive textiles, on the one hand, are easily acquired, and allow quick prototyping of antennas with regular conductive structures. For these simple conductive structures, such as rectangular antenna patches or ground planes with regular aperture shapes, the (stretchable) fabrics offer the most flexible option. Metal-on-polymer laminations, on the other hand, allow highly accurate fabrication by means of photolithographical processes, and resist high temperatures, which allows components to be soldered onto the fabricated conductive structures. This makes metal-on-polymer laminations, such as copper-on-polyimide, the preferred technology for more complex structures, such as feed networks with integrated (active) components.

For the substrates, we make a distinction between the feed substrate and the an-

tenna substrate. On the one hand, to limit back-radiation from the feed circuit, a thin feed substrate with a high permittivity is preferred. On the opposite hand, for the antenna substrate, a thicker substrate with a low permittivity improves antenna efficiency [48]. In a low-permittivity substrate, the fringing fields, depicted in Fig. 1.1(b), are less confined to the substrate, improving antenna radiation. Increasing the substrate's height, the radiating apertures formed between the patch and the groundplane, as discussed earlier, become larger, and thus, antenna radiation is improved. For both the feed and antenna substrate, low loss materials are preferred, in order to minimize the dielectric losses. In Fig. 1.3, some examples of flexible/textile materials used in the design of wearable antennas are depicted. These will be further discussed throughout the dissertation.

1.2.3 Antenna analysis techniques

Different analysis techniques exist to determine the microstrip patch antenna's characteristics. The transmission line and cavity models [44], for example, offer simplified, but insightful methods for microstrip patch analysis. Nowadays, for antenna design and optimization, more rigorous techniques, known as full-wave analysis, are used. Computer-aided design (CAD) tools yield a numerical solution of Maxwell's equations, and provide highly accurate and complete analyses of microstrip patch antennas and other microwave devices. A widely used technique is solving the boundary integral equation by means of the method-of-moments (MoM), which was also the main method used in the antenna design processes in this work. The MoM allows to solve the mixed potential integral equation (MPIE) derived from the Maxwell equations for planar structures in a multi-layered dielectric background medium. The unknown magnetic and electric surface currents are discretized by meshing the metalization and slot layers, and applying an expansion in a finite number of subsectional basis functions. Inserting these current expansions in the integral equations and applying the Galerkin testing technique, the equations are transformed into a discrete matrix equation. Solving this matrix equation then yields the unknown surface currents. This method is applied in Agilent's Advanced Design System (ADS) Momentum solver. Other popular methods include the finite difference time domain (FDTD), the finite element method (FEM) and the finite integration technique (FIT) [49].

1.2.4 Antenna parameters

Next, a brief overview is given of the fundamental antenna parameters. These are used throughout this work to describe the characteristics and the performance of the presented antenna designs. For more in-depth information, the reader is referred to antenna textbooks, such as [44], [48].

Input impedance

A transmitting antenna can be represented by the equivalent circuit depicted in Fig. 1.4(a), where the antenna is connected to a generator (not shown) via a

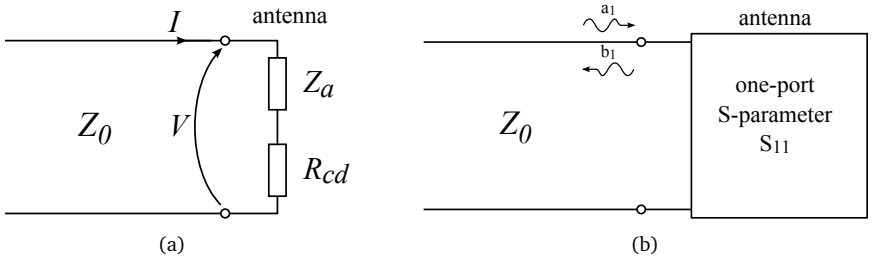

Figure 1.4: Circuit representation of an antenna in transmit mode (a) and S-parameter representation of an antenna (b).

transmission line with characteristic impedance Z_0. Looking at the antenna from its terminals, the input impedance can be determined as:

$$Z_{in} = \frac{V}{I} = Z_a + R_{cd}.$$

Here, Z_a represents the antenna's radiation impedance, and

$$Z_a = R_a + jX_a,$$

where the radiation resistance R_a relates to the power radiated in the far-field, and the radiation reactance X_a relates to the antenna energy in the near-field. R_{cd} represents the antenna losses, including the effects of conductive and dielectric losses. The antenna is connected to a transmission line with characteristic impedance Z_0. This characteristic impedance is usually 50 Ω in microwave circuits. From the antenna's input impedance and the characteristic impedance of the transmission line, the reflection coefficient Γ can be calculated as

$$\Gamma = \frac{Z_{in} - Z_0}{Z_{in} + Z_0},$$

which relates to the mismatch factor M as

$$M = 1 - |\Gamma|^2.$$

When $\Gamma = 0$, or equivalently, $M = 1$, there is no mismatch between the transmission line and the antenna, and a maximum amount of power is transferred to the antenna terminals. In Fig. 1.4(b), the antenna is represented by a one-port scattering parameter S_{11}, normalized with respect to the characteristic impedance Z_0 of the transmission line connected to the antenna terminals. In high frequency analysis, scattering parameters are widely used, and the reflection coefficient Γ corresponds to S_{11}. S_{11} is equal to the ratio of the incoming wave a_1 to the reflected wave b_1, where the squared amplitudes of a_1 and b_1 correspond to incoming and reflected power waves. Hence, $|S_{11}|^2 = \frac{|b_1|^2}{|a_1|^2}$ is a measure for the reflected power.

This measure is usually evaluated on a logarithmic scale as $20\log_{10}|S_{11}|$, and in the rest of this work, as in most of literature, the notation $|S_{11}|$ is used to represent $20\log_{10}|S_{11}|$. A value of $|S_{11}| < -10\ dB$, for example, means that less than 10 % of the injected power is reflected back to the generator, and, hence 90 % of the power is injected into the antenna.

The $|S_{11}|$ is a frequency-dependent value, and the range in which $|S_{11}| < -10\ dB$ is denominated as the antenna bandwidth, a widely used performance parameter in antenna design.

Power gain

The power gain, or gain, of an antenna provides a measure of how much power is radiated in a certain direction, compared to a perfect isotropic radiator. The radiation intensity $U(\theta,\phi)$ represents the power an antenna radiates along a given direction in a unit solid angle, and can be expressed as:

$$U(\theta,\phi) = \frac{|\boldsymbol{F}(\theta,\phi)|^2}{2Z_c},$$

where $Z_c = \sqrt{\frac{\mu}{\epsilon}}$ is the characteristic impedance of the medium in which the antenna is transmitting, and $\boldsymbol{F}(\theta,\phi)$ is the radiation vector, used to express the far-field of the transmitting antenna (at a distance $R > \frac{2d^2}{\lambda}$, d being the largest dimension of the antenna) by:

$$\boldsymbol{e(r)} = \boldsymbol{F}(\theta,\phi)\frac{e^{-jkR}}{R},$$

with $k = \omega\sqrt{\epsilon\mu}$. For an ideal isotropic antenna, to which a power P_t is delivered, we obtain:

$$U_{iso} = \frac{P_t}{4\pi},$$

since the power at the antenna terminals is radiated isotropically over the unit sphere. Taking the ratio of an antenna's radiation intensity to the radiation intensity of the ideal isotropic antenna, results in the antenna gain:

$$G(\theta,\phi) = \frac{U(\theta,\phi)}{U_{iso}} = 4\pi\frac{U(\theta,\phi)}{P_t}.$$

As seen in the discussion on the input impedance, an antenna does not radiate all of the power that is delivered to the terminals. Due to the conductor and dielectric losses, the radiated power will be

$$P_{rad} = e_{cd}P_t,$$

where e_{cd} represents the conduction-dielectric efficiency. The directivity of an antenna does not take into account conduction-dielectric losses, and is equal to

$$D(\theta,\phi) = 4\pi\frac{U(\theta,\phi)}{P_{rad}},$$

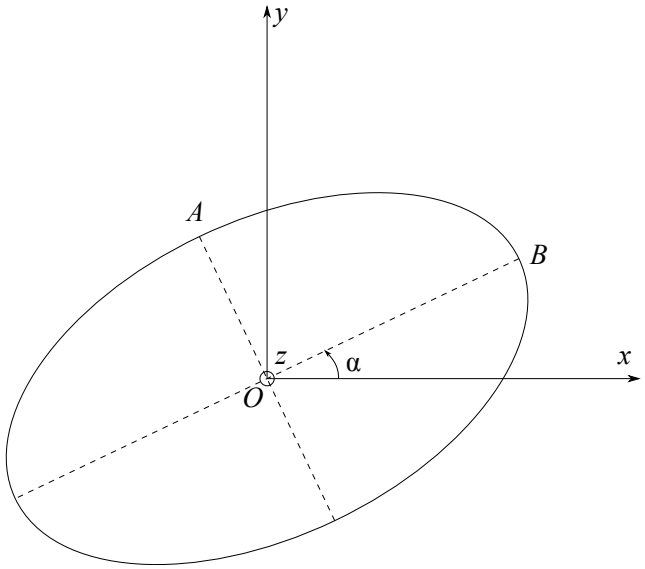

Figure 1.5: Polarization ellipse.

so it is easily seen that the relation between antenna gain and directivity is

$$G(\theta,\phi) = e_{cd} D(\theta,\phi).$$

In literature, the gain is often presented as a two- or three-dimensional plot, the so-called gain pattern.

Polarization

The antenna polarization, or rather, the polarization of the wave radiated by the antenna, indicates how the electric field vector's orientation and size change when the wave propagates in a certain direction. When looking in the far-field, the electric and magnetic fields of the antenna can be seen locally as plane waves, propagating along the radial direction $\hat{r}$, meaning that the field vectors rotate in the plane perpendicular to $\hat{r}$. The figure described by the field vector is, in general, an ellipse, as depicted in Fig. 1.5. This ellipse can be described by it's eccentricity $\tau = \frac{\overline{OA}}{\overline{OB}}$, being the ratio between the minor and major axis, and its tilt angle α, which is the angle formed between the ellipse's major axis and the x axis of the local reference system. The value of τ is limited by $0 \leq |\tau| \leq 1$. When $\tau = 0$, the antenna is linearly polarized, and when $|\tau| = 1$ the antenna is circularly polarized. For the remaining values of τ, the antenna is said to be elliptically polarized. The sign of τ indicates the polarization sense: if $\tau > 0$, the wave is right-handed polarized (RHP), if $\tau < 0$, it is left-handed polarized (LHP).

If the polarization ellipses of a transmitting and a receiving antenna coincide, and the polarization has an opposite sense (direction of rotation), seen from the receiv-

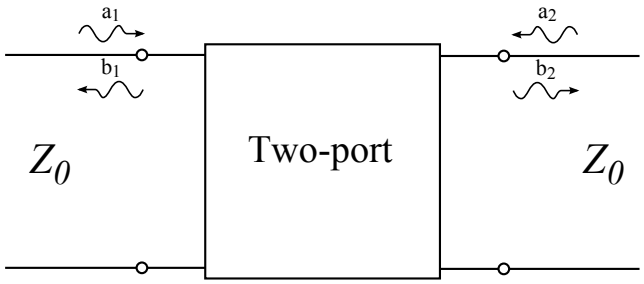

Figure 1.6: Two-port circuit with incident and reflected power waves.

ing antenna's point of view, then a wave traveling directly from the one antenna to the other will be perfectly received. In this case, no polarization mismatch occurs. The other extreme, a complete polarization mismatch, occurs when the transmit and receive antennas are cross-polarized. An example is a the case of two orthogonally linearly polarized antennas, or the case of a left -handed circularly polarized (LHCP) and a right-handed circularly polarized (RHCP) antenna.

The polarization of an antenna is, in practice, quantified by the axial ratio (AR), giving essentially the same information as the absolute value of the eccentricity $|\tau|$. In this work, the axial ratio for circular polarization is often used. It is defined as

$$AR = 20\log_{10}(\frac{1}{|\tau|}).$$

The AR is valued between 0 and $+\infty$, where a value of 0 corresponds to a perfect circular polarization, and a value of $+\infty$ corresponds to a perfect linear polarization. In the design of circularly polarized antennas, sufficient circular polarization purity is ensured in the bands of interest by requiring the AR to remain under the limit of 3 dB. The axial ratio is a direction dependent value, and, like the gain pattern, can be displayed as a function of θ and ϕ, to form the axial ratio pattern.

1.2.5 Two-port S-parameters

Since later in this work LNA design and measurements, as well as antenna arrays are discussed, here, we expand the explanation on one-port parameters from subsection 1.2.4 to two-port S-parameters [50]. In Fig. 1.6, analogous to the one-port case, a two-port network is depicted. Considering the incident waves a_1, a_2 as an excitation, and the reflected waves b_1, b_2 as a response, the circuit can be described as follows:

$$\begin{bmatrix} b_1 \\ b_2 \end{bmatrix} = \begin{bmatrix} S_{11} & S_{12} \\ S_{21} & S_{22} \end{bmatrix} \begin{bmatrix} a_1 \\ a_2 \end{bmatrix}.$$

Again, like in the one-port case, the notation $|S_{ij}|$ is used to represent $20\log_{10}|S_{ij}|$.

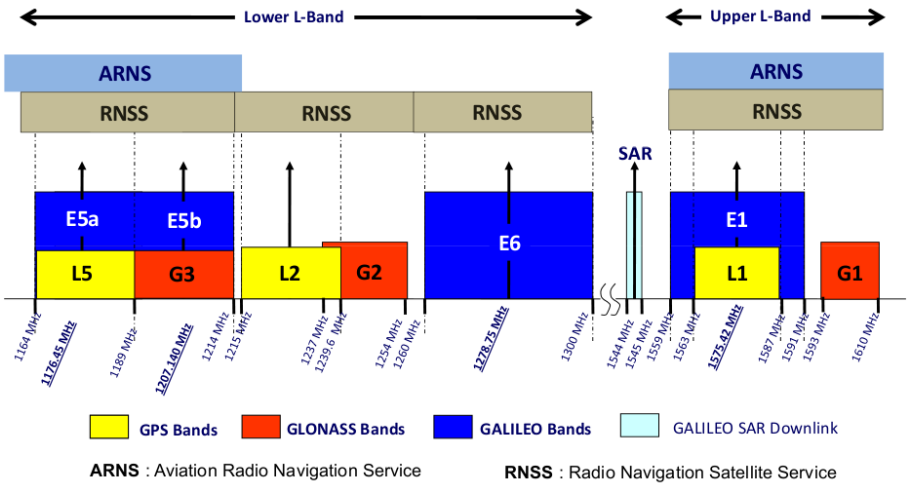

Figure 1.7: GNSS spectrum.

1.3 Global navigation satellite systems

Not only was space-based positioning one of the first methods for navigation, at this moment it is also one of the most advanced and widely used ones. In older days, travelers used the sun and the stars to guide the way, whereas today's space-based navigation uses satellites to provide highly accurate positioning. Starting with the conception of the Global Positioning System (GPS) in the 1970s, nowadays, different satellite-based navigation systems have reached maturity or are being developed. In Fig. 1.7, the spectrum of the different Global Navigation Satellite Systems (GNSS) is depicted, showing the frequency bands allocated to the different services. These frequency bands are located within the so-called L-band, stretching from 1 to 2 GHz. In general, within the allocated frequency bands, the navigation satellites transmit navigation messages containing time information. From the time difference between sending and receiving, a ground user can calculate the distance to a satellite. Basically, when three satellites are in sight, the ground user can uniquely determine his position. Currently, the American GPS and the Russian GLONASS are fully operational, whereas full completion of the European Galileo system is expected by 2019.

From the antenna point of view, GNSSs use circularly polarized antennas. This remedies positioning errors due to multipath. The RHCP GNSS signals can be received by RHCP ground user antennas. Signals reaching the receiving antenna via an indirect path, however, will change their polarization sense after reflection, and thusly become LHCP. As discussed in section 1.2.4, this results in a polarization mismatch, preventing the antenna from receiving multipath signals, at least from first-order reflections.

Wearable GNSS antennas benefit greatly from the direct integration of processing electronics on the antenna backside. Aside from the benefits towards overall robustness and miniaturization of the complete wearable system, active antennas are of particular interest for GNSS applications. Since the space signal is very weak when it reaches a ground user, often a low-noise amplifier (LNA) is connected directly to the GNSS antenna [51]. In this way, the signal-to-noise ratio (SNR) is increased, improving the quality of reception. Moreover, integration of an LNA onto the antenna backside mitigates the effect of the attenuation caused by interconnections between the antenna and the GNSS receiver, further improving the SNR.

1.4 Outline

In the second chapter of this work, a method to integrate additional functionalities in a wearable antenna in a compact way, by means of adding active electronics on the antenna's backside, is presented. In this chapter, the design of an active wearable dual-band GPS/Iridium antenna, intended for integration into a firefighter garment, is discussed. A chip LNA is integrated onto a circularly polarized aperture-coupled microstrip patch antenna. Prototypes of this antenna are fabricated using textile/flexible materials, and their performance is evaluated by means of elaborate measurements, including measurements of the antenna in bent and on-body conditions. These measurements show excellent off- and on-body performance, even compared to traditional, rigid antennas.

Chapter 3 presents a novel dedicated design paradigm for autonomous active textile antenna systems that may serve as platforms for body-centric sensing, localization and wireless communication systems in professional rescue worker applications. On the one hand, the large amount of real estate available in professional rescue worker garments may be exploited to deploy multiple textile antennas. On the other hand, the size of each radiator may be designed large enough to ensure high radiation efficiency when deployed on the body. This antenna area is then reused by placing active electronics directly underneath and energy harvesters directly on top of the antenna patch. We illustrate this design paradigm by means of recent textile antenna prototypes integrated in professional garments, providing sensing, positioning and communication capabilities. In particular, a novel wearable active Galileo E1-band antenna is presented and fully characterized, including noise figure and linearity performance.

In the fourth chapter a design strategy is presented that is able to produce antennas that are optimized over a wide bandwidth for often conflicting characteristics such as impedance matching, axial ratio, efficiency and gain, and, moreover, that is able to account for the tolerances that apply for the characteristics of the unconventional materials used in smart textile systems. This strategy incorporates a multi-objective constrained Pareto-optimization, and is applied to the design of a Galileo E6-band antenna with optimal return loss and axial ratio characteristics.

Subsequently, different prototypes of the optimized antenna are fabricated and measured to validate the proposed design strategy.

Chapter 5 builds further on the strategy presented in chapter 4, and proposes an improved version that relies on surrogate modeling to achieve a greater computational efficiency. This is of particular importance when using more advanced antenna topologies, which can be used to incorporate more functionalities into a single wearable antenna, but often require longer simulation times compared to simpler designs. Therefore a strategy is presented that performs a multi-objective constrained Pareto-optimization by means of surrogate models for reducing the computational cost caused by more complex antenna designs. This strategy is applied to the design of a wearable stacked patch antenna, intended for GNSS reception in the lower and upper L-band.

In the sixth chapter, a novel fabrication method for active wearable antennas is presented. In an effort to improve the flexibility of active wearable aperture coupled patch antennas applied in smart textile systems, a laser shaping technique for the antenna feed substrate is used. The technique consists of the removal of most of the antenna feed substrate, up to very close distances to the microstrip interconnects and in close vicinity to the coupling slots in the antenna ground plane. One the one hand, this changes the effective dielectric constant of the substrate, influencing the performance of the impedance-controlled designed RF circuitry, and the aperture coupling between the feed lines and the radiating structure. On the other hand, the removal of lossy, textile substrate material surrounding the RF interconnections has the potential to reduce losses in the feed circuit. By taking into account the effects of this altered substrate, design guidelines can be defined to produce high performance, light-weight and flexible active wearable antenna designs. The proposed feed substrate trimming technique is validated by means of two antenna prototypes, one with a full feed substrate, and one with a reduced substrate.

References

[1] J. Cheng, P. Lukowicz, N. Henze, A Schmidt, O. Amft, G. Salvatore, and G. Tröster, "Smart textiles: from niche to mainstream", *IEEE Pervasive Comput.*, vol. 12, no. 3, pp. 81–84, 2013.

[2] A Lymberis and R. Paradiso, "Smart fabrics and interactive textile enabling wearable personal applications: R & D state of the art and future challenges", in *Engineering in Medicine and Biology Society 2008 (EMBS 2008), 30th Annual International Conference of the IEEE*, 2008, pp. 5270–5273.

[3] D. Marculescu, R. Marculescu, N. Zamora, P. Stanley-Marbell, P. Khosla, S. Park, S. Jayaraman, S. Jung, C. Lauterbach, W. Weber, T. Kirstein, D. Cottet, J. Grzyb, G. Troster, M. Jones, T. Martin, and Z. Nakad, "Electronic textiles: a platform for pervasive computing", *Proceedings of the IEEE*, vol. 91, no. 12, pp. 1995–2018, 2003.

[4] H.-J. Yoo, J. Yoo, and L. Yan, "Wireless fabric patch sensors for wearable healthcare", in *Engineering in Medicine and Biology Society (EMBC), 2010, Annual International Conference of the IEEE*, 2010, pp. 5254–5257.

[5] J. Yeo, S.-G. Moon, and J.-Y. Jung, "Design of antennas for a battery-assisted RFID tag with a thin and flexible film battery", in *IEEE Antennas and Propagation Society International Symposium, 2007*, 2007, pp. 5463–5466.

[6] S. Kim, A Georgiadis, A Collado, and M. Tentzeris, "An inkjet-printed solar-powered wireless beacon on paper for identification and wireless power transmission applications", *IEEE Trans. Microw. Theory Tech.*, vol. 60, no. 12, pp. 4178–4186, 2012.

[7] S. Lemey, F. Declercq, and H. Rogier, "Dual-band substrate integrated waveguide textile antenna with integrated solar harvester", *IEEE Antennas Wireless Propag. Lett.*, vol. 13, pp. 269–272, 2014.

[8] A. Dierck, S. Agneessens, F. Declercq, B. Spinnewyn, G.-J. Stockman, P. Van Torre, L. Vallozzi, D. Vande Ginste, T. Vervust, J. Vanfleteren, *et al.*, "Active textile antennas in professional garments for sensing, localisation and communication", *International Journal of Microwave and Wireless Technologies*, pp. 1–11,

[9] F. Declercq, A Georgiadis, and H. Rogier, "Wearable aperture-coupled shorted solar patch antenna for remote tracking and monitoring applications", in *Proceedings of the 5th European Conference on Antennas and Propagation (EUCAP)*, 2011, pp. 2992–2996.

[10] G. Orecchini, L. Yang, M. Tentzeris, and L. Roselli, “"Smart shoe": an autonomous inkjet-printed RFID system scavenging walking energy”, in *2011 IEEE Int. Symp. on Antennas and Propagation (APSURSI)*, 2011, pp. 1417 –1420.

[11] N. Shenck and J. Paradiso, “Energy scavenging with shoe-mounted piezoelectrics”, *Micro, IEEE*, vol. 21, no. 3, pp. 30–42, 2001.

[12] W. Y. Toh, Y. K. Tan, W. S. Koh, and L. Siek, “Autonomous wearable sensor nodes with flexible energy harvesting”, *Sensors Journal, IEEE*, vol. 14, no. 7, pp. 2299–2306, 2014.

[13] G. Andia Vera, A Georgiadis, A Collado, and S. Via, “Design of a 2.45 ghz rectenna for electromagnetic (EM) energy scavenging”, in *2010 IEEE Radio and Wireless Symposium (RWS)*, 2010, pp. 61–64.

[14] L. Francioso, C. De Pascali, I Farella, C. Martucci, P. Creti, P. Siciliano, and A Perrone, “Flexible thermoelectric generator for wearable biometric sensors”, in *IEEE Sensors 2010*, 2010, pp. 747–750.

[15] Y. Minami and E. Nakamachi, “Development of enhanced piezoelectric energy harvester induced by human motion”, in *Engineering in Medicine and Biology Society (EMBC), 2012, Annual International Conference of the IEEE*, 2012, pp. 1627–1630.

[16] A Collado and A Georgiadis, “Conformal hybrid solar and electromagnetic (EM) energy harvesting rectenna”, *IEEE Trans. Circuits Syst. I*, vol. 60, no. 8, pp. 2225–2234, 2013.

[17] R. Paradiso and D. De Rossi, “Advances in textile sensing and actuation for e-textile applications”, in *Engineering in Medicine and Biology Society (EMBS), 2008, 30th Annual International Conference of the IEEE*, 2008, pp. 3629–3629.

[18] M. Catrysse, R. Puers, C. Hertleer, L. V. Langenhove, H. van Egmond, and D. Matthys, “Towards the integration of textile sensors in a wireless monitoring suit”, *Sensors and Actuators A: Physical*, vol. 114, pp. 302 –311, 2004, Selected papers from Transducers 03.

[19] T. Seesaard, P. Lorwongtragool, and T. Kerdcharoen, “Wearable electronic nose based on embroidered amine sensors on the fabric substrates”, in *9th International Conference on Electrical Engineering/Electronics, Computer, Telecommunications and Information Technology (ECTI-CON), 2012*, 2012, pp. 1–4.

[20] S. Corbellini, F. Ferraris, and M. Parvis, “A system for monitoring workers’ safety in an unhealthy environment by means of wearable sensors”, in *IEEE Instrumentation and Measurement Technology Conference Proceedings (IMTC), 2008.*, 2008, pp. 951–955.

[21] F. Kelly, L. Meunier, C. Cochrane, and V. Koncar, “Evaluation of solid or liquid phase conducting polymers within a flexible textile electrochromic device”, *Journal of Display Technology*, vol. 9, no. 8, pp. 626–631, 2013.

[22] C. Zysset, N. Munzenrieder, T. Kinkeldei, K. Cherenack, and G. Troster, "Woven active-matrix display", *IEEE Trans. Electron Devices*, vol. 59, no. 3, pp. 721–728, 2012.

[23] T. Tamura, T. Yoshimura, M. Sekine, M. Uchida, and O. Tanaka, "A wearable airbag to prevent fall injuries", *IEEE Trans. Inf. Technol. Biomed.*, vol. 13, no. 6, pp. 910–914, 2009.

[24] B. Huyghe, H. Rogier, J. Vanfleteren, and F. Axisa, "Design and manufacturing of stretchable high-frequency interconnects", *IEEE Trans. Adv. Packag.*, vol. 31, no. 4, pp. 802–808, 2008.

[25] D. Cottet, J. Grzyb, T. Kirstein, and G. Troster, "Electrical characterization of textile transmission lines", *IEEE Trans. Adv. Packag.*, vol. 26, no. 2, pp. 182–190, 2003.

[26] G. Conway and W. Scanlon, "Antennas for over-body-surface communication at 2.45 ghz", *IEEE Trans. Antennas Propag.*, vol. 57, no. 4, pp. 844–855, 2009.

[27] I Locher and G. Troster, "Fundamental building blocks for circuits on textiles", *IEEE Trans. Adv. Packag.*, vol. 30, no. 3, pp. 541–550, 2007.

[28] A. Tronquo, H. Rogier, C. Hertleer, and L. Van Langenhove, "Robust planar textile antenna for wireless body LANs operating in 2.45 GHz ISM band", *Electron. Lett.*, vol. 42, no. 3, pp. 142–143, 2006.

[29] T. Kellomaki, J. Heikkinen, and M. Kivikoski, "Wearable antennas for fm reception", in *First European Conference on Antennas and Propagation (EuCAP), 2006.*, 2006, pp. 1–6.

[30] T. Kennedy, P. Fink, A. Chu, N. Champagne, G. Lin, and M. Khayat, "Body-worn E-Textile antennas: The good, the low-mass, and the conformal", *IEEE Trans. Antennas Propag.*, vol. 57, no. 4, pp. 910–918, 2009.

[31] E. Kaivanto, M. Berg, E. Salonen, and P. de Maagt, "Wearable circularly polarized antenna for personal satellite communication and navigation", *IEEE Trans. Antennas Propag.*, vol. 59, no. 12, pp. 4490 –4496, 2011.

[32] A. Dierck, H. Rogier, and F. Declercq, "A wearable active antenna for global positioning system and satellite phone", *IEEE Trans. Antennas Propag.*, vol. 61, no. 2, pp. 532–538, 2013.

[33] A. Dierck, T. De Keulenaer, F. Declercq, and H. Rogier, "A wearable active GPS antenna for application in smart textiles", eng, in *Proc. of the 32nd ESA Antenna Workshop on Antennas for Space Applications*, Noordwijk, the Netherlands, 2010.

[34] B. Gupta, S. Sankaralingam, and S. Dhar, "Development of wearable and implantable antennas in the last decade: A review", in *2010 Mediterranean Microwave Symp. (MMS)*, 2010, pp. 251 –267.

[35] P. G. Elliot, E. N. Rosario, B. Rama Rao, R. J. Davis, and N. M. Marcus, "E-textile microstrip patch antennas for gps", in *Position Location and Navigation Symposium (PLANS), 2012 IEEE/ION*, 2012, pp. 66–73.

[36] S. Agneessens, P. Van Torre, E. Tanghe, G. Vermeeren, W. Joseph, and H. Rogier, "On-body wearable repeater as a data link relay for in-body wireless implants", *IEEE Antennas Wireless Propag. Lett.*, vol. 11, pp. 1714–1717, 2012.

[37] M. L. Scarpello, D. Kurup, H. Rogier, D. Vande Ginste, F. Axisa, J. Vanfleteren, W. Joseph, L. Martens, and G. Vermeeren, "Design of an Implantable Slot Dipole Conformal Flexible Antenna for Biomedical Applications", *IEEE Trans. Antennas Propag.*, vol. 59, no. 10, 3556–3564, 2011.

[38] F.-J. Huang, C.-M. Lee, C.-L. Chang, L.-K. Chen, T.-C. Yo, and C.-H. Luo, "Rectenna application of miniaturized implantable antenna design for triple-band biotelemetry communication", *IEEE Trans. Antennas Propag.*, vol. 59, no. 7, pp. 2646–2653, 2011.

[39] C. Hertleer, H. Rogier, L. Vallozzi, and L. Van Langenhove, "A textile antenna for off-body communication integrated into protective clothing for firefighters", *IEEE Trans. Antennas Propag.*, vol. 57, no. 4, pp. 919–925, 2009.

[40] R. Paradiso, G. Loriga, and N. Taccini, "A wearable health care system based on knitted integrated sensors", *IEEE Trans. Inf. Technol. Biomed.*, vol. 9, no. 3, pp. 337–344, 2005.

[41] J. Lilja, V. Pynttari, T. Kaija, R. Makinen, E. Halonen, H. Sillanpaa, J. Heikkinen, M. Mantysalo, P. Salonen, and P. de Maagt, "Body-worn antennas making a splash: lifejacket-integrated antennas for global search and rescue satellite system", *IEEE Antennas Propag. Mag.*, vol. 55, no. 2, pp. 324–341, 2013.

[42] A. Serra, P. Nepa, and G. Manara, "A wearable two-antenna system on a life jacket for cospas-sarsat personal locator beacons", *IEEE Trans. Antennas Propag.*, vol. 60, no. 2, pp. 1035–1042, 2012.

[43] G. A. Deschamps, "Microstrip Microwave Antennas", in *3rd USAF Symposium on Antennas*, 1953.

[44] R. Garg, P. Bhartia, I. Bahl, and A. Ittipiboon, *Microstrip Antenna Design Handbook*. Artech House, 2001.

[45] C. Hertleer, A. Tronquo, H. Rogier, L. Vallozzi, and L. Van Langenhove, "Aperture-coupled patch antenna for integration into wearable textile systems", *IEEE Antennas Wireless Propag. Lett.*, vol. 6, pp. 392–395, 2007.

[46] P. Salonen, Y. Rahmat-Samii, and M. Kivikoski, "Wearable antennas in the vicinity of human body", in *2004 IEEE Antennas and Propagation Society Int. Symp.*, IEEE, vol. 1, 2004, pp. 467–470.

[47] G. Kumar and K. Ray, *Broadband microstrip antennas*. Artech House, 2002.

[48] H. Rogier, *Antennas and Propagation*. Course notes, 2014.

[49] D. B. Davidson, *Computational electromagnetics for RF and microwave engineering*. Cambridge University Press, 2005.

[50] H. Rogier, *Circuit- en EMC-concepten - Deel 1: circuittheorie*. Course notes, 2014.

[51] J. Wang, "Antennas for Global Navigation Satellite System (GNSS)", *Proceedings of the IEEE*, vol. 100, no. 7, pp. 2349–2355, 2012.

2

A wearable active antenna for global positioning system and satellite phone

Arnaut Dierck, Frederick Declercq, and Hendrik Rogier

Based on the article published in IEEE Transactions on Antennas and Propagation

★ ★ ★

A wearable multiband circularly polarized active antenna is presented for use in Global Positioning System and Iridium satellite phone applications. The square patch antenna is constructed using flexible foam and fabric substrates and conductors etched on thin copper-on-polyimide films. The feed substrate integrates a compact low-noise amplifier chip directly underneath the antenna patch. The antenna performance is studied under bending conditions and in the presence of a human body. The active antenna exhibits a gain higher than 25 dBi and a 3 dB axial ratio bandwidth exceeding 183 MHz in free-space conditions and is robust to bending and on-body placement.

2.1 Introduction

In the recent years, interest in wearable electronics has boomed. By using suitable materials such as textiles and foams, the electronic systems can be unobtrusively integrated into clothing. These so-called smart textile systems can be deployed in a variety of fields, and have been shown to function desirably in garments ranging

from sporting apparel to public service outfits [1]–[9]. A comfortable integration into clothing, however, causes some design challenges in order to guarantee optimal performance of the active circuits and antennas present in the wearable electronic systems. Textile/foam substrates introduce additional losses, and, while flexibility is necessary for conformal integration into clothing, it makes the antennas susceptible to bending, which might affect their performance. Also, proximity to the body and other electronic devices must be taken into account.

Key in these designs is to maintain a high wearability and, at the same time, to provide a highly reliable communications link. In this respect, miniaturization of the on-body electronic system is vital, on the one hand making the electronic circuitry and antennas less bulky and in the meanwhile improving wearability, and, on the other hand, combining functionalities of different circuits/antennas into more compact electronic units, reducing potential weak links between these devices. When looking at the antenna side of things, it is thus advisable to replace multiple antennas by a single, broad band radiator. Electronics required for the different functionalities serviced by this antenna can then also be centralized and reduced in size. From this point of view, we investigated the possibility of integrating Global Positioning System (GPS) and Iridium satellite phone capabilities into one active antenna. The active part of the antenna consists of a low-noise amplifier (LNA) chip amplifying the incoming signal. This enhances both GPS and Iridium signal reception.

Performance studies of wearable antennas under different adverse conditions were already reported. In [10], [11] the influence of antenna bending and crumpling is evaluated, which affects the antenna impedance bandwidth and causes shifts in resonance frequency. In [12], effects of moisture absorption by the textile substrate, depending on the relative humidity, were studied. Increased humidity raises the relative permittivity and loss tangent of the substrate, in this way changing the resonant frequency and bandwidth of the antenna. When placed on-body [13], [14], antenna radiation pattern distortion, resonant frequency shift and bandwidth changes are measured. Several circularly polarized wearable patch antennas [15] for GPS [16], [17] and GPS/Iridium [18] were reported in literature. These antennas are inset [15] or probe [16]–[18] fed and make use of asymmetries in the patch to excite circular polarization. This provides good matching and axial ratio characteristics, albeit in a limited frequency range. Due to the above-mentioned challenges present in wearable antenna design, resonance frequency and bandwidth can shift, resulting in reduced performance. Also, the probe feed presents a weakness when the antenna is exposed to stress from bending, stretching or compression, whereas the inset feed necessitates integration of additional (active) components on the radiating side of the antenna, making them vulnerable to interference. This can be circumvented by using a probe to connect the inset-fed antenna to components on the antenna backside, leading however to the aforementioned probe-fed related drawbacks. While the cited publications present antennas with sufficient bandwidth to cover both GPS L1 and Iridium bands, the nature of the techniques used to realize circular polarization leads to circular polarization in

a small frequency range that is insufficient to cover both GPS and Iridium bands (e.g. [17]: < 35 MHz centered around the GPS L1 frequency; [18]: ~ 25 MHz centered around the Iridium frequency). By using a hybrid coupler, it is our aim to increase the bandwidth in which the antenna is circularly polarized. The 183 MHz wide bandwidth in which the antenna in our contribution is circularly polarized with an AR < 3 dB clearly demonstrates this feature. Moreover, the extra bandwidth provided by the hybrid coupler ensures robustness against fabrication tolerances. For example, in [16], the total impedance bandwidth is indeed large enough to cover both GPS and Iridium frequencies. However, due to fabrication tolerances and inaccuracies in the measured electromagnetic properties of the used materials, the fabricated antenna bandwidth differs from the simulated bandwidth, leading to an $|S_{11}|$ exceeding -10 dB at the GPS frequency (and even worse under certain bending conditions).

In this chapter, we present a robust active wearable circularly polarized GPS antenna. We propose an aperture fed topology [1], [2], thereby eliminating probes through the antenna substrate and increasing robustness and flexibility. Circular polarization is achieved by using a discrete hybrid coupler, which provides a wideband circular polarization to ensure satisfactory performance at GPS and Iridium frequencies under bending and on-body conditions. To ensure proper signal reception, an LNA chip is integrated onto the antenna feed plane, providing a high level of integration to increase overall on-body system compactness and ruggedness, while amplifying the received signal for further processing. In this chapter, to the authors' knowledge for the first time in literature, we present an active wearable antenna that has a chip LNA and discrete hybrid coupler directly integrated onto the textile antenna. Moreover, this topology results in an impedance bandwidth of 340 MHz and a 3 dB axial ratio bandwidth of 183 MHz, which is much wider than currently found in literature for wearable antennas. Thereby, the new antenna provides stable coverage of both GPS and Iridium bands, when deployed on body and when subjecting the antenna to different bending conditions. The single-band active wearable GPS antenna discussed in [1], [2], which bears some resemblance in terms of topology to the currently presented design, but which made use of discrete components to implement the LNA, only partly satisfied the specifications for the GPS band. In particular, the discrete element LNA did not fulfill the matching requirements at the GPS frequency ($|S_{11}| < -10$ dB). Moreover, the many discrete components formed weak links in the design that easily break when bending the antenna and the large footprint of the active circuit reduced the breathability of the design. Therefore, it was replaced by a more compact circuit based on an LNA chip with only three additional discrete components. This topology was then optimized to provide appropriate and robust matching at the desired frequencies, even when bending the antenna and deploying it on the human body. In the following text, we will first discuss the active antenna topology and design in Section 2.2. The design evaluation is outlined in Section 2.3.

2.2 Active antenna design and topology

2.2.1 Active antenna design specifications

The active antenna is designed to meet the requirements to adequately receive GPS and Iridium signals. First, this necessitates an antenna able to cover the 2.046 MHz wide GPS L1-band centered around 1.575 GHz and the Iridium spectrum ranging from 1.616 GHz to 1.6265 GHz [19]. Second, this calls for an antenna with a right-handed circularly polarized radiation characteristic in the aforementioned frequency range. The circular polarization is quantified by means of the axial ratio, and a 3 dB upper limit is set as a circular polarization figure of merit. Moreover, the antenna should be planar and low-profile to facilitate integration into clothing. To account for bending and body influence on the antenna bandwidth, attention is paid to ensure proper functionality under these adverse conditions. To minimize the influence of the body on the antenna, a topology radiating away from the body is preferred.

2.2.2 Active antenna topology

To provide a low-profile planar antenna that can be easily integrated into clothing, a microstrip patch antenna topology is selected. This ensures radiation away from the body in a semi-hemisphere, allowing sufficient beam width for a good coverage. As depicted in Fig. 2.1, the microstrip patch is aperture coupled to two perpendicular feed lines through rectangular slots in the ground plane. The ground plane effectively shields the antenna patch from the active circuitry, integrated on the feed plane, and from the human body. The feed lines are connected to a discrete quadrature hybrid coupler. The coupler that was used in the design is the Anaren XC1400P-03S [20]. This coupler provides a fixed 90 degree phase difference between the feedlines, exciting circular polarization. At the other end, this coupler is connected to an LNA chip and a 50 Ω termination. To generate circular polarization, a hybrid coupler was preferred over other techniques, such as irregularities in the patch or feed geometry, to provide a broad band and robust circular polarization. This reduces the sensitivity of the antenna to fabrication tolerances and to frequency shifts caused by antenna bending. A discrete component was chosen instead of a microstrip realization to reduce the footprint size, leaving place for the LNA chip to be integrated under the antenna patch while also reducing the vulnerability of this component to influences of antenna bending. The antenna layout is symmetric about the plane perpendicular to the xy-plane forming a +45° angle with the x-axis. For the fabrication, flexible materials were used to ensure the wearability of the design. The conducting surfaces were etched on a copper-on-polyimide (PI) film, in which a 9 µm copper layer is laminated onto a 25 µm polyimide sheet. The antenna substrate consists of a polyurethane foam layer (typically found in the shoulder pads of protective garments) with a thickness of 7.25 mm. This height was chosen to guarantee wideband performance of the patch antenna while conserving a relatively simple feed structure in order

Table 2.1: Electromagnetic properties of the active antenna materials.

Substrate	ϵ_r	tan δ	Height	Materials
Antenna substrate	1.25	0.02	7.25 mm	Polyurethane foam
LNA substrate	1.775	0.02	450 µm	Aramid textile fabric + polyimide layer

Table 2.2: Antenna dimensions.

Parameter	Value [mm]
L	70.85
L_{ground}	100
L_{slot}	30
W_{slot}	5
L_{stub}	18
W_{stub}	1.62
L_{elbow}	2.17

to guarantee an easy-to-fabricate, robust design. For the feed substrate, 400 µm thick aramid fabric is used, a textile typically used as an outer layer in protective garments. This layer is kept thin to minimize radiation from the feed circuit. The different layers were glued together by means of thermally activated adhesive sheets. The electromagnetic properties of the substrates are listed in Table 2.1. The listed height of 450 µm of the LNA substrate includes the thickness of the polyimide film of the feed and ground plane. We fabricated two versions of the antenna, one passive, the other one active. The active antenna comprises a discrete Maxim MAX2659 LNA chip [21], which provides high gain and low noise figure in a small package that can be compactly integrated into the antenna. The layout of the chip LNA is depicted in Fig. 2.2. This layout implements a simple capacitor-inductor input matching network, formed by capacitor C_1 (470 pF) and inductor L_1 (6.8 nH), to connect to the 50 Ω discrete hybrid coupler. The DC feed voltage is decoupled through capacitor C_2 (33 nF). The 50 Ω microstrip lines (1.62 mm wide) in the layout are kept short to minimize losses. The LNA output is interfaced to the receiving equipment through a low-profile UFL-connector.

2.2.3 Active Antenna Modeling

An initial design based on the aforementioned antenna topology was modeled in ADS Momentum. This design was subsequently tuned and optimized from within the ADS schematic editor. Since the discrete hybrid coupler is a 50 Ω matched component, the passive radiator and the LNA are designed to a 50 Ω match. The optimized antenna dimensions are listed in Table 2.2.

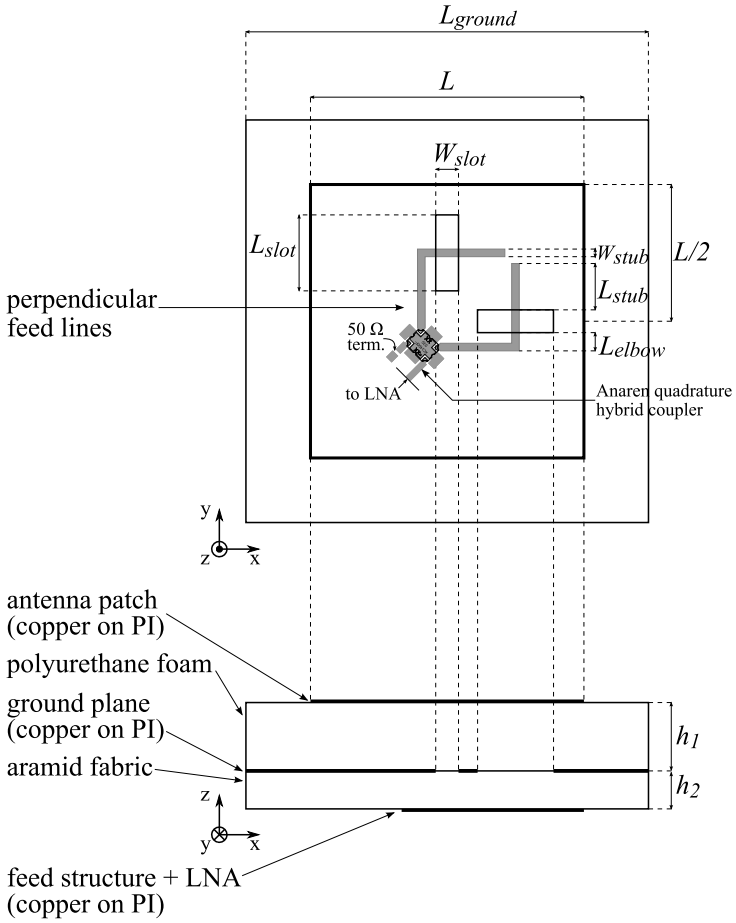

Figure 2.1: Wearable GPS/Iridium active antenna topology.

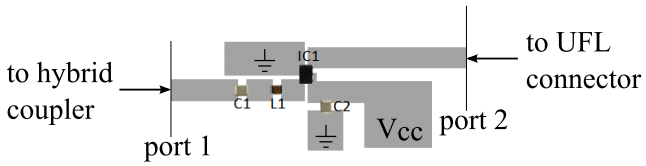

Figure 2.2: Layout of LNA with chip amplifier.

2.3 Evaluation

In this section, the measurement results are discussed and compared to the simulations. First, we elaborate on the LNA measurements. Second, we treat the antenna

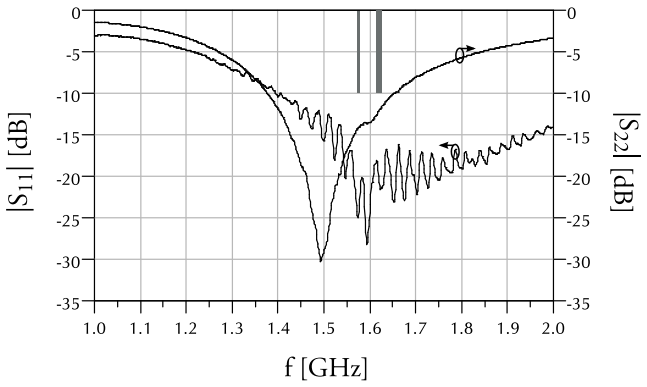

Figure 2.3: Measured $|S_{11}|$ and $|S_{22}|$ of chip LNA.

measurements.

2.3.1 LNA evaluation

Using the Agilent Technologies N5241A PNA-X Vector Network Analyzer, the scattering parameters and noise performance of the LNA were measured. These separate LNA measurements were carried out in order to validate the performance of the LNA circuit when implemented on a textile substrate. The LNA was connected to a 3 V source. The noise measurement was performed using the source-corrected noise measurement technique embedded in the PNA-X system [22]. In Fig. 2.3, the measured $|S_{11}|$ and $|S_{22}|$ of the LNA are depicted. We obtain a good in- and output match in the desired frequency range. In Fig. 2.4, the measured $|S_{21}|$ and $|S_{12}|$ are shown. A gain larger than 18 dB is observed in the GPS and Iridium frequency ranges. In Fig. 2.5, it is seen that the measured noise figure remains below 1.4 dB in the desired frequency range.

2.3.2 Antenna evaluation

The passive and active antennas were measured in an anechoic chamber by means of the N5241A PNA-X VNA. A photograph of the complete active antenna prototype is depicted in Fig. 2.6. First, conventional free-space antenna measurements, without influence of bending or human proximity, were performed. Next, the antennas were also studied while subjected to bending in free-space and when integrated into a rescue worker jacket at different locations. To study the influence of free-space bending, both antennas were attached to a plastic cylinder with a 5 cm radius of curvature to emulate the geometry of a human arm. In this way, the antenna was bent in four directions according to the axes displayed in Fig. 2.1: along the x-axis, y-axis, and $y \pm 45°$ axes. This is depicted in Fig. 2.7(a). For the on-body measurements, the antenna was placed in the rear section of a firefighter

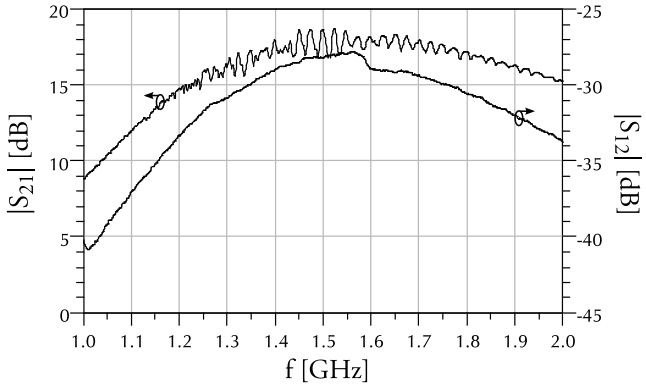

Figure 2.4: Measured $|S_{21}|$ and $|S_{12}|$ of chip LNA.

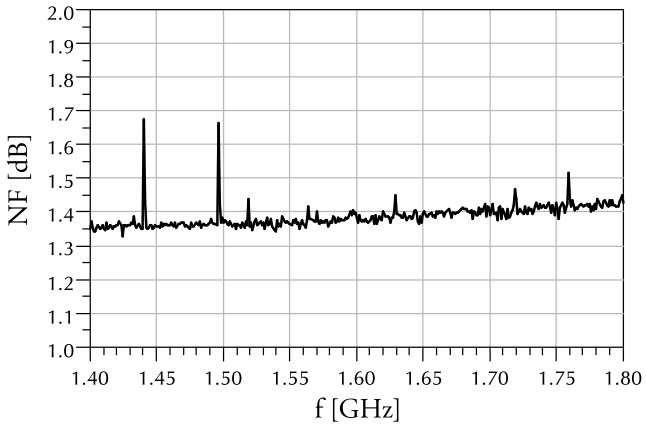

Figure 2.5: Measured noise figure of chip LNA.

jacket and in the upper part of the sleeve, behind the outer shell fabric and the thermal and moisture barrier. In the rear section, the antenna was not subjected to any bending. In the sleeve, the antenna was subjected to bending along the upper arm, following the directions depicted in Fig. 2.7(a). The circumference of the upper arm is 20 cm, corresponding to a radius of 3.2 cm. The positions of the antenna integrated in the firefighter jacket are depicted in Fig. 2.7(b). This jacket was worn by a male of average height and weight. To power the active antenna, it was connected to a portable battery-operated adjustable power supply, delivering 3 V. First, we treat the passive antenna, second the active antenna.

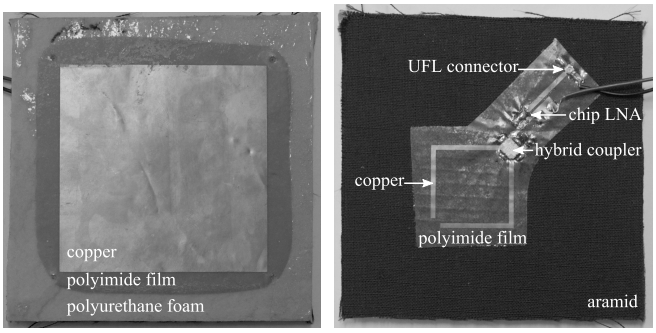

(a) (b)

Figure 2.6: Photograph of active antenna prototype top (a) and bottom (b).

Passive antenna evaluation

The radiation pattern of the passive antenna in free-space is depicted in Fig. 2.8, together with the active antenna radiation pattern. The properties of the radiation pattern are listed in Table 2.3. The measured $|S_{11}|$, as a function of frequency, is displayed in Fig. 2.9 for the passive antenna under free-space and on-body conditions, both in planar and bent state. The $|S_{11}|$ in free space is lower than -10 dB from 1.512 GHz to 1.7 GHz and beyond. Data for frequencies exceeding 1.7 GHz were not measured during the radiation pattern measurements, since the standard gain horn that was used is not calibrated for measurements in this higher frequency range. A separate measurement of the antenna $|S_{11}|$ over a larger frequency range revealed matching up to 1.8 GHz, resulting in an almost 300 MHz matching bandwidth. Here, the influence of the discrete hybrid coupler, which is matched to 50 Ω, can clearly be seen. When subjecting the antenna to proximity of the body and to different bending conditions, the matching bandwidth does not significantly change. The hybrid coupler provides a robust, broad band 50 Ω match. The measured antenna gain is depicted in Fig. 2.10. In free space, it reaches a maximum value of 5.5 dBi at 1.619 GHz. It remains within 1 dB of the maximum value from 1.556 to 1.662 GHz, resulting in a 1 dB gain bandwidth of 106 MHz. In the different measurement scenarios, this 1 dB gain bandwidth is not significantly influenced, but maximum gain value and frequency are altered. The largest decrease in gain occurs when bending the antenna along the y-axis on the arm, resulting in a gain that is about 2.5 dB lower than in free-space conditions. The RHCP and LHCP gains are plotted in Fig. 2.11. We see that the RHCP gain is fairly insensitive to the different conditions imposed on the antenna. The LHCP gain, however, shows significant variations. In all scenarios, for GPS and Iridium frequencies, the RHCP gain remains at least 5.595 dB above the LHCP gain.

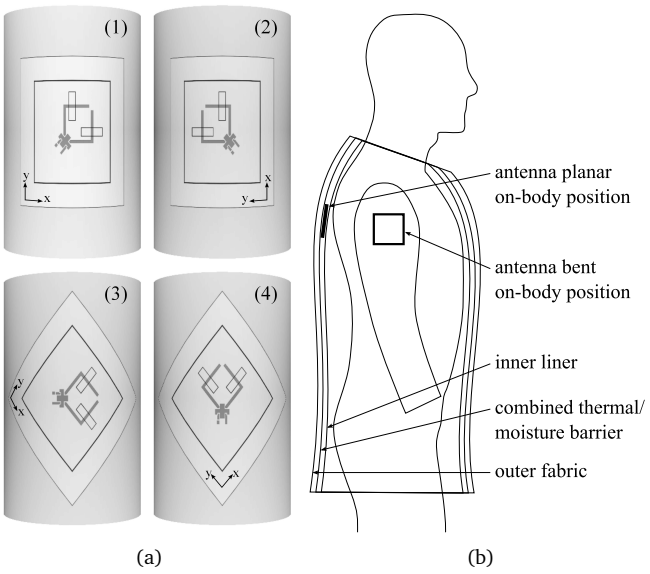

Figure 2.7: (a): different bending directions of the antenna ((1) along the x-axis; (2) along the y-axis; (3) along the $y + 45°$-axis; (4) along the $y - 45°$-axis); (b): position of the antenna integrated in the firefighter jacket.

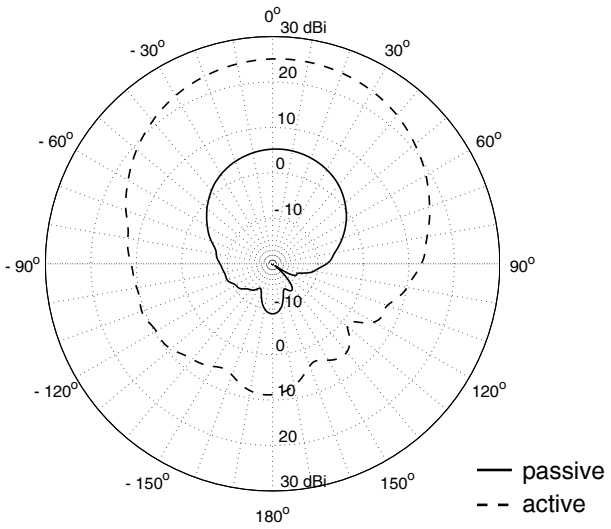

Figure 2.8: Measured radiation pattern of passive and active antenna at 1.6 GHz in the xz-plane.

Table 2.3: Axial ratio data of the different antennas measured at 1.6 GHz

Antenna	Gain [dBi]	3 dB beam width	Axial ratio [dB]	3 dB AR beam width
Passive	5.2	66°	2.476	78°
Active	25.1	68°	1.866	106°

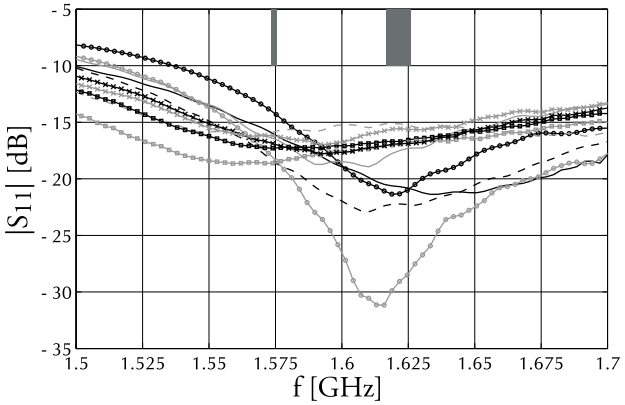

Figure 2.9: Measured $|S_{11}|$ of passive antenna (— planar; - - on-body; -o- bent x; — bent y; - - bent y + 45°; -o- bent y − 45°; -□- arm x; -□- arm y; -×- arm y + 45°; -×- arm y − 45°).

Active antenna evaluation

The free-space radiation pattern of the active antenna is depicted in Fig. 2.8. It exhibits a similar shape as the passive antenna radiation pattern, of course, providing a higher gain thanks to the integrated LNA. The active antenna forward gain is about 20 dB higher than the passive antenna forward gain. This is a little bit higher than what could be expected from the measured LNA gain of 18 dB. Fabrication tolerances could, however, lead to slight variations between the standalone LNA and the LNA integrated into the active antenna. The properties of the active antenna radiation pattern are listed in Table 2.3. Although the antenna radiator topology is the same for the passive and active antenna, the axial ratio performance also slightly differs. The axial ratio is dependent on the alignment of the feed lines to the slots and the patch. The alignment of the prototypes is performed by hand, leading to variations. The measured $|S_{11}|$ is displayed in Fig. 2.12, as a function of frequency, for the active antenna under free-space and on-body conditions, both in planar and bent state. Compared to the passive antenna's $|S_{11}|$, the active antenna's $|S_{11}|$ exhibits a downward shift of the matching frequency. As the active

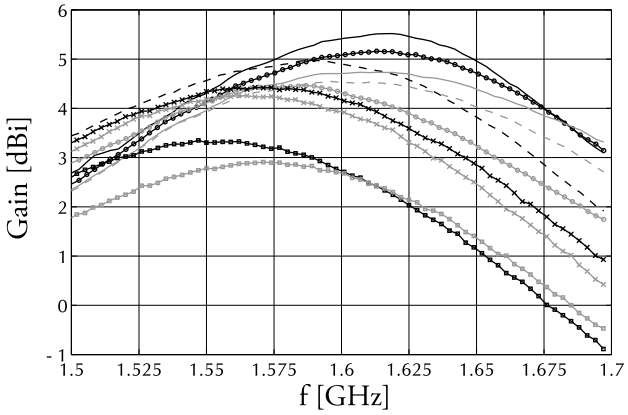

Figure 2.10: Measured gain of passive antenna (— planar; - - on-body; -o- bent x; — bent y; - - bent y + 45°; -o- bent y − 45°; -□- arm x; -□- arm y; -×- arm y + 45°; -×- arm y − 45°).

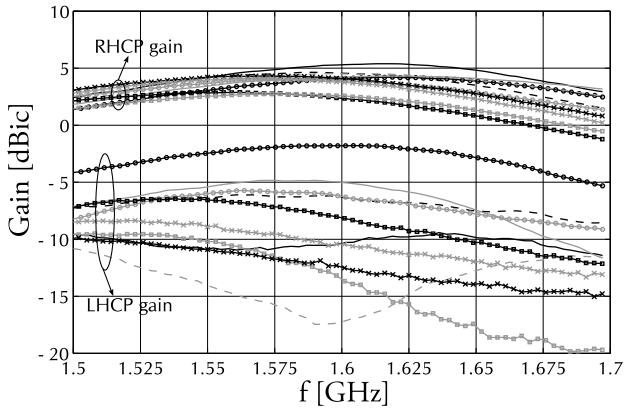

Figure 2.11: Measured RHCP and LHCP gain of passive antenna (— planar; - - on-body; -o- bent x; — bent y; - - bent y + 45°; -o- bent y − 45°; -□- arm x; -□- arm y; -×- arm y + 45°; -×- arm y − 45°).

antenna accommodates an LNA chip with a matching network exhibiting a different $|S_{11}|$ characteristic than the hybrid coupler, this was to be expected. It must be noted that, under all circumstances, the $|S_{11}|$ of the active antenna remains lower than -13 dB for the Iridium frequencies. However, it would be safer to move the center frequency of the matching upwards. This was not done in order to minimize the amount of additional discrete components. The $|S_{11}|$ is a characteristic of the matching network which is built into the chip LNA. Adding capacitors and/or coils can indeed change this characteristic, but would make the LNA layout more

complex. The $|S_{11}|$ in free-space is lower than -10 dB over the complete displayed frequency range. A separate measurement of the antenna revealed that the $|S_{11}|$ is lower than -10 dB from 1.36 GHz to 1.7 GHz, resulting in a matching bandwidth of 340 MHz. Subjecting the antenna to proximity of the body and to different bending conditions does not significantly change the matching bandwidth. The hybrid coupler and LNA provide a robust, broad band 50 Ω match. The measured antenna gain is depicted in Fig. 2.13. In free-space, it reaches a maximum value of 25.43 dBi at 1.625 GHz. It stays within 1 dB of the maximum value from 1.558 to 1.677 GHz, resulting in a 1 dB gain bandwidth of 119 MHz. This value is not significantly altered in the different measurement setups, however the maximum gain value and frequency change under influence of bending and on-body placement. The largest gain degradation occurs when bending the antenna on the arm along the y-axis. In Fig. 2.14, the measured RHCP and LHCP gain are depicted. Again, the RHCP gain is fairly insensitive to the different conditions imposed on the antenna, whereas the LHCP gain exhibits larger variations. For GPS and Iridium frequencies, the RHCP gain remains at least 10.44 dB higher than the LHCP gain. In Fig. 2.15, the measured axial ratio of the active antenna in free-space, on-body and bent positions is plotted as a function of frequency. For the free-space case, the axial ratio is lower than 3 dB for frequencies starting from 1.517 GHz and extending beyond the measurement upper limit of 1.7 GHz, resulting in a 3 dB axial ratio bandwidth of over 183 MHz. When bent in free-space, the axial ratio exceeds 3 dB for most cases, though, with exception of the antenna bent along $y - 45°$, the axial ratio never exceeds 5 dB for the GPS and Iridium frequencies. It must be noted that this kind of bending represents a worst case scenario, which would only occur if the antenna was placed attached directly onto the human arm. When implemented in the lining of a jacket, the observed bending will be less severe. When placed on-body without bending, the axial ratio shifts downwards, resulting in a 3 dB axial ratio bandwidth larger than 200 MHz. When placed on a human arm, so that the antenna is subjected to both body presence and bending, the axial ratio stays below 3 dB for two out of the four bending directions. In terms of on-body axial ratio performance, it is optimal to place this antenna so that bending occurs along the x or $y + 45°$-axis.

2.4 Conclusion

In this chapter, we discussed the design of a combined GPS and Iridium active antenna. The antenna was constructed using flexible, wearable materials. Passive and active antennas were prototyped. The active receive antenna contains an LNA directly integrated on the antenna backside. Both antennas are robustly matched over a broad frequency range under bending and on-body conditions. The discrete hybrid coupler allows circular polarization over a wide frequency range. The active antenna realizes a gain larger than 25 dBi in a 1 dB gain bandwidth of 119 MHz. Circular polarization is ensured in a wide frequency range starting at 1.517 GHz and extending beyond 1.7 GHz in unbent state. When bent in free-

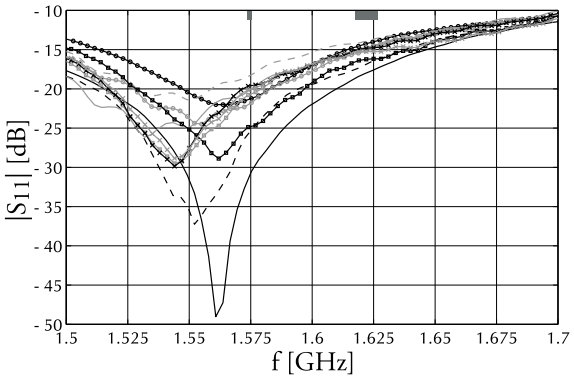

Figure 2.12: Measured $|S_{11}|$ of active antenna (— planar; - - on-body; -o- bent x; — bent y; - - bent $y + 45°$; -o- bent $y - 45°$; -□- arm x; -□- arm y; -×- arm $y + 45°$; -×- arm $y - 45°$).

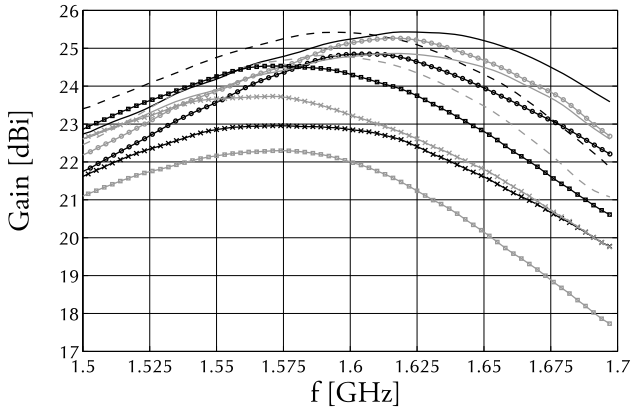

Figure 2.13: Measured gain of active antenna (— planar; - - on-body; -o- bent x; — bent y; - - bent $y + 45°$; -o- bent $y - 45°$; -□- arm x; -□- arm y; -×- arm $y + 45°$; -×- arm $y - 45°$).

space and on-body, the antenna's axial ratio remains lower than 5 dB for GPS and Iridium frequencies, except for the antenna bent along $y - 45°$, whose axial ratio exceeds 5 dB for Iridium frequencies. For the antenna placed on-body, the planar positions and the x and $y + 45°$ bending positions result in an axial ratio which remains lower than 3 dB. Each of these positions provides a sufficiently wide axial ratio bandwidth for proper GPS and Iridium reception. In the future, the possibility to coat the antenna with a breathable, water-resistant TPU coating [23] will be examined, increasing robustness by encapsulating the discrete components and solder joints, and at the same time providing an effective waterproof cover to withstand cleaning and washing. Moreover, the accuracy of the fabrication and

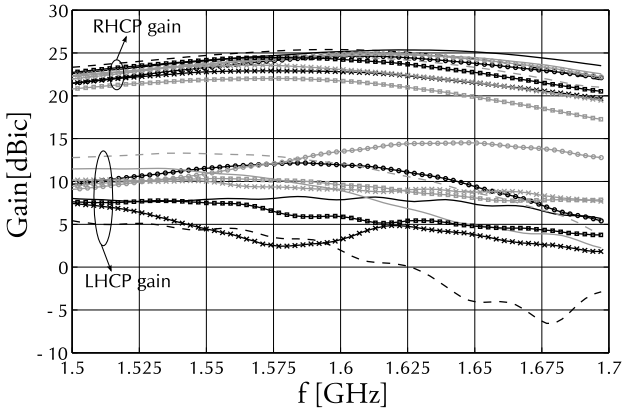

Figure 2.14: Measured RHCP and LHCP gain of active antenna (— planar; - - on-body; -o- bent x; — bent y; - - bent y + 45°; -o- bent y − 45°; -□- arm x; -□- arm y; -×- arm y + 45°; -×- arm y − 45°).

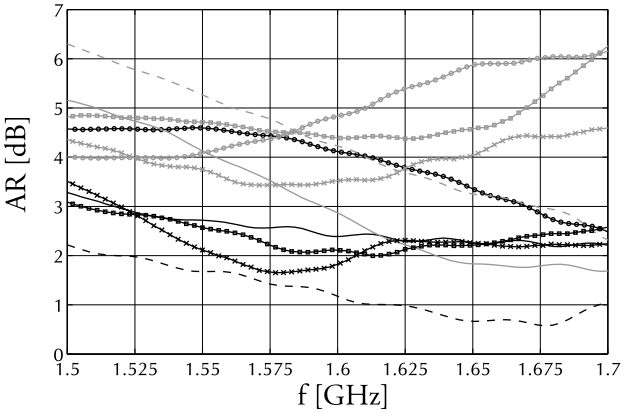

Figure 2.15: Measured axial ratio of active antenna (— planar; - - on-body; -o- bent x; — bent y; - - bent y + 45°; -o- bent y − 45°; -□- arm x; -□- arm y; -×- arm y + 45°; -×- arm y − 45°).

alignment of the conductive structures will be augmented by using a laser powered cutting/alignment device, in this way providing a more consistent axial ratio performance in different prototypes.

References

[1] A. Dierck, T. De Keulenaer, F. Declercq, and H. Rogier, “A wearable active GPS antenna for application in smart textiles”, eng, in *Proc. of the 32nd ESA Antenna Workshop on Antennas for Space Applications*, Noordwijk, the Netherlands, 2010.

[2] A. Dierck, F. Declercq, and H. Rogier, “Review of active textile antenna co-design and optimization strategies”, in *2011 IEEE Int. Conference on RFID-Technologies and Applications (RFID-TA)*, 2011, pp. 194 –201.

[3] G. Orecchini, L. Yang, M. Tentzeris, and L. Roselli, “"Smart shoe": an autonomous inkjet-printed RFID system scavenging walking energy”, in *2011 IEEE Int. Symp. on Antennas and Propagation (APSURSI)*, 2011, pp. 1417 –1420.

[4] B. Gupta, S. Sankaralingam, and S. Dhar, “Development of wearable and implantable antennas in the last decade: A review”, in *2010 Mediterranean Microwave Symp. (MMS)*, 2010, pp. 251 –267.

[5] L. Vallozzi, W. Vandendriessche, H. Rogier, C. Hertleer, and M. L. Scarpello, “Wearable textile GPS antenna for integration in protective garments”, eng, in *Proc. of the Fourth European Conference on Antennas and Propagation (EuCAP), 2010*, Barcelona, Spain: IEEE, 2010, p. 4.

[6] L. Vallozzi, P. Van Torre, C. Hertleer, H. Rogier, M. Moeneclaey, and J. Verhaevert, “Wireless communication for firefighters using dual-polarized textile antennas integrated in their garment”, *IEEE Trans. Antennas Propag.*, vol. 58, no. 4, pp. 1357–1368, 2010.

[7] L. Vallozzi, H. Rogier, and C. Hertleer, “Dual polarized textile patch antenna for integration into protective garments”, *IEEE Antennas Wireless Propag. Lett.*, vol. 7, pp. 440–443, 2008.

[8] A. Tronquo, H. Rogier, C. Hertleer, and L. Van Langenhove, “Robust planar textile antenna for wireless body LANs operating in 2.45 GHz ISM band”, *Electron. Lett.*, vol. 42, no. 3, pp. 142–143, 2006.

[9] T. Kennedy, P. Fink, A. Chu, N. Champagne, G. Lin, and M. Khayat, “Body-worn E-Textile antennas: The good, the low-mass, and the conformal”, *IEEE Trans. Antennas Propag.*, vol. 57, no. 4, pp. 910–918, 2009.

[10] Q. Bai and R. Langley, “Crumpling of PIFA textile antenna”, *IEEE Trans. Antennas Propag.*, vol. 60, no. 1, pp. 63 –70, Jan. 2012.

[11] P. Salonen and Y. Rahmat-Samii, “Textile antennas: Effects of antenna bending on input matching and impedance bandwidth”, *IEEE Aerosp. Electron. Syst. Mag.*, vol. 22, no. 3, pp. 10–14, 2007.

[12] C. Hertleer, A. Van Laere, H. Rogier, and L. Van Langenhove, "Influence of relative humidity on textile antenna performance", *Textile Research Journal*, vol. 80, no. 2, p. 177, 2010.

[13] C. Hertleer, A. Tronquo, H. Rogier, L. Vallozzi, and L. Van Langenhove, "Aperture-coupled patch antenna for integration into wearable textile systems", *IEEE Antennas Wireless Propag. Lett.*, vol. 6, pp. 392–395, 2007.

[14] P. Salonen, Y. Rahmat-Samii, and M. Kivikoski, "Wearable antennas in the vicinity of human body", in *2004 IEEE Antennas and Propagation Society Int. Symp.*, IEEE, vol. 1, 2004, pp. 467–470.

[15] I. Locher, M. Klemm, T. Kirstein, and G. Tröster, "Design and Characterization of Purely Textile Patch Antennas", *IEEE Trans. Adv. Packag.*, vol. 29, no. 4, pp. 777 –788, 2006.

[16] P. Salonen, Y. Rahmat-Samii, M. Schaffrath, and M. Kivikoski, "Effect of textile materials on wearable antenna performance: a case study of GPS antennas", in *2004 IEEE Antennas and Propagation Society Int. Symp.*, vol. 1, 2004, 459 –462 Vol.1.

[17] L. Vallozzi, W. Vandendriessche, H. Rogier, C. Hertleer, and M. Scarpello, "Design of a protective garment GPS antenna", *Microwave and optical technology lett.*, vol. 51, no. 6, pp. 1504–1508, 2009.

[18] E. Kaivanto, M. Berg, E. Salonen, and P. de Maagt, "Wearable circularly polarized antenna for personal satellite communication and navigation", *IEEE Trans. Antennas Propag.*, vol. 59, no. 12, pp. 4490 –4496, 2011.

[19] S. Pratt, R. Raines, C. Fossa, and M. Temple, "An operational and performance overview of the iridium low earth orbit satellite system", *IEEE Commun. Surveys Tuts.*, vol. 2, no. 2, pp. 2–10, 1999.

[20] Anaren, *Anaren XC1400P-03S datasheet*.

[21] Maxim Integrated Products, *GPS/GNSS Low Noise Amplifier, MAX2659 data sheet*, 2011.

[22] K. Wong. (2008). Advancements in Noise Measurement, [Online]. Available: `http://www.ewh.ieee.org/r6/scv/ims/archives/May2008Wong.pdf`.

[23] M. L. Scarpello, I. Kazani, C. Hertleer, H. Rogier, and D. Vande Ginste, "Stability and efficiency of screen-printed wearable and washable antennas", *IEEE Antennas Wireless Propag. Lett.*, vol. 11, pp. 838 –841, 2012.

3

Active textile antennas in professional garments for sensing, localization and communication

Arnaut Dierck, Sam Agneessens, Frederick Declercq, Bart Spinnewyn, Gert-Jan Stockman, Patrick Van Torre, Luigi Vallozzi, Dries Vande Ginste, Thomas Vervust, Jan Vanfleteren and Hendrik Rogier

Based on the article published in International Journal of Microwave and Wireless Technologies

★★★

New wireless wearable monitoring systems integrated in professional garments require a high degree of reliability and autonomy. Active textile antenna systems may serve as platforms for body-centric sensing, localization and wireless communication systems, in the meanwhile being comfortable and invisible to the wearer. We present a new dedicated comprehensive design paradigm and combine this with adapted signal processing techniques that greatly enhance the robustness and the autonomy of these systems. On the one hand, the large amount of real estate available in professional rescue worker garments may be exploited to deploy multiple textile antennas. On the other hand, the size of each radiator may be designed large enough to ensure high radiation efficiency when deployed on the body. This antenna area is then reused by placing active electronics directly underneath and energy harvesters directly on top of the antenna patch. We illustrate this design paradigm by means of recent textile antenna prototypes integrated in professional garments, providing sensing, positioning and communication capabilities. In particular, a novel wearable active Galileo E1-band antenna is presented and fully characterized, including noise figure and linearity performance.

3.1 Introduction

In recent years, lots of research was devoted to increase the operational safety and efficiency of police, army and rescue services. In particular, wearable electronic systems greatly enhance the functionality of professional rescue worker garments by providing sensing, localization and wireless communication capabilities. Smart fabrics and interactive textiles (SFIT) [1], [2], which are unobtrusively integrated into garments, do not hinder the movements during interventions, and, in the meanwhile, continuously monitor life signs, activities and environmental conditions, relaying these data wirelessly to a remote location for supervision by the operations coordinator. In addition, in hazardous situations, alarms and specific instructions can be fed back to each individual in action.

As SFIT systems are to be deployed in harsh conditions and during critical operations, their reliability and autonomy are two key concerns of the designers. To ensure sufficient autonomy without the use of heavy batteries, the electronics must be highly energy-efficient. As a lot of power is consumed in establishing wireless communication links, textile antennas are critical components, so they should preferably exhibit high gain and large radiation efficiency. Garments provide the space needed to deploy antennas with such characteristics, and by making use of a large ground plane, absorption of antenna radiation by the human body is also avoided. Yet, special care must be taken by designers of wearable antennas to counter degradation of antenna performance due to bending, wrinkling and crumpling of the large flexible textile antenna [3]–[7] as the wearer moves around. Moreover, a good selection of materials is needed to avoid excessive substrate losses due to humidity trapped in the substrate fabric [8] and a thermoplastic

polyurethane (TPU) coating may be required to protect the antenna during washing [9]. In addition to increasing the power-efficiency of SFIT systems, energy harvesters may be added to scavenge energy from one or more energy sources available in the neighborhood of the body, in order to increase the operational autonomy.

In this chapter, we propose a dedicated comprehensive design paradigm to implement energy-efficient active wearable antennas with stable performance when integrated in professional garments that are worn during interventions. To improve reliability and autonomy of the active antenna modules, we integrate electronics on the planar textile antenna's feed plane, directly underneath its ground plane, and position energy harvesters directly on the antenna plane. We outline the measures taken to ensure that the antenna performance is not reduced due to the integration of these additional components. We then pinpoint how this strategy resulted in several implementations for different applications in the context of interventions by rescue workers and public regulatory services, as recently proposed in literature.

In Section 3.2, we present the comprehensive design paradigm to design autonomous active textile antennas based on full-wave/circuit co-design and co-optimization. Integrating active electronic circuits directly underneath the wearable antenna, results in a compact communication module and avoids weak connections that easily break when put under stress during interventions. Moreover, by placing the active electronic circuits directly on the antenna feed plane, the length of radio-frequency (RF) connections is minimized, thereby reducing signal attenuation and improving signal integrity and electromagnetic compatibility of the device. In a next step, energy harvesters can be deployed on the active antennas to increase their autonomy. This is shown by integrating a set of solar cells on top of the antenna patch of a wearable module, without disturbing its radiation characteristics. We then move on to discuss two recent antenna designs for sensing, localization and wireless communication applications. Section 3.3 describes a wearable low-cost through-wall Doppler radar that may be deployed in rescue worker garments to detect moving persons behind walls and victims lying under rubble. In Section 3.4, we outline the design and validation of a wearable active Galileo E1-band antenna, additionally covering the Galileo Search-and-Rescue (SAR) downlink and Glonass L1 frequencies. Finally, we wrap up by drawing some conclusions in Section 3.5.

3.2 Textile antenna design paradigm

In order to provide additional functionalities to technical garments for rescue workers, wearable, robust and autonomous modules are required. To this aim, we put forward the dedicated design strategy outlined in Figure 3.1. Starting from the nominal application-specific design specifications, the particular operating conditions in which the wearable modules have to operate, dictate the final design re-

quirements, the choice of topology and the material selection. Antenna bending, body presence and environmental parameters, such as heat or moisture, for example, can cause frequency shifts, which may be anticipated by adding safety margins to the frequency range in which the antenna has to comply with the specifications. These adjusted conservative requirements lead to a consequent choice of the active antenna topology. The preliminary circuit and antenna designs are subsequently co-optimized according to the principles described in subsection 3.2.1. As outlined in subsection 3.2.2, energy harvesters can then be integrated onto the active antenna, producing a compact, autonomous module that is evaluated in realistic testing conditions.

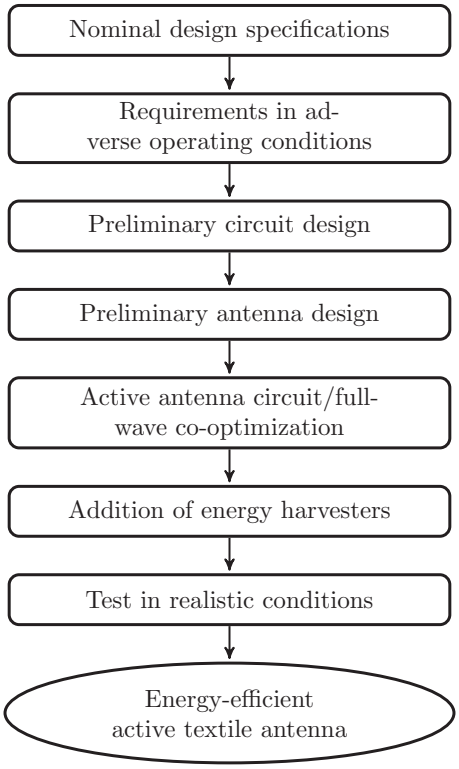

Figure 3.1: Dedicated energy-efficient active textile antenna design paradigm.

3.2.1 Active antenna circuit/full-wave co-optimization

Direct integration of active electronics circuits onto the wearable antenna reduces the number of connections and keeps RF paths short. This is, in particular, beneficial for circuits implemented on textile substrates and interconnections with e-textiles, as, on the one hand, substrate and conductive losses are typically more

important compared to conventional rigid printed circuit board materials, and, on the other hand, soldering or press-fitting connectors onto conductive textiles results in weak links prone to breaking when subjected to stress incurred, for example, by movements. In addition, via connections should also be avoided, if possible, as these may also come loose when pressure is exerted onto the textile or foam substrate.

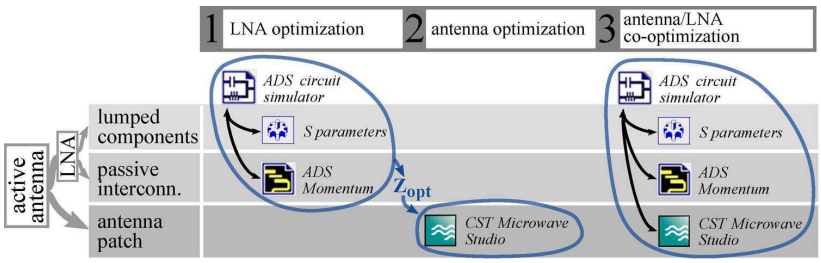

Figure 3.2: Design strategy for optimal noise characteristics.

The design of active antennas requires a joint circuit/full-wave optimization to simultaneously design the antenna and the active electronics to meet the desired specifications [10]–[13]. Typically, impedance matching and circular polarization may be desired for the antenna together with large available gain, input and output matching, as well as low noise figure for the low-noise amplifier (LNA) attached to the antenna output. Given the large number of design variables available for optimization, we devised two dedicated strategies to keep the design process manageable [10]. The first process puts forward an optimal complex radiation impedance for the passive textile antenna, resulting in a minimal noise figure at the LNA's output. This impedance is found in the first step of the full-wave/circuit co-optimization procedure for the active electronics only, producing a preliminary optimal LNA design. In the process, a full-wave simulator is applied to generate an N-port scattering matrix describing the interconnections of the active electronics circuit. This scattering matrix is combined with N-port descriptions of the different active and passive lumped components in the circuit in a subsequent circuit simulation. In a second step, full-wave optimization of the passive antenna is performed to fix the antenna dimensions that provide the optimal radiation impedance. In third and final step, the complete active antenna is co-optimized to jointly maximize the performance of both the antenna and the active electronics. This design flow for optimal noise characteristics without the need of a matching network is sketched in Fig. 3.2. It guarantees short RF connections and avoids excess losses due to components added for matching. The strategy makes use of the most suited simulators for each part of the active textile antenna. In particular, the passive antenna was modeled in the 3D full-wave frequency domain simulator of CST Microwave Studio, which is able to take into account the finite conductivity of the electro-textile Flectron, used as antenna plane and ground plane. As the LNA circuit is implemented on a thin polyimide flex, its interconnections can be modeled

by means of the planar-3D full-wave simulator ADS Momentum. The reader is referred to [10], [14] for further details.

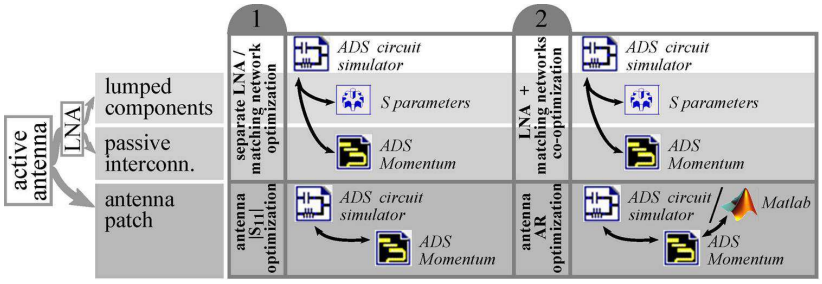

Figure 3.3: Design strategy for optimal impedance matching.

Antennas for satellite communication typically exhibit stringent requirements in terms of circular polarization. Deforming the radiating structure together with optimization of the feed point may not suffice to meet the requirement that the axial ratio remains below 3 dB over a sufficiently large bandwidth. If this is the case, the use of a quadrature hybrid should be considered. As implementations in wearable microstrip technology are typically too large at GPS frequencies, miniaturized off-the-shelf lumped hybrids are preferred. Moreover, a filter between the receiving antenna and the LNA may be required to suppress interference and noise. For satellite communication, such filters typically require very steep filter flanks and narrow transition regions between pass band and stop bands. Again, a microstrip implementation of a filter of sufficiently large order will be prohibitively large and an off-the-shelf discrete ceramic, surface acoustic wave (SAW) or bulk acoustic wave (BAW) filter is preferred. As these components have a fixed impedance level of 50 Ω at their ports, the above described co-optimization strategy must be modified. Now, in a first step, to accommodate the discrete component, the antenna output and the LNA input are both separately matched to 50 Ω. This requires a matching network to guarantee optimal noise performance for the LNA. In a second step, at the antenna side, axial ratio and antenna impedance are jointly optimized, whereas a full-wave/circuit co-optimization is performed on the complete LNA circuit. This design flow for optimal impedance matching of both the passive antenna and the LNA is sketched in Fig. 3.3. As all conductive layers are implemented by means of copper patterns on polyimide flex, only the planar-3D full-wave simulator ADS Momentum is used in the design process. More details are found in [10], [15].

3.2.2 Integration of energy harvesters onto wearable antennas

An important remaining issue standing in the way of a commercial breakthrough of SFIT systems for professional garments concerns ensuring sufficient autonomy

without the need of heavy batteries and frequent recharging. Therefore, recent research concentrated on adding energy-scavengers to these systems, in order to collect energy from the body and its environment to power the system [16]–[19]. For modules in SFIT garments, solar energy and kinetic energy originating from body movement are the most important sources. In [16], it is shown that the antenna patch may serve as a platform for flexible amorphous silicon (a-Si:H) solar cells, thereby reusing the space consumed by the large antenna. In Fig. 3.4, we show the aperture-coupled shorted wearable solar patch antenna for communication in the 902–928 MHz UHF band. By adopting a PIFA topology for the textile antenna and by routing the feed wires of the flexible solar cells along the shorting-wall of the antenna, the antenna radiation is not influenced by the presence of the energy harvester glued onto the antenna patch. Furthermore, only the positive polarity of the solar cell has to be routed through the antenna substrate. The solar cell's cathode can be directly connected to the patch of the antenna since the patch provides DC grounding through the antenna's shorting wall.

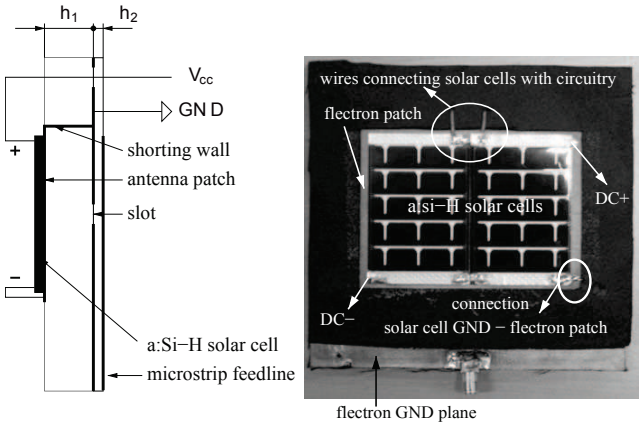

Figure 3.4: Aperture-coupled shorted wearable solar patch antenna for 902–928 MHz UHF band.

The antenna substrate is a flexible polyurethane foam with a thickness $h_1 = 11$ mm, a relative permittivity $\varepsilon_r = 1.16$ and a loss tangent $tan\ \delta = 0.010$. The feed substrate is an assembly of two aramid textile layers with a thickness $h_2 = 0.95$ mm, an $\varepsilon_r = 1.97$ and a loss tangent $tan\ \delta = 0.020$. The conductive patch and ground plane are made out of a copper coated woven nylon fabric, whereas the microstrip feedline is constructed from copper foil. All layers are assembled by means of an adhesive sheet. The antenna design used the time domain solver of CST Microwave Studio in which antenna patch size, microstrip feedline stub length and aperture size were optimized in order to accomplish impedance matching in the 902-928 MHz frequency band. The available antenna surface (= conductive patch) for integration of solar cells is 62 mm × 80 mm, resulting in sufficient space for two solar cells as shown in Fig. 3.4.

Under ideal illumination conditions, measuring 100 mW/cm^2, the solar cell can deliver up to 57.3 mW (maximum power point). This illumination level represents sunlight directly overhead on a clear bright day on earth. The current configuration is based on two solar cells and can provide a maximum DC power of about 114 mW. However, in real life applications, the DC output power will be lower since the orientation of the solar cell with respect to the sun and the illumination strength will differ from these optimal conditions. Furthermore, the load connected to the solar cell configuration must be optimal in order to operate in the solar cell's maximum power point.

In order to investigate the influence of the solar cells on the antenna characteristics, both a reflection coefficient and radiation pattern measurement of the antenna with and without solar cells were executed. The simulated reflection coefficient, the measured reflection coefficients of the antenna in free space with and without solar cells, and the measured $|S_{11}|$ with the antenna positioned on the chest of a human body are presented in Fig. 3.5. The simulated and measured bandwidth is about 48 MHz whereas the on-body bandwidth increased to 64 MHz due to the additional losses induced by the proximity of the human body. Moreover, a slightly larger bandwidth is observed because of the presence of the solar cells which incur a small additional loss. However, this excess loss is much smaller than the extra losses observed when the antenna operates in the vicinity of the human body. The simulated and measured antenna gains in the XZ and YZ-plane are displayed in Fig. 3.6. Again, a comparison is made between the radiation pattern of the antenna with and without solar cells. The maximum gain of the antenna is about 3 dBi, and from these measurements we can conclude that the solar cells have a minor influence on the radiation performance of the antenna.

3.3 Wearable through-wall Doppler radar

The design procedure outlined in Section 3.2 was applied to construct a low-cost, low-weight, wearable Doppler radar system capable of detecting moving objects behind a barrier, operating at 2.35 GHz. In rescue operations, wearability is critical, since the user's range of motion should not be limited by the radar system. The novelty of this radar system lies in the wearability and its comfortable integration into a garment, which is why a simple, power-efficient Doppler radar architecture was chosen, requiring minimal data processing. As shown in Fig. 3.7, the transmit part of the Doppler radar consists of a four-element phased array of textile antennas. The beam emitted by this array is right-hand circularly polarized along all scanning angles and provides 9.2 dBi gain. The element spacing of 8.5 cm results in a large aperture and allows beamsteering from -15° to +15° with respect to boresight. In Fig. 3.8, the $|S_{11}|$ and $|S_{21}|$ are depicted. It can be seen that the array is broadly matched in its intended frequency range (2.3 - 2.4 GHz), ensuring functionality when affected by potential frequency shifts due to antenna bending and body proximity. Moreover, we note that the individual array elements are ad-

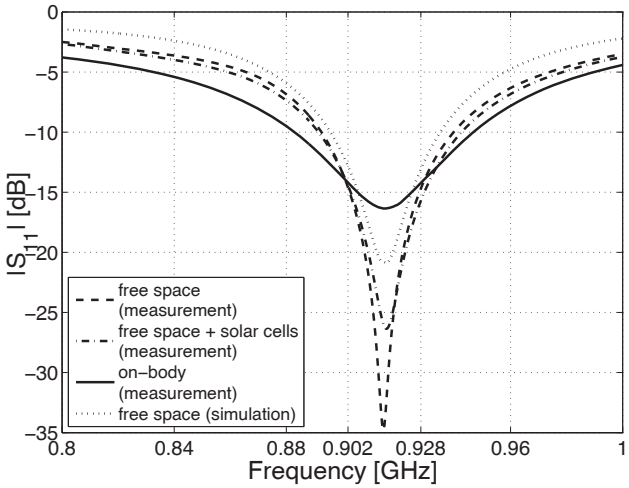

Figure 3.5: Measured and simulated $|S_{11}|$ of the aperture coupled shorted wearable solar patch antenna.

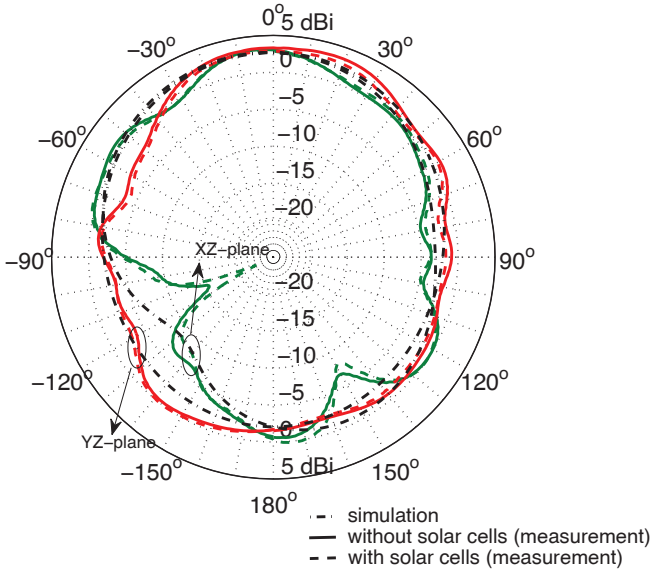

Figure 3.6: Measured and simulated antenna radiation patterns in the XZ and YZ-plane of the aperture coupled shorted wearable solar patch antenna at 915 MHz.

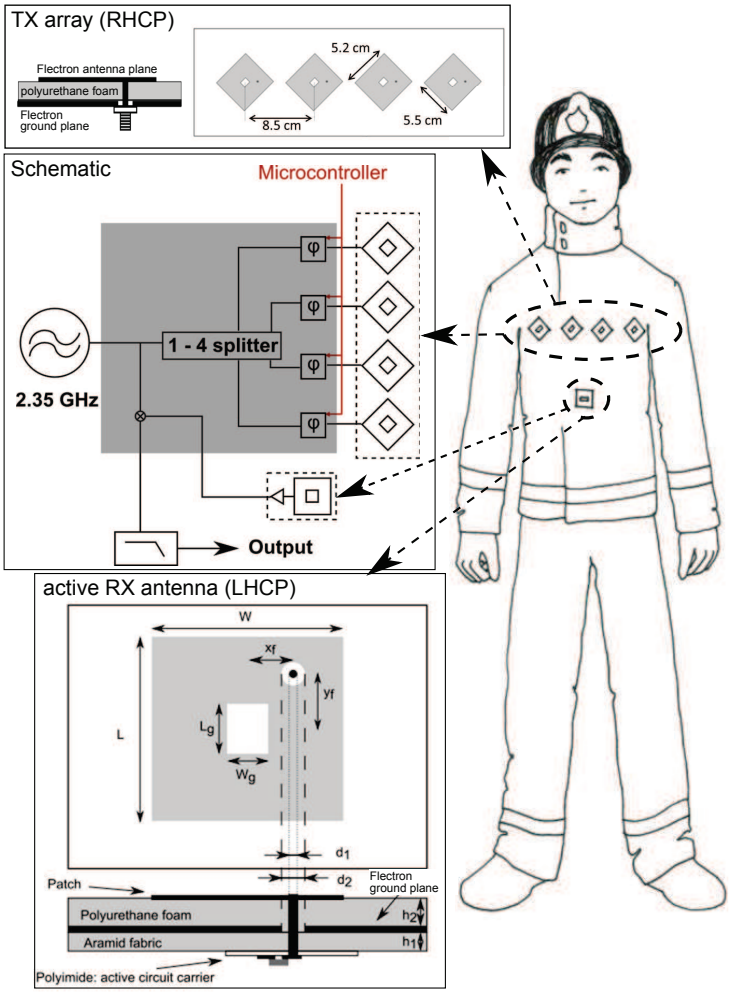

Figure 3.7: Wearable through-wall Doppler radar (firefighter drawing by Laura Goethals).

equately isolated from each other. In Fig. 3.9, the radiation pattern of the transmit array is depicted for beams steered in the -10°, 0° and 15° direction. Note that, for these steering directions, there is a single main beam and grating lobes are absent. At the receiving end, textile fabrics found in professional garments were used to develop an active wearable receive antenna. Applying the design strategy for optimal noise characteristics outlined in Section 3.2 and shown in Fig. 3.2 results in 15.7 dBi gain, 1.1 dB noise figure, left-hand circular polarization, and a 3 dB axial ratio beamwidth larger than 50°. The transmit and receive antennas both consist of microstrip patch antennas with a sufficiently large ground plane, providing ra-

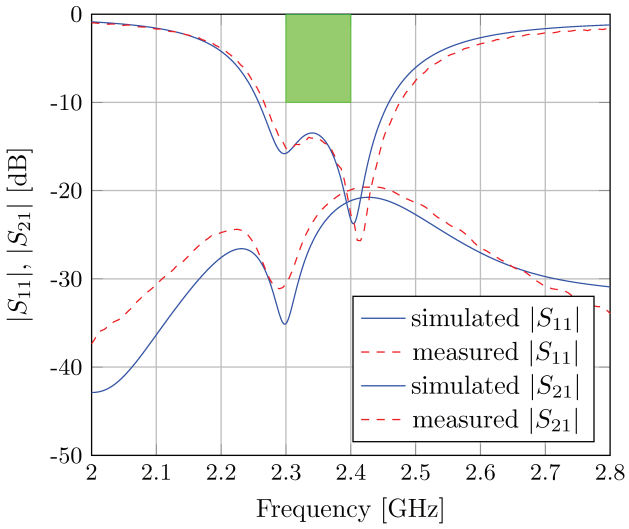

Figure 3.8: Simulated and measured $|S_{11}|$ and $|S_{21}|$ of the wearable four-element array.

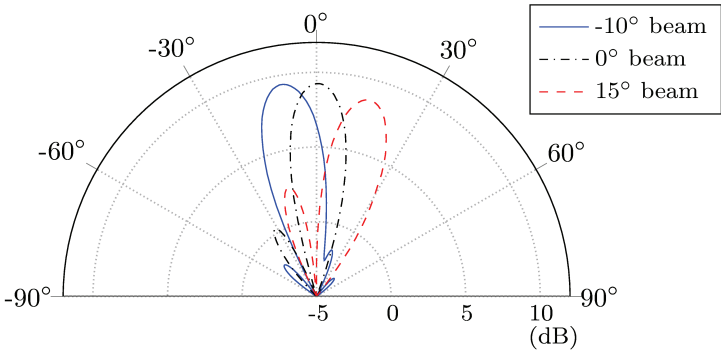

Figure 3.9: Radiation pattern of the transmit array with beam steered in -10°, 0° and 15° direction.

diation in a semi-hemisphere away from the body. Therefore, the ground plane effectively shields the antenna from the body or electronics integrated on the antenna backside. In Fig. 3.10, the measured radiation pattern of the active receive antenna is depicted. The maximum gain is found along the broadside direction and equals 15.7 dBi. Fig. 3.11 shows the spectrogram measured by the radar worn by a rescue worker standing in front of a fire-retardant door, detecting a person walking at 1.5 m/s at a position of 15° with respect to boresight, behind that door. A full description of the design, fabrication and validation of the wearable radar is found in [20].

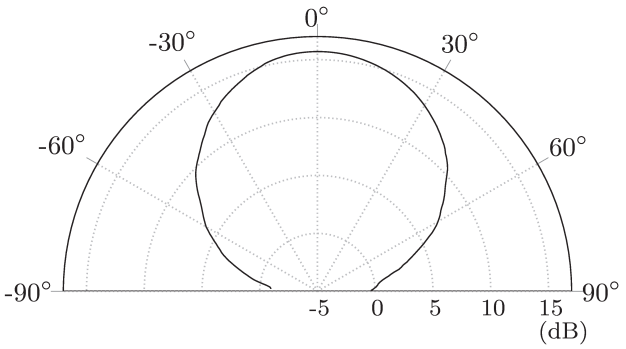

Figure 3.10: Measured radiation pattern of the active receive antenna.

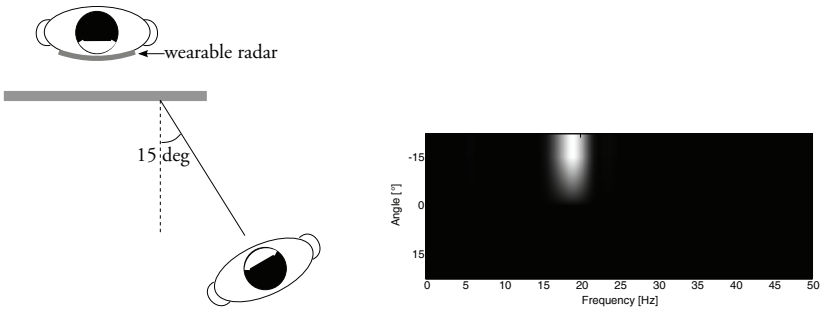

(a) (b)

Figure 3.11: Measurement setup with a rescue worker wearing the radar, trying to detect a person walking at 15° behind a closed fire-retardant door (a) and measured spectrogram (b).

3.4 Wearable active Galileo E1-band antenna

The second design strategy outlined in Section 3.2, following Fig. 3.3, was applied to design an active wearable Galileo E1-band antenna, additionally servicing the Galileo SAR downlink and the Glonass L1 band. In order to provide the aforementioned functionalities, the antenna has to cover a frequency spectrum ranging from 1.544 GHz to 1.611 GHz, while being right-handed circularly polarized. Moreover, in terms of application scenario, the antenna is intended for use in rescue-worker garments. This requires a module that is not only compact and flexible, ensuring the wearer's movements are not hindered, but also robust, guaranteeing performance in harsh conditions. In order to achieve these requirements, an aperture-coupled microstrip patch topology [15], as shown in Fig. 3.12, has been selected. This topology is low-profile and the ground plane shields the antenna from the body, reducing its influence on the radiation performance, and allowing the inte-

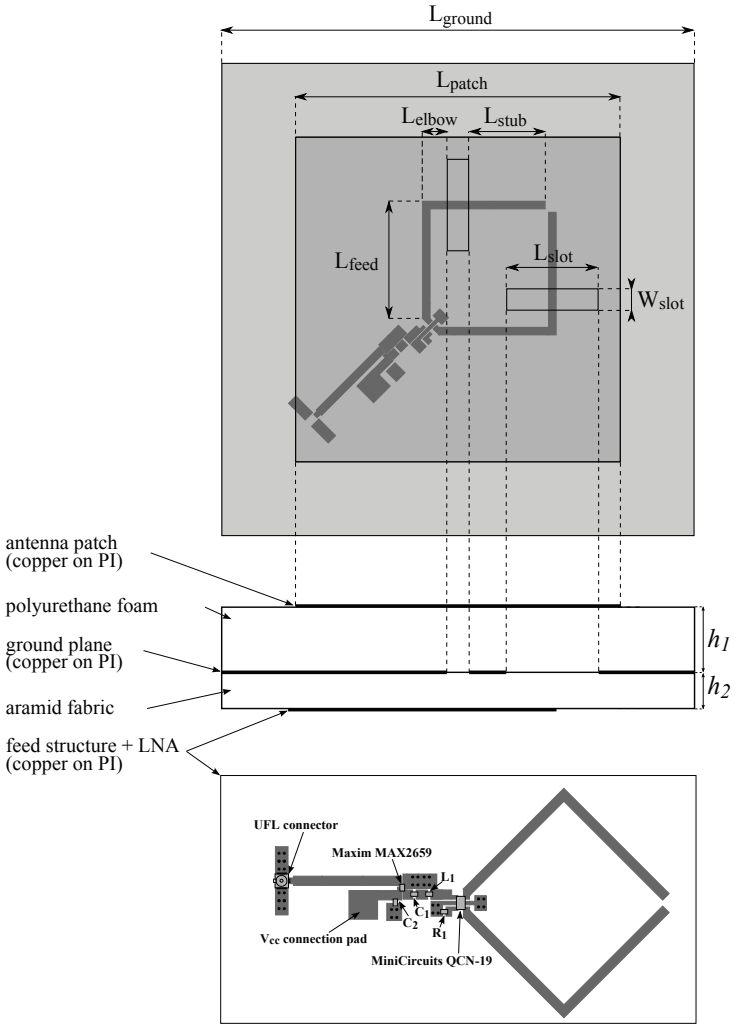

Figure 3.12: Wearable active Galileo E1-band antenna.

gration of active electronics on the antenna backside, eliminating potential weak links that would otherwise be present between the antenna and the electronic system. The aperture coupling helps to reduce the amount of vias in the design, increasing robustness to stresses occurring when the antenna is bent or compressed. In order to achieve a wideband circular polarization, a discrete hybrid coupler was preferred over other techniques [21]–[23]. Moreover, we opted for a compact discrete component instead of a microstrip realization, leaving space for the low-noise amplifier and reducing the vulnerability of the coupler to bending influences. This hybrid coupler is connected to the Maxim MAX2659 LNA [24], providing a high

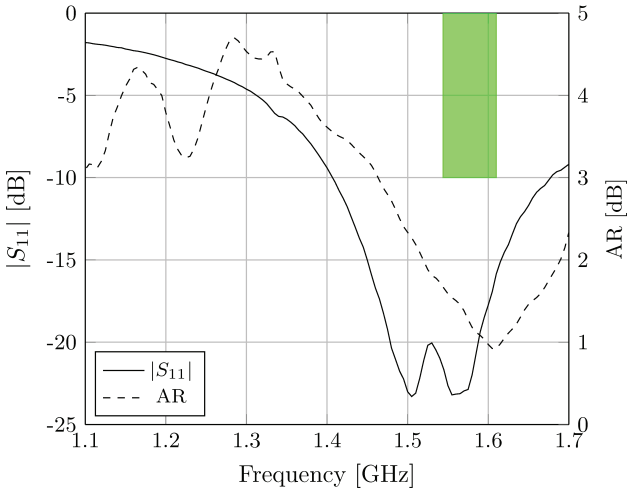

Figure 3.13: Measured $|S_{11}|$ and axial ratio of the wearable active Galileo E1-band antenna.

gain and a low noise figure in a small package that can be conveniently integrated into the feed plane of the antenna. The detailed view in Fig. 3.12 presents the feed circuit layout, in which the discrete hybrid coupler is connected to the LNA input via an inductor-capacitor matching network ($L_1 = 6.8$ nH and $C_1 = 470$ pF). Apart from the discrete coupler, the LNA and the two-element matching network, only two additional components are required (50 Ω termination R_1 and 33 nF decoupling capacitor C_2), permitting a small and rugged circuit. The LNA is powered by a voltage $V_{cc} = 3V$. Its DC power consumption is 12 mW. As depicted in Fig. 3.13, measurements indicate that the active antenna is robustly matched over a frequency band ranging from 1.41 GHz to 1.675 GHz. The antenna's axial ratio is lower than 3 dB from 1.465 GHz to 1.765 GHz. This wideband circular polarization is achieved by using the discrete hybrid coupler. As depicted in Fig. 3.14, the antenna gain reaches a maximum of 25.45 dB at 1.595 GHz. It stays within 3 dB of this maximum value from 1.54 to 1.66 GHz.

To characterize the noise and linearity performance of the active antenna, noise measurements were performed on the LNA integrated on an aramid textile substrate, and linearity measurements were performed on the complete active antenna. The noise figure (NF) of the stand-alone LNA at 1.575 GHz is measured to be 0.95 dB, obtained after deembedding the attenuation of the SubMiniature version A - U.FL series ultra small surface mount coaxial connector (SMA-U.FL) adapter and the U.FL-cable connected to the LNA input. This value is slightly higher than the one listed in the datasheet. The LNA examined here is integrated onto a textile substrate glued to a copper-on-polyimide laminate, on which the circuit is etched. This layered substrate is characterized by a $tan\ \delta = 0.02$, resulting in a larger attenuation in the circuit's interconnections compared to rigid,

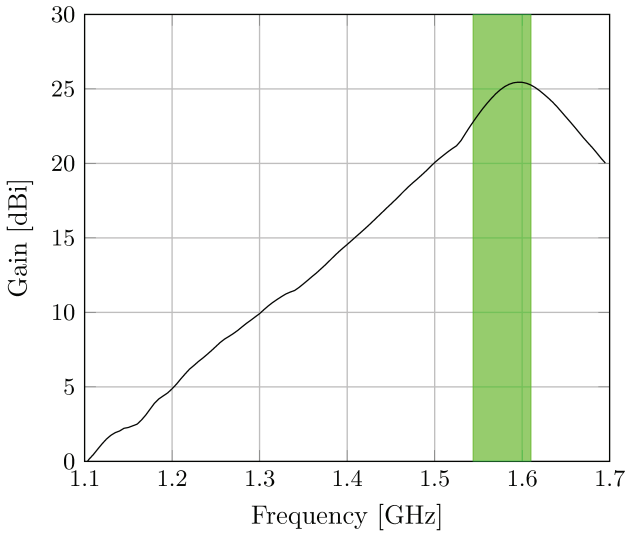

Figure 3.14: Measured gain of the wearable active Galileo E1-band antenna.

high-frequency laminates. However, thanks to the short transmission lines in the LNA circuit, the attenuation and its effect on the noise figure are limited. Nevertheless, the vias in the textile substrate are fabricated by threading copper wires through the substrate, introducing additional inductance in the ground connection of the LNA chip, potentially affecting its performance. Next, by using the Gain Compression and Swept IMD applications available on the Agilent N5242A PNA-X Vector Network Analyzer, which use an external power meter to calibrate the PNA-X receivers as reliable power meters, the 1-dB input compression point (P1dB) and third-order input intercept point (IIP3) of the active antenna were determined. For these measurements, the setup displayed in Fig. 3.15 was used. Port 1 of the PNA-X is connected to a highly linear low-noise amplifier, which in turn is connected to a standard gain horn. As discussed in [25], the high OIP3 (43 dB from 700 to 1600 MHz) of the MiniCircuits ZRL-3500+ amplifier allows it to be driven with an input power level up to 0 dBm before intermodulation distortion is generated, providing ample range for the linearity characterization of the active antenna under test. At a distance of 3.55 m from the horn, the active antenna, displayed on the figure as a separate antenna and LNA block, is aligned with the horn. The active antenna is fed by two AA batteries, resulting in a 3.15 V feed voltage. The active antenna is then connected to port 2 of the PNA-X. In Fig. 3.15, detailed descriptions and gains/losses of the different elements of the setup are specified. In this setup, the PNA-X is located in a Faraday cage, while the other components were positioned in an anechoic chamber. To be able to compare the results with the values listed in the MAX2659 datasheet, the same 5 MHz tone spacing and -40 dBm/tone power (at the LNA input) were used for the IIP3 mea-

surement. The values for the P1dB and IIP3 returned by the PNA-X measurements were corrected with the term $G_{LNA1} + G_{Horn} + L + G_{ant}$ = -4.9 dB to take into account the gains/losses that occur before the signal transmitted at port 1 of the PNA-X actually reaches the LNA integrated into the active antenna. In this way, a P1dB of -9.965 dBm and a IIP3 of -4.23 dBm at 1.575 GHz were measured. These results are in in good agreement with the values indicated in the datasheet.

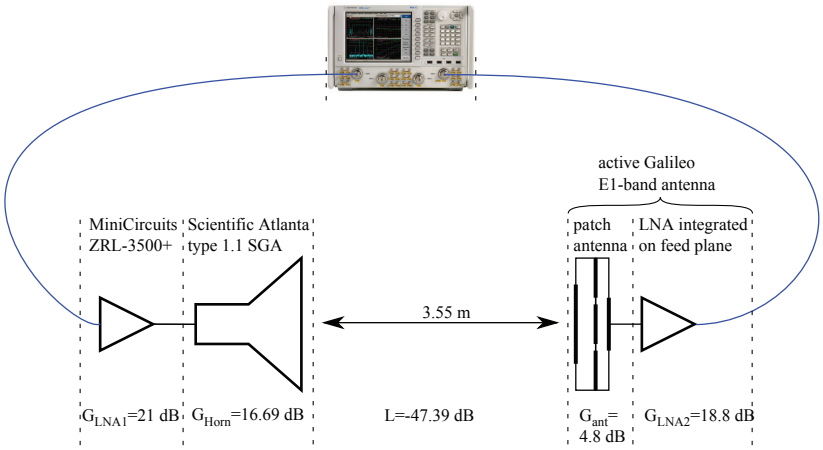

Figure 3.15: Setup for the active antenna P1dB and IIP3 measurements.

3.5 Conclusion

Smart electronic systems for sensing, localization and wireless communications should exhibit robustness, reliability and a high degree of autonomy while not adding too much weight, nor hindering the movements of the wearer. In this chapter, we exploit the large area available in professional garments to integrate flexible textile antennas. In turn, the wearable antenna is used as a platform for the integration of active electronics, on the feed plane directly below the ground plane, as well as for the integration of solar cells directly on top of the antenna patch. We presented a comprehensive dedicated design paradigm that yields optimal active antenna characteristics. The two outlined full-wave/circuit co-optimization strategies were applied to the design of a wearable through-wall Doppler radar for the detection of moving persons behind barriers and of a wearable active Galileo E1-band antenna, whose noise and linearity performance were characterized. The large area available in garments can also be exploited to deploy multiple antennas to improve the signal quality by means of diversity and MIMO techniques. For more details, we refer to [26]–[29].

References

[1] D. Curone, E. Secco, L. Caldani, A. Lanata, R. Paradiso, A. Tognetti, and G. Magenes, "Assessment of sensing fire fighters uniforms for physiological parameter measurement in harsh environment", *IEEE Trans. Inf. Technol. Biomed.*, vol. 16, no. 3, pp. 501–511, 2012.

[2] T. Kennedy, P. Fink, A. Chu, N. Champagne, G. Lin, and M. Khayat, "Body-worn E-Textile antennas: The good, the low-mass, and the conformal", *IEEE Trans. Antennas Propag.*, vol. 57, no. 4, pp. 910–918, 2009.

[3] A. Tronquo, H. Rogier, C. Hertleer, and L. Van Langenhove, "Robust planar textile antenna for wireless body LANs operating in 2.45 GHz ISM band", *IEE Electronic Letters*, vol. 42, no. 3, pp. 142–146, 2006.

[4] I. Locher, M. Klemm, T. Kirstein, and G. Troster, "Design and characterization of purely textile patch antennas", *IEEE Trans. Adv. Packag.*, vol. 29, no. 4, pp. 777–788, 2006.

[5] P. Salonen and Y. Rahmat-Samii, "Textile antennas: effects of antenna bending on input matching and impedance bandwidth", *IEEE Aerosp. Electron. Syst. Mag.*, vol. 22, no. 12, pp. 18–22, 2007.

[6] C. Hertleer, H. Rogier, L. Vallozzi, and L. Van Langenhove, "A textile antenna for off-body communication integrated into protective clothing for firefighters", *IEEE Trans. Antennas Propag.*, vol. 57, no. 4, pp. 919–925, 2009.

[7] J. Lilja, P. Salonen, T. Kaija, and P. de Maagt, "Design and manufacturing of robust textile antennas for harsh environments", *IEEE Trans. Antennas Propag.*, vol. 60, no. 9, pp. 4130–4140, 2012.

[8] C. Hertleer, A. Van Laere, H. Rogier, and L. Van Langenhove, "Influence of relative humidity on textile antenna performance", *Textile Research Journal*, vol. 80, no. 2, 177–183, 2010.

[9] M. L. Scarpello, I. Kazani, C. Hertleer, H. Rogier, and D. Vande Ginste, "Stability and Efficiency of Screen-Printed Wearable and Washable Antennas", *IEEE Antennas Wireless Propag. Lett.*, vol. 11, 838–841, 2012.

[10] A. Dierck, F. Declercq, and H. Rogier, "Review of active textile antenna co-design and optimization strategies", in *2011 IEEE Int. Conference on RFID-Technologies and Applications (RFID-TA)*, 2011, pp. 194 –201.

[11] M. Del Prete, D. Masotti, N. Arbizzani, and A. Costanzo, "Remotely identify and detect by a compact reader with mono-pulse scanning capabilities", *IEEE Trans. Microw. Theory Tech.*, vol. 61, no. 1, pp. 641–650, 2013.

[12] D. Masotti, P. Francia, A. Costanzo, and V. Rizzoli, "Rigorous electromagnetic/circuit-level analysis of time-modulated linear arrays", *IEEE Trans. Antennas Propag.*, vol. 61, no. 11, pp. 5465–5474, 2013.

[13] D. Masotti, A. Costanzo, M. Prete, and V. Rizzoli, "Genetic-based design of a tetra-band high-efficiency radio-frequency energy harvesting system", *IET Microwaves, Antennas & Propagation*, vol. 7, no. 15, pp. 1254–1263, 2013.

[14] F. Declercq and H. Rogier, "Active Integrated Wearable Textile Antenna With Optimized Noise Characteristics", *IEEE Trans. Antennas Propag.*, vol. 58, no. 9, 3050–3054, 2010.

[15] A. Dierck, H. Rogier, and F. Declercq, "A wearable active antenna for global positioning system and satellite phone", *IEEE Trans. Antennas Propag.*, vol. 61, no. 2, pp. 532–538, 2013.

[16] F. Declercq, A. Georgiadis, and H Rogier, "Wearable aperture-coupled shorted solar patch antenna for remote tracking and monitoring applications", in *Proceedings of the 5th European Conference on Antennas and Propagation (EUCAP)*, Rome, Italy, 2011, 2992–2996.

[17] A. Collado and A. Georgiadis, "Conformal hybrid solar and electromagnetic (EM) energy harvesting rectenna", *IEEE Trans. Circuits Syst. I*, vol. 60, no. 8, pp. 2225–2234, 2013.

[18] S. V. Shynu, M. Roo Ons, M. Ammann, S. McCormack, and B. Norton, "Dual band a-Si:H solar-slot antenna for 2.4/5.2 GHz WLAN applications", in *3rd European Conference on Antennas and Propagation (EuCAP), 2009.*, 2009, pp. 408–410.

[19] M. B. Schubert and J. H. Werner, "Flexible solar cells for clothing", *Materials Today*, vol. 9, no. 6, pp. 42 –50, 2006.

[20] S. Agneessens, P. Van Torre, F. Declercq, B. Spinnewyn, G.-J. Stockman, H. Rogier, and D. Vande Ginste, "Design of a Wearable, Low-Cost, Through-Wall Doppler Radar System", English, *International Journal of Antennas and Propagation*, no. 840924, 2012.

[21] E. Kaivanto, M. Berg, E. Salonen, and P. de Maagt, "Wearable circularly polarized antenna for personal satellite communication and navigation", *IEEE Trans. Antennas Propag.*, vol. 59, no. 12, pp. 4490 –4496, 2011.

[22] L. Vallozzi, W. Vandendriessche, H. Rogier, C. Hertleer, and M. L. Scarpello, "Wearable textile GPS antenna for integration in protective garments", in *Proc. of the Fourth European Conference on Antennas and Propagation (EuCAP), 2010*, Barcelona, Spain, 2010, p. 4.

[23] P. Salonen, Y. Rahmat-Samii, M. Schaffrath, and M. Kivikoski, "Effect of textile materials on wearable antenna performance: a case study of GPS antennas", in *2004 IEEE Antennas and Propagation Society Int. Symp.*, vol. 1, 2004, 459 –462 Vol.1.

[24] Maxim Integrated Products, *GPS/GNSS Low Noise Amplifier, MAX2659 data sheet*, 2011.

[25] A. Biondi, F. Declercq, D. De Zutter, H. Rogier, and L. Vallozzi, "Electromagnetic compatibility aware design and testing of intermodulation distortion under multiple co-located sources illumination", *IET Science Measurement & Technology*, vol. 6, no. 2, 105–112, 2012.

[26] L. Vallozzi, P. Van Torre, C. Hertleer, H. Rogier, M. Moeneclaey, and J. Verhaevert, "Wireless Communication for Firefighters Using Dual-Polarized Textile Antennas Integrated in Their Garment", *IEEE Trans. Antennas Propag.*, vol. 58, no. 4, 1357–1368, 2010.

[27] P. Van Torre, L. Vallozzi, C. Hertleer, H. Rogier, M. Moeneclaey, and J. Verhaevert, "Indoor Off-Body Wireless MIMO Communication With Dual Polarized Textile Antennas", *IEEE Trans. Antennas Propag.*, vol. 59, no. 2, 631–642, 2011.

[28] P. Van Torre, M. L. Scarpello, L. Vallozzi, H. Rogier, M. Moeneclaey, D. Vande Ginste, and J. Verhaevert, "Indoor Off-Body Wireless Communication: Static Beamforming versus Space-Time Coding", *IEEE Trans. Antennas Propag.*, 2012.

[29] P. Van Torre, L. Vallozzi, L. Jacobs, H. Rogier, M. Moeneclaey, and J. Verhaevert, "Characterization of Measured Indoor Off-Body MIMO Channels with Correlated Fading, Correlated Shadowing and Constant Path Loss", *IEEE Trans. Wireless Commun.*, vol. 11, no. 2, 712–721, 2012.

4

Dedicated multi-objective constrained Pareto optimization for design of textile antennas

Arnaut Dierck, Frederick Declercq, Thomas Vervust, and Hendrik Rogier

Submitted to International Journal of Antennas and Propagation

★ ★ ★

Designing textile antennas for real-life applications requires a design strategy that is able to produce antennas that are optimized over a wide bandwidth for often conflicting characteristics such as impedance matching, axial ratio, efficiency and gain, and, moreover, that is able to account for the tolerances that apply for the characteristics of the unconventional materials used in smart textile systems. In this chapter, such a strategy, incorporating a multi-objective constrained Pareto optimization, is presented and applied to the design of a Galileo E6-band antenna with optimal return loss and axial ratio characteristics. Subsequently, different prototypes of the optimized antenna are fabricated and measured to validate the proposed design strategy.

4.1 Introduction

With the advent of ubiquitous computing, the need for ever smaller, cheaper and more powerful electronic devices has increased significantly. Smart fabrics and interactive textiles (SFIT) offer great potential to increase the functionality in a wide

gamut of applications at a low cost, as well in terms of price as space. From healthcare to civil services, by using suitable materials such as (conductive) textiles, foams and 3D-fabrics to realize active circuits and antennas, electronic systems can be unobtrusively integrated into clothing, implementing features that would otherwise require additional, often cumbersome, devices that have to be carried around [1]–[8]. For rescue workers, having access to services such as positioning, victim localization, vital signs monitoring and environmental hazard sensing can mean the difference between life and death. Replacing the traditional, rigid, handheld devices by electronics directly integrated into the wearer's garment, however, does not come without specific design challenges. The placement of the wearable systems inside of a garment makes them susceptible to influences of the proximity of the body. Moreover, the foam and fabric substrates give rise to additional losses and their flexibility, while indispensable for a conformal integration into clothing, makes the antennas vulnerable to bending, potentially affecting their performance [9], [10]. Additionally, the off-the-shelf foam/textile materials, not having been specifically designed and fabricated as radio frequency (RF) substrates, can exhibit high tolerances on their RF properties when looking at different product batches. These tolerances can cause an unwanted shift in the antenna frequency response, which can reduce performance in the required frequency range. As wearable applications often require a low-profile antenna, the antenna thickness, mainly determined by the height of the antenna substrate, is a key aspect in the design process. A thinner antenna substrate offers a more comfortable integration into the garment, but, at the same time, limits the margins the designer can introduce to ruggedize the antenna to material tolerances by increasing the antenna bandwidth. In order to meet the stringent requirements for modern applications, both in terms of performance and wearability, it is not only important to base the design on a suitable antenna topology that is subsequently optimized in view of the different design objectives, but also to be able to cope with the potentially large tolerances of the used foam/textile materials.

Aperture-coupled circularly polarized patch antennas provide a versatile topology for wearable, robust user-terminal antennas for satellite communications [1], [2]. The intricate effect of the different design parameters on the antenna performance, combined with the tolerances on the applied substrate materials, demand a dedicated design strategy, employing a multi-objective optimization approach in tandem with a final post-optimization step to accommodate for potential tolerances in the foam/textile substrates. Multi-objective optimization has been successfully applied to several areas of electromagnetic design, such as antennas [11], [12], antenna arrays [13], [14] and filters [15], [16]. Here, we propose a novel dedicated textile antenna design strategy based on a multi-objective constrained Pareto optimization that is able to combine resources from suitable simulators and databases to achieve a design that is jointly optimized for different, often conflicting, objectives, followed by a final post-optimization step to accomodate for unexpected deviations in the substrate characteristics. This scheme is illustrated by considering the design of a wearable Galileo E6-band antenna, taking as a starting point

the GPS/E1-band antenna topology presented in [1], which is then optimized in terms of wearablility, by applying a substrate that is almost 50 % thinner, and enhanced for Galileo E6-band reception, by using a different feed line geometry. This antenna is optimized using the proposed strategy to jointly take into account the antenna impedance matching and it's circular polarization, expressed by the axial ratio (AR). Afterwards, different antenna prototypes are fabricated using a foam antenna substrate with variable dielectric properties, and subsequently optimized to accommodate for the substrate deviations.

This chapter is organized as follows. In section 4.2, the Galileo E6-band antenna and its requirements are described. In section 4.3, the proposed dedicated design strategy is sketched.

4.2 Aperture coupled Galileo E6-band antenna

GNSS (Global Navigation Satellite System) services for Civil Protection can benefit greatly from wearable technology. To extend the functionality of wearable satellite based positioning systems, which usually rely on reception of E1/L1-band signals, we propose a compact, wearable textile antenna intended for Galileo signal reception in the E6-band. In terms of specifications, this means that the antenna has to cover a frequency range from 1.26 to 1.3 GHz. In this range, an $|S_{11}|$ lower than -10 dB is enforced, as well as an AR not exceeding 3 dB, in order to ensure right-hand circular polarization. This antenna is designed for integration into rescue-worker garments. This requires a module that is not only compact and flexible, minimizing hindrance of the wearer's range of motion, but also robust, guaranteeing stable performance in harsh conditions. In order to achieve the above-listed requirements, an aperture-coupled microstrip patch topology, as shown in Fig. 4.1, has been selected. This topology is low-profile and the ground plane shields the antenna from the body, reducing its influence on the radiation performance. The aperture coupling reduces the number of vias in the design, increasing robustness to stress occurring when the antenna is bent or compressed. To achieve circular polarization, a Minicircuits QCN-19 [17] discrete hybrid coupler was selected, on the one hand providing a robust circular polarization over a wide frequency range compared to other techniques involving deforming the feed and/or radiating structure, and, on the other hand, leveraging a compact feed circuit, leaving space for the integration of additional electronics on the antenna backside and reducing the vulnerability of the feed circuit to bending influences. The wide band AR characteristic makes the antenna robust against potential frequency shifts incurred by the integration of the antenna into a garment, exposing it to bending and body proximity. The antenna (excluding a small part of the feed network before the quadrature hybrid) is diagonally symmetrical, as indicated in Fig. 4.1. Compared to the antenna presented in [1], the antenna has been redesigned using a substrate with a lower height and a smaller hybrid coupler to enable easier and more

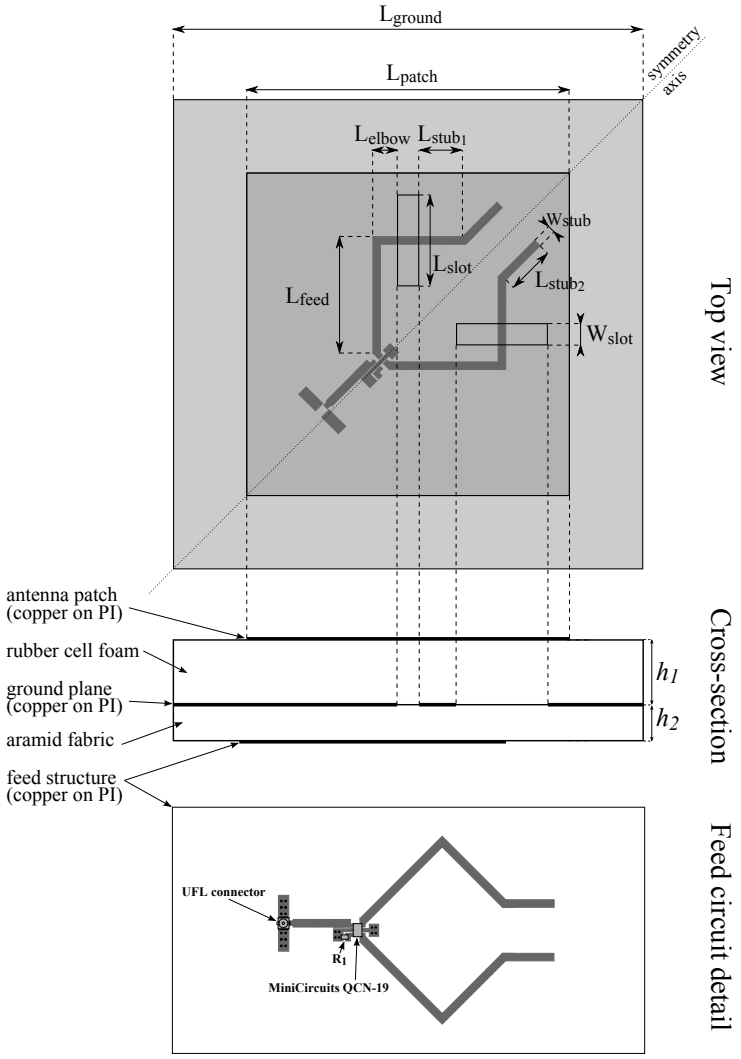

Figure 4.1: Topology of the E6-band Galileo antenna.

comfortable integration into a garment. Moreover, the feedline stubs have been extended along the diagonal to allow more headroom for matching purposes. The materials used in the construction of this antenna are: for the antenna substrate, a closed-cell expanded rubber foam ($h_1 = 3.94$ mm, $\epsilon_r = 1.56$, $tan\ \delta = 0.02$) that is fire-retardant; for the feed substrate, aramid fabric ($h_2 = 400$ µm, $\epsilon_r = 2.15$, $tan\ \delta = 0.02$), commonly found as an outer layer in protective garments; and, for the conductors, copper-on-polyimide film, offering good flexibility and robustness, while allowing an accurate manufacturing process by means of photolithography.

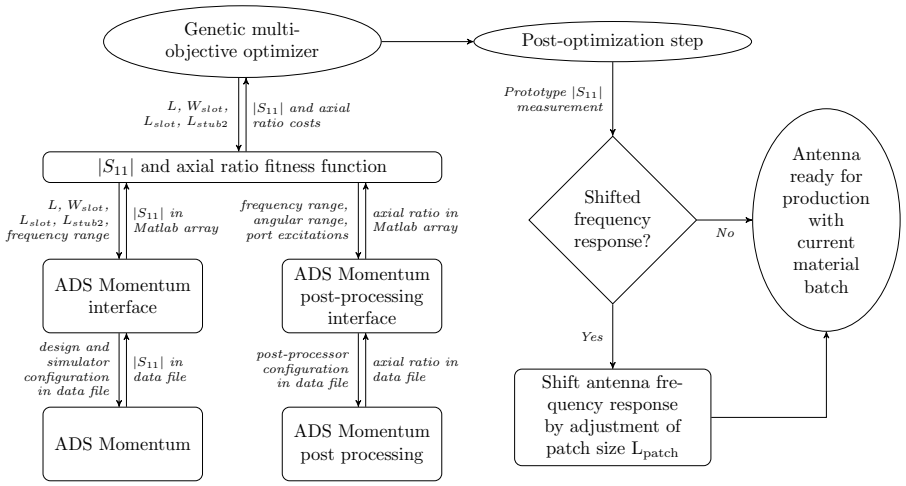

Figure 4.2: Dedicated optimization scheme for the design of the Galileo E6-band antenna.

Of these materials, deviations in the dielectric properties of the antenna substrate have the highest effect on the performance of the manufactured prototype, inducing shifts in the antenna frequency response. The significant geometrical parameters for optimization of the antenna performance are the patch length L_{patch}, the slot width W_{slot}, the slot length L_{slot} and the stub length L_{stub2}. The patch length L_{patch} controls the resonance frequency of the microstrip patch, the slot dimensions W_{slot} and L_{slot} are used to tune the coupling between the feed lines and the patch, and the length of diagonal extension of the feed stubs L_{stub2} is varied to ensure good matching of the antenna to the 50 Ω hybrid coupler. Parameter sweeps, carried out during early design space exploration, show the conflicting nature of the optimization of the antenna bandwidth, on the one side, and the AR, on the other side. While the antenna patch dimensions generally determine the frequency range in which the antenna will operate, increasing the slot dimensions, for example, increases the bandwidth of the antenna by providing a better coupling from the feed lines to the patch at the lower frequencies, but at the same time, it decreases the AR performance at these frequencies. Increasing the feed line stub length improves the AR performance, but, at the same time, decreases the bandwidth. The simultaneous optimization of these parameters is necessary to achieve a right-hand circularly polarized antenna that optimally performs within the Galileo E6-band.

4.3 Dedicated multi-objective constrained Pareto optimization strategy

In Fig. 4.2, the dedicated optimization scheme is outlined. Because the design objectives are conflicting, as discussed in section 4.2, the optimization will not result in a single optimal point, but in a set of Pareto-optimal points, representing the solutions for which an improvement in one objective comes at the cost of another objective. By subsequently constraining this Pareto-front using the design specifications, this allows the designer to make a well-considered trade-off between the conflicting design objectives. At the start, a genetic multi-objective optimizer [18] is used to construct a set of Pareto optimal solutions in terms of $|S_{11}|$ and AR, relying on a suitable combination of simulation tools. After this optimization, a final post-optimization step is applied by measuring the $|S_{11}|$ of a first prototype, allowing a final adjustment to take into account deviations occurring between different material batches of the antenna's protective foam substrate.

4.3.1 Genetic multi-objective optimization

In the first step of the optimization strategy, a genetic optimizer is used to avoid getting stuck in local minima in the large design space. To calculate the fitness functions in terms of $|S_{11}|$ and AR, we rely on Agilent's Advanced Design System (ADS) Momentum and the ADS Momentum post-processing environment, respectively, using interfaces to pass the data from and to Matlab in a suitable format. The $|S_{11}|$ and AR cost functions are defined by:

$$cost_{|S_{11}|} = \sum_i [|S_{11}(f_i)| - |S_{11,lim}|] \tag{4.1}$$

$$cost_{AR} = \sum_i \sum_j [AR(f_i, \theta_j) - AR_{lim}] \tag{4.2}$$

For the $|S_{11}|$ cost function, the limit $|S_{11,lim}|$ was set to -12 dB from 1.26 GHz to 1.3 GHz. Since the hybrid coupler we intend to use is matched to 50 Ω over a broad frequency range, we do not include it in the optimization of the antenna $|S_{11}|$, because it could hide the reflection characteristics of the antenna itself. For the AR, a limit of $AR_{lim} = 2$ dB was imposed for an elevation angle ranging from -30° to 30° in the frequency range from 1.26 GHz to 1.3 GHz, with a 20 MHz step size. To keep the simulation time low, this step size was not chosen smaller, because every frequency at which the AR should be calculated requires an explicit simulation of the antenna structure. For optimization, the antenna's geometrical parameters are allowed to vary within the following ranges:

$$\begin{aligned} &80 \text{ mm} < L_{patch} < 90 \text{ mm} \qquad 4 \text{ mm} < W_{slot} < 8 \text{ mm} \\ &20 \text{ mm} < L_{slot} < 30 \text{ mm} \qquad 10 \text{ mm} < L_{stub2} < 25 \text{ mm} \end{aligned} \tag{4.3}$$

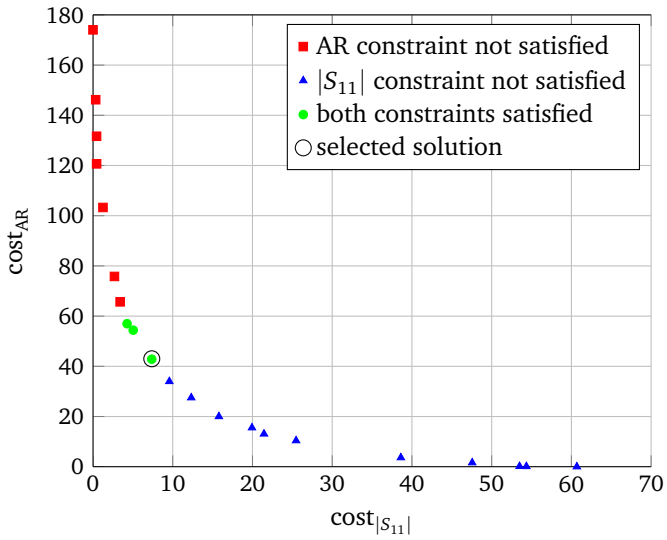

Figure 4.3: Constrained Pareto front resulting from the E6-band antenna optimization (constraints imposed: AR $<$ 3 dB and $|S_{11}| < -10$ dB).

Table 4.1: Dimensions of the optimized antenna.

Parameter	Value [mm]
L_{patch}	84.64
L_{slot}	24.77
W_{slot}	5
L_{stub1}	9.12
L_{stub2}	18.36
W_{stub}	1.6
L_{elbow}	5

The antenna structure is simulated using the ADS Momentum planar 3D full-wave EM-solver available in Agilent's ADS 2009. This solver allows efficient calculation of the planar microstrip patch antenna's characteristics, speeding up the optimization process. For the evaluation of the AR, the ADS Momentum post-processor is used. Reusing the simulation data from the ADS Momentum simulator, this allows a quick calculation of the AR. The reason we combine two ADS simulation tools with an external optimizer, and not with the built-in ADS optimizer, is that the ADS optimizer does not allow automatic optimization of the far-field properties of the antenna. Using our dedicated optimization scheme, manual optimization of two conflicting antenna characteristics is circumvented, and the efficient ADS Momentum electromagnetic full-wave field solver can be used for a comprehensive

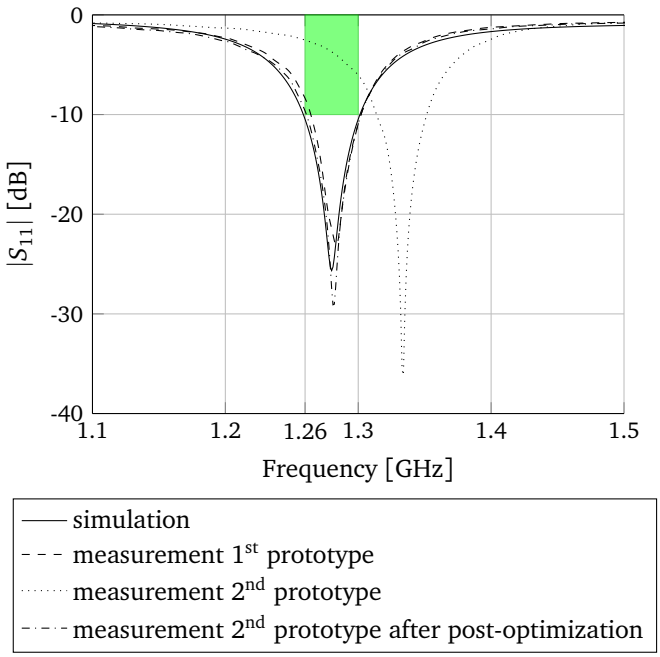

Figure 4.4: Simulated $|S_{11}|$(without hybrid coupler) of the optimized Galileo E6-antenna, together with the -10 dB limit specified by the design requirements (green).

antenna optimization, producing the Pareto front shown in Fig. 4.3. This Pareto front has been constrained using the design requirements for the E6-band antenna put forward in Section 4.2, being $|S_{11}| < -10$ dB and AR < 3 dB from 1.26 GHz up to 1.3 GHz. The green circles indicate the solutions for which both the $|S_{11}|$ and AR constraints are fulfilled. From these Pareto optimal points, we have selected the design with the lowest AR error as the final optimal solution. The dimensions of the optimal antenna are given in Table 4.1.

4.3.2 Post-optimization step

The second step in the optimization strategy takes into account the tolerances on the characteristics of the antenna substrate materials. To this aim, a prototype is constructed using substrate material from a specific material batch. If the dielectric constant of the antenna substrate material deviates from the value applied in the design process, a shift in the antenna's frequency response is noticed. A cost- and time-effective post-optimization step that takes this material tolerance into account, consists of slightly varying the antenna patch size to compensate for the induced frequency shift. The patch is a simple structure, that is quickly manufactured and replaced on an existing prototype. To illustrate this post-optimization

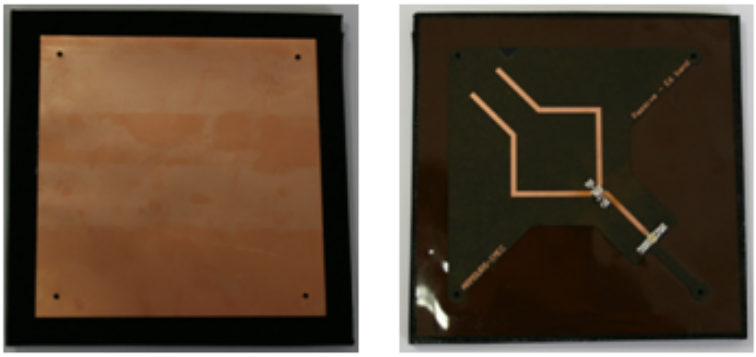

(a) (b)

Figure 4.5: Back (a) and front (b) of the manufactured Galileo E6-band antenna.

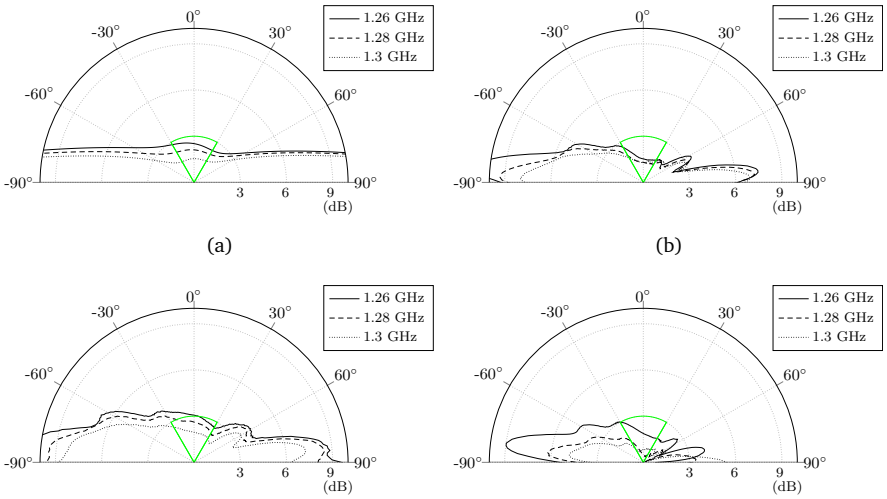

(a) (b)

(c) (d)

Figure 4.6: Simulated (a) and measured ((b), (c) and (d): prototype 1, prototype 2 before post-optimization and prototype 2 after post-optimization, respectively) AR of the Galileo E6-antenna, together with the 3 dB limit specified by the design requirements (green).

step, the optimized antenna was fabricated using antenna substrate foam from two different batches. The fabrication process for both prototypes is the same. The feed layer conductors are defined by means of a specialized photolithographic process for copper-on-polyimide FCBs (flexible circuit boards). The feed circuit is then laminated onto the aramid fabric feed substrate and laser-cut to the desired shape. The antenna ground plane and patch are laser-cut. Making use of accurately defined alignment holes and a custom alignment fixture, the different layers are aligned and glued together by means of a thermally activated adhesive sheet to assemble the complete antenna. The performance of the antenna prototypes is measured in an anechoic room by means of an Agilent PNA-X N5242A Vector Network Analyzer (VNA).

In Fig. 4.4, the measured $|S_{11}|$ of the prototypes is depicted, together with the simulated $|S_{11}|$. Note that the $|S_{11}|$ depicted in Fig. 4.4 is the $|S_{11}|$ of the antenna without the hybrid coupler, as pointed out earlier. The $|S_{11}|$ of the first prototype agrees well with the simulated $|S_{11}|$, whereas the $|S_{11}|$ from the second prototype differs from the simulations. Based on this $|S_{11}|$ measurement, an estimation of the deviation of the dielectric constant of the second material batch is made, and subsequently a new patch size is determined. Compared to the ϵ_r of 1.56 that was used in the first stage of the design, the second substrate material batch exhibits an ϵ_r of 1.46. This is compensated by assembling the second prototype with a patch with a size of 88.2415 x 88.2415 mm. The measured $|S_{11}|$ of this final optimized prototype is also depicted in Fig. 4.4.

The simulated and measured AR of the antenna prototypes is depicted in Fig. 4.6, together with the 3 dB limit specified by the design requirements. The post-optimization step significantly improves the performance of the second prototype. In this way, the antennas fabricated using the second material batch also meet the design requirements.

4.4 Conclusion

A flexible dedicated multi-objective computer-aided optimization scheme for textile antennas is presented, allowing a proprietary design using a genetic multi-objective Pareto optimization linked with appropriately selected simulation tools, together with a material batch-specific post-optimization step consisting of altering the patch size based on a prototype $|S_{11}|$ measurement, to account for tolerances of the unconventional substrate materials used in the textile antenna design process. This optimization scheme is applied to the design of a Galileo E6-band antenna with optimal return loss and AR characteristics. The validity of the strategy is confirmed by means of the construction of two prototypes, using different batches of antenna substrate material. Both antenna prototypes (one after applying the post optimization step to account for the different material batch) meet the design requirements, showing that the proposed optimization strategy is able to efficiently take into account the tolerances on the antenna substrate material.

Acknowledgment

This work was co-funded by the European Commission in the context of the EC-FP7 Galileo.2011.3.1- 2: Collaborative Project, Grant agreement no.: 287166.

References

[1] A. Dierck, H. Rogier, and F. Declercq, “A wearable active antenna for global positioning system and satellite phone”, *IEEE Trans. Antennas Propag.*, vol. 61, no. 2, pp. 532–538, 2013.

[2] A. Dierck, S. Agneessens, F. Declercq, B. Spinnewyn, G.-J. Stockman, P. Van Torre, L. Vallozzi, D. Vande Ginste, T. Vervust, J. Vanfleteren, *et al.*, “Active textile antennas in professional garments for sensing, localisation and communication”, *International Journal of Microwave and Wireless Technologies*, pp. 1–11,

[3] S. Agneessens, P. Van Torre, F. Declercq, B. Spinnewyn, G.-J. Stockman, H. Rogier, and D. Vande Ginste, “Design of a wearable, low-cost, through-wall doppler radar system”, *International Journal of Antennas and Propagation*, vol. 2012, p. 9, 2012.

[4] J. Lilja, P. Salonen, T. Kaija, and P. de Maagt, “Design and manufacturing of robust textile antennas for harsh environments”, *IEEE Trans. Antennas Propag.*, vol. 60, no. 9, pp. 4130–4140, 2012.

[5] J. Lilja, V. Pynttari, T. Kaija, R. Makinen, E. Halonen, H. Sillanpaa, J. Heikkinen, M. Mantysalo, P. Salonen, and P. de Maagt, “Body-worn antennas making a splash: lifejacket-integrated antennas for global search and rescue satellite system”, *IEEE Antennas Propag. Mag.*, vol. 55, no. 2, pp. 324–341, 2013.

[6] E. Kaivanto, M. Berg, E. Salonen, and P. de Maagt, “Wearable circularly polarized antenna for personal satellite communication and navigation”, *IEEE Trans. Antennas Propag.*, vol. 59, no. 12, pp. 4490 –4496, 2011.

[7] G. Orecchini, L. Yang, M. Tentzeris, and L. Roselli, “"Smart shoe": an autonomous inkjet-printed RFID system scavenging walking energy”, in *2011 IEEE Int. Symp. on Antennas and Propagation (APSURSI)*, 2011, pp. 1417 –1420.

[8] A. Serra, P. Nepa, and G. Manara, “A wearable multi antenna system on a life jacket for Cospas Sarsat rescue applications”, in *2011 IEEE Int. Symp. on Antennas and Propagation (APSURSI)*, 2011, pp. 1319 –1322.

[9] Q. Bai and R. Langley, “Crumpling of PIFA textile antenna”, *IEEE Trans. Antennas Propag.*, vol. 60, no. 1, pp. 63 –70, Jan. 2012.

[10] F. Boeykens, H. Rogier, and L. Vallozzi, “An efficient technique based on polynomial chaos to model the uncertainty in the resonance frequency of textile antennas due to bending”, *IEEE Trans. Antennas Propag.*, vol. 62, no. 3, pp. 1253–1260, 2014.

[11] S. Koulouridis, D. Psychoudakis, and J. Volakis, "Multiobjective optimal antenna design based on volumetric material optimization", *IEEE Trans. Antennas Propag.*, vol. 55, no. 3, pp. 594–603, 2007.

[12] S. Koziel and S. Ogurtsov, "Multi-objective design of antennas using variable-fidelity simulations and surrogate models", *IEEE Trans. Antennas Propag.*, vol. 61, no. 12, pp. 5931–5939, 2013.

[13] D. Bianchi, S. Genovesi, and A. Monorchio, "Constrained pareto optimization of wide band and steerable concentric ring arrays", *IEEE Trans. Antennas Propag.*, vol. 60, no. 7, pp. 3195–3204, 2012.

[14] T. H. Nguyen, H. Morishita, Y. Koyanagi, K. Izui, and S. Nishiwaki, "A multilevel optimization method using PSO for the optimal design of an l-shaped folded monopole antenna array", *IEEE Trans. Antennas Propag.*, vol. 62, no. 1, pp. 206–215, 2014.

[15] C. Gazda, I. Couckuyt, H. Rogier, D. Vande Ginste, and T. Dhaene, "Constrained multiobjective optimization of a common-mode suppression filter", *IEEE Trans. Electromagn. Compat.*, vol. 54, no. 3, pp. 704–707, 2012.

[16] S. Goudos and J. Sahalos, "Pareto optimal microwave filter design using multiobjective differential evolution", *IEEE Trans. Antennas Propag.*, vol. 58, no. 1, pp. 132–144, 2010.

[17] Mini-Circuits, *Ultra-small ceramic power splitter/combiner, QCN-19 data sheet*.

[18] K. Deb, *Multi-Objective Optimization using Evolutionary Algorithms*. Chichester, England, 2001: John Wiley & Sons, Ltd., 2001.

5

Dedicated surrogate-model based optimization strategy for a wearable multi-band aperture-coupled stacked patch antenna

Arnaut Dierck, Frederick Declercq, Thomas Vervust, Prashant Singh, Ivo Couckuyt and Hendrik Rogier

Ongoing research

★ ★ ★

Designing robust, wearable antennas for rescue worker systems requires a design strategy that is able to produce antennas that are optimized over a wide bandwidth for often conflicting characteristics, such as impedance matching, axial ratio, efficiency and gain. Advanced antenna topologies can be used to incorporate more functionalities into a single wearable antenna. These advanced topologies require longer simulation times compared to simpler designs. Therefore, in this chapter, a strategy is presented that performs a multi-objective constrained Pareto-optimization by means of surrogate models for reducing the computational cost caused by more complex antenna designs. This strategy is applied to the design of a wearable stacked patch antenna, intended for GNSS reception in the lower and upper L-band.

5.1 Introduction

Smart fabrics and interactive textiles (SFIT) present a great opportunity to increase the functionality of a broad range of applications, providing communication, localization and sensing capabilities in fields ranging from military to search-and-rescue and other civil services. Both in terms of price, by using off-the-shelf fabrics and foams available in textile production processes, as in terms of space, by integrating the antennas into otherwise unused areas of a garment, the cost can be kept low. By applying suitable materials such as (conductive) textiles, foams and 3D-fabrics to realize active circuits and antennas, electronic systems can be unobtrusively integrated into clothing, implementing features that would otherwise require additional, often cumbersome, devices that have to be carried around [1]–[8]. These electronic systems can provide access to services such as positioning, victim localization, vital signs monitoring and environmental hazard sensing, vastly improving the safety and survival chances of both the wearer of the technical garment and the distressed people being aided. Replacing the traditional, rigid, hand-held devices by electronics directly integrated into the wearer's garment, however, does not come without specific design challenges. The placement of the wearable systems inside of a garment makes them susceptible to influences of the proximity of the body. Moreover, the foam and fabric substrates give rise to additional losses and their flexibility, while indispensable for a conformal integration into clothing, makes the antennas vulnerable to bending, potentially affecting their performance [9], [10]. To provide a highly reliable communications link in these conditions, miniaturization of the on-body electronic system is crucial. This approach produces less bulky electronic circuitry, and antennas and improves wearability. The functionalities of different circuits/antennas are combined into more compact electronic units, reducing potential weak links between these devices. When looking at miniaturization from the antenna designer's perspective, it is thus advisable to replace multiple antennas by a single, broad band radiator. Electronics implementing the different functionalities serviced by this antenna can then also be centralized and reduced in size. Circularly polarized aperture-coupled patch antennas provide a versatile topology for wearable, robust user-terminal antennas for satellite communications [1], [2]. To extend the functionality of single-patch antennas without further increasing their footprint, a stacked patch topology can be utilized [11]–[13]. The intricate effect of the different design parameters on the antenna performance, requires a co-optimization of the complete antenna, taking into account the behaviour of feed network, in order to produce an optimally performing design. Designing a high performance antenna means that not only the antenna's impedance matching, in terms of, e.g., $|S_{11}|$, but also it's far-field characteristics have to be optimized. This necessitates a multi-objective optimization, with the goal of finding the Pareto-front, representing the best possible trade-offs for the conflicting design objectives. Pareto fronts, however, require a vast amount of objective function evaluations, increasing the computation time. In order to reduce the computational cost of the optimization procedure, a surrogate model is constructed of the circularly polarized stacked patch antenna. This results in a

dedicated surrogate model-based co-optimization strategy that is able to combine resources from the most suitable simulators and databases to achieve a design that is jointly optimized for different objectives. This strategy is presented by means of the design of a wearable stacked patch antenna for GNSS applications. To our knowledge for the first time in literature, a circularly polarized aperture-coupled stacked patch antenna is designed using textile/flexible materials, resulting in a single, unobtrusive wearable antenna to cover the lower and upper L-band, covering GNSS services such as GPS, Galileo, GLONASS and Beidou [14]. The combination of these services will lead to increased availability, reliability and accuracy. This is a crucial aspect when relying on GNSS in the aforementioned fields such as military applications, rescue worker systems, search-and-rescue equipment and other civil services. This chapter is organized as follows. In section 5.2, the wearable multi-band stacked patch antenna and its requirements are described. In section 5.3, the devised simulation flow and surrogate model-based co-optimization strategy is presented.

5.2 Wearable multi-band stacked patch antenna

To extend the functionality of wearable satellite based positioning systems, which usually rely on reception of E1/L1-band signals, we propose a compact, wearable textile antenna intended for reception of GNSS signals in both the upper and lower L-band. In the lower L-band, coverage from 1.16 to 1.3 GHz is required, enabling Galileo E5/E6, GPS L2/L5 and GLONASS G2/G3 reception. In the upper L-band, coverage from 1.54 to 1.61 GHz is desired, enabling the reception of Galileo E1 (including SAR downlink), GPS L1 and GLONASS G1. In the proposed frequency ranges, an $|S_{11}|$ lower than -10 dB is enforced at the antenna output. Moreover, considering the far-field requirements, the boresight gain should exceed 3 dBi, the axial ratio should not exceed 3 dB, in order to ensure right-hand circular polarization, and the efficiency should remain above 50 %. Since this antenna is designed for integration into rescue-worker garments, a module is required that is not only compact and flexible, minimizing hindrance of the wearer's range of motion, but also robust, guaranteeing stable performance in harsh conditions. In order to achieve the above-listed requirements, an aperture-coupled stacked patch antenna topology, as shown in Fig. 5.1, has been selected. This topology is low-profile and the ground plane shields the antenna from the wearer's body, reducing its influence on the radiation performance. The aperture coupling reduces the number of vias in the design, increasing robustness to stresses occurring when the antenna is bent or compressed. To achieve circular polarization, a feed network consisting of one 180° coupler, followed by two 90° hybrid couplers has been designed. For the 180° coupler, a MiniCircuits SYPJ-2-33+ has been chosen, whereas two MiniCircuits QCN-19 quadrature hybrids form the necessary 90° hybrid couplers. Using discrete elements for the couplers, on the one hand pro-

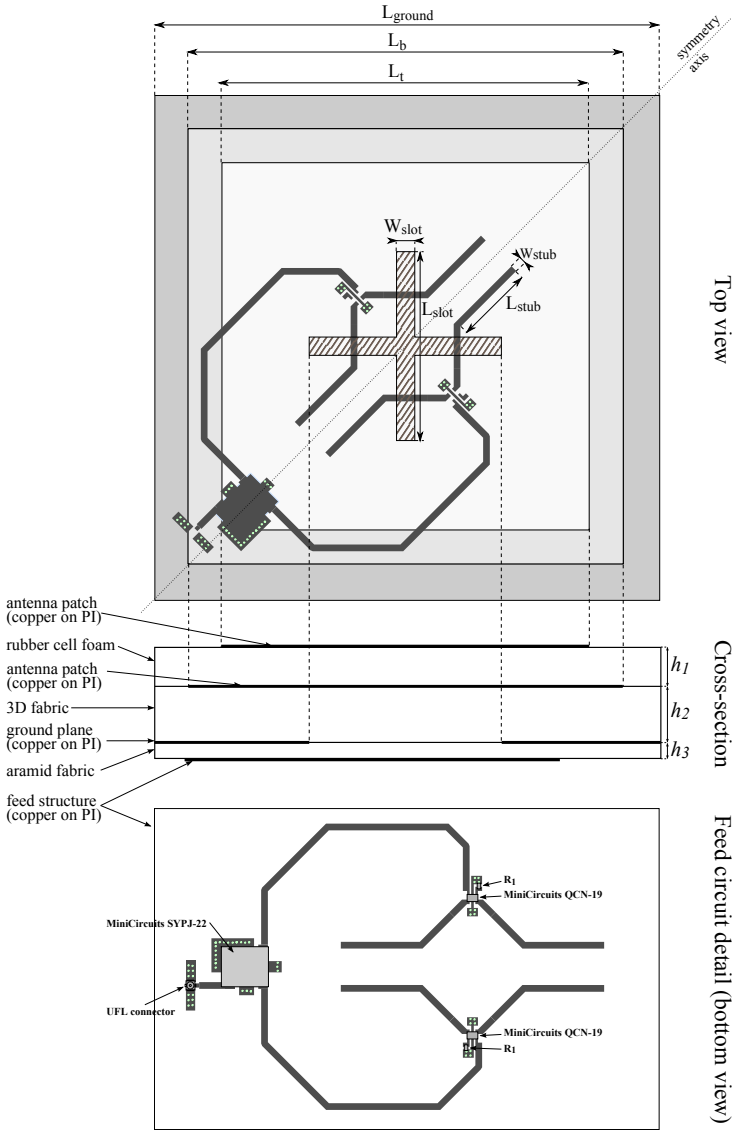

Figure 5.1: Topology of the wearable multi-band stacked patch antenna.

vides a robust circular polarization over a wide frequency range compared to other techniques involving deforming the feed and/or radiating structure, and, on the other hand, leverages a compact feed circuit, leaving space for the integration of additional electronics on the antenna backside and reducing the vulnerability of the feed circuit to bending influences. The wide-band specifications of the discrete

Table 5.1: Electromagnetic properties of the antenna materials.

Substrate	ϵ_r	tan δ	Height (mm)	Materials
Top antenna substrate	1.56	0.02	3.94	Closed-cell rubber-foam
Bottom antenna substrate	1.05	0.001	7.5	3D-fabric
Feed substrate	2.15	0.02	0.4	Aramid fabric

components enable a wide-band circular polarization and matching, making the antenna robust against potential frequency shifts incurred by the integration of the antenna into a garment, by bending or by body proximity. The feed network couples to the stacked antenna patches through a cross-shaped slot, centered in the antenna ground plane. The central position improves the symmetry of the antenna, yielding better circular polarization characteristics. The antenna (excluding small details in the feed network to accommodate the discrete components) is diagonally symmetrical, as indicated in Fig. 5.1. Several high-performance textile materials were used as substrates in the design of the antenna. The top antenna substrate consists of a 3.94 mm thick layer of closed-cell expanded rubber foam that is shock-absorbing and fire-retardant. The bottom antenna substrate is formed by a 3D fabric with a height of 7.5 mm, which is breathable, lightweight and shock absorbing. For the feed substrate, a 400 µm thick layer of tear and flame resistant aramid fabric, commonly found as an outer layer in protective garments, is used. These materials, along with their properties, are listed in Table 5.1. The conductive layers were realized on copper-on-polyimide laminates, consisting of an 18 µm copper film on a 50 µm polyimide carrier. These laminates offer excellent flexibility and robustness, while allowing a highly accurate manufacturing process by means of a dedicated photolithographic process.

The significant geometrical parameters for optimization of the antenna performance are the top patch length L_t, the bottom patch length L_b, the slot width W_{slot}, the slot length L_{slot} and the stub length L_{stub2}. The top and bottom patch lengths L_t and L_b have to be determined simultaneously, as their strong coupling does not allow them to resonate independently. The slot dimensions W_{slot} and L_{slot} are used to tune the coupling between the feed lines and the bottom patch. The length of diagonal extension of the feed stubs L_{stub2} is varied to ensure good matching of the antenna to the 50 Ω hybrid couplers.

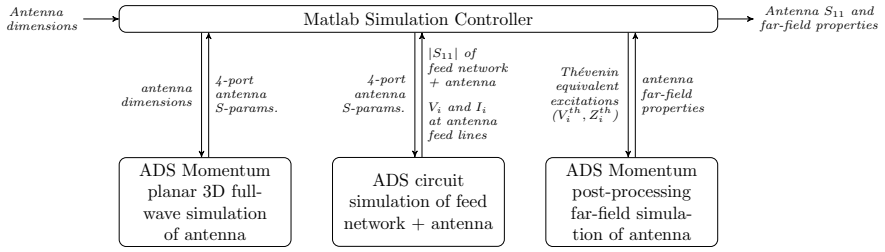

Figure 5.2: Simulation flow for the stacked patch antenna.

5.3 Dedicated surrogate-model based co-optimization strategy

In this section the dedicated surrogate-model based co-optimization strategy will be discussed. First, in section 5.3.1, the devised simulation flow that takes into account the interaction of the antenna feed network and the antenna patch, is presented. Second, the co-optimization of the complete antenna, relying on surrogate models to allow an efficient computation of the optimal result, is further discussed in section 5.3.2.

5.3.1 Proposed co-simulation flow

The complete antenna structure is simulated using Agilent's Advanced Design System (ADS), directed by a dedicated simulation controller implemented in Matlab. The antenna layout is simulated in the ADS Momentum planar 3D full-wave solver. This solver allows an efficient calculation of the planar microstrip patch antenna's characteristics. For incorporating the discrete components, the layout of the feed network is imported into the ADS schematic solver, where the S-parameter representations of the discrete components are connected to the feed circuit layout. For the evaluation of the far-field properties, the ADS Momentum post-processor is used. Reusing the layout simulation data from the ADS Momentum simulator, allows a quick calculation of the far-field behavior. The reason the different ADS simulation tools are combined using an external simulation controller, is that ADS does not allow automatic calculation of the far-field properties of the antenna while taking into account the discrete components in the feed network. Our dedicated simulation flow circumvents manual simulation of the different antenna characteristics, allowing an automatic, efficient co-simulation of the antenna and its feed network. The general outline of the proposed simulation flow is depicted in figure 5.2. To perform a co-simulation of the feed structure and the radiating patch, the different simulation steps are coupled by means of a central simulation controller. This controller takes as input a vector with the dimensions of the antenna, and outputs the antenna $|S_{11}|$ and far-field characteristics (gain, AR and efficiency), invoking the simulation tools in the order required for taking into account the in-

teractions between the feed structure and the antenna structure. At the basis of the simulation, is the antenna designed in ADS Momentum. In the simulation flow, this antenna design is split into two parts, as depicted in Fig. 5.3. The one part consists of the feed network. The layout of the feed network, consisting of the microstrip transmission lines interconnecting the different discrete components, is simulated in ADS Momentum, and subsequently coupled to the S-parameter models of the discrete components that are supplied by the manufacturer, in the ADS schematic simulation environment. In this way, a 5-port S-parameter description of the feed network is obtained. The other part of the antenna design consists of the stacked antenna patches and their feed lines. This structure is designed in ADS Momentum, and subsequently imported into Matlab to allow manipulation of the antenna's geometry. In the first step of the simulation flow, the antenna geometry is updated based on the input values of the simulation controller, and, subsequently, a Momentum simulation is performed on the updated antenna structure. In a second step, the resulting 4-port S-parameters of the radiating stacked patch antenna element are combined with the 5-port S-parameter description of the antenna feed network, in order to calculate both the resulting reflection coefficient at the feed network input, as well as the voltages and currents that are imposed on the antenna feed lines when connected to the feed network. The currents and voltages are defined as shown in Fig. 5.4. These voltages and currents are used to calculate the Thévenin equivalent excitations at the antenna terminals. By relying on the Z-matrix representation of the feed network

$$\begin{bmatrix} V_1 \\ V_2 \\ \vdots \\ V_5 \end{bmatrix} = \begin{bmatrix} Z_{11} & Z_{12} & \cdots & Z_{15} \\ Z_{21} & Z_{22} & \cdots & Z_{25} \\ \vdots & \vdots & \ddots & \vdots \\ Z_{51} & Z_{52} & \cdots & Z_{55} \end{bmatrix} \begin{bmatrix} I_1 \\ I_2 \\ \vdots \\ I_5 \end{bmatrix},$$

it is seen that

$$V_i = Z_{ii} I_i + \sum_{\substack{j=1 \\ j \neq i}}^{5} Z_{ij} I_j,$$

from which the Thévenin equivalent voltages and impedances can be identified as

$$V_i^{th} = \sum_{\substack{j=1 \\ j \neq i}}^{5} Z_{ij} I_j$$

and

$$Z_i^{th} = Z_{ii}.$$

In a third and final step, the Thevenin equivalent generators are connected to the appropriate antenna terminals, as shown in Fig. 5.5, in order to simulate the antenna's far-field behavior by calling ADS Momentum's post-processing environment. The $|S_{11}|$ and far-field characteristics of the complete antenna are subsequently delivered as the output of the simulation controller.

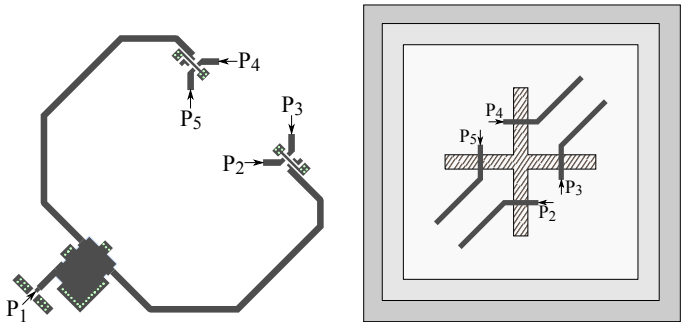

Figure 5.3: Feed network (a) and radiating stacked patches (b) of the dual-band aperture-coupled stacked patch antenna.

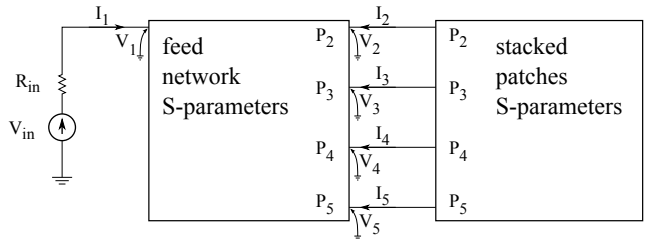

Figure 5.4: Calculation of the voltages and currents on the antenna terminals under excitation by the feed network using ADS AC simulation.

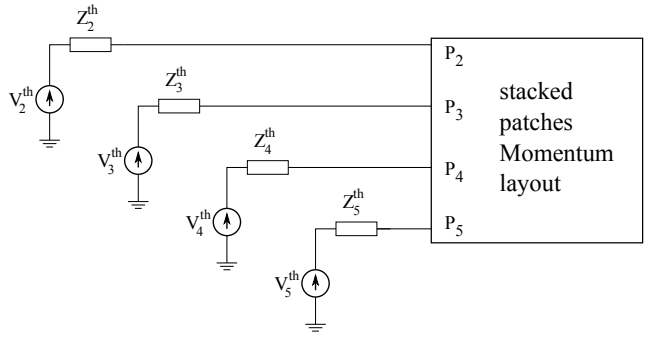

Figure 5.5: Stacked patch antenna connected to Thévenin equivalent excitations for far-field simulation using Momentum post-processing simulation.

5.3.2 Surrogate model-based co-optimization

To speed up the optimization process, a surrogate modeling approach is implemented, by means of the SUrogate MOdelling (SUMO) Toolbox [15], [16]. The surrogate-based optimization (SBO) [17], [18] allows to determine Pareto-optimal solutions, while avoiding prohibitively large amounts of expensive simulations. First, an initial cheap surrogate model is constructed to guide the sampling process. A multi-objective formulation of the probability of improvement (PoI) is used as a sampling scheme. This directs the selection of new samples that have to be evaluated to regions where improvement of the objectives is expected, avoiding unnecessary, expensive simulations. In this way, a multi-objective optimization is performed, optimizing antenna $|S_{11}|$, gain and axial ratio, where the $|S_{11}|$ should be lower than -10 dB, the gain should be higher than 3 dB, and the AR should be lower than 3 dB. The resulting Pareto-front is constrained according to the specifications. The design variables that are optimized are the top patch length L_t, the bottom patch length L_b, the slot width W_{slot}, the slot length L_{slot} and the stub length L_{stub}. During the optimization, these parameters are allowed to vary within the following ranges:

$$\begin{aligned} &70 \text{ mm} < L_b < 95 \text{ mm} \qquad 2 \text{ mm} < W_{slot} < 8 \text{ mm} \\ &70 \text{ mm} < L_t < 95 \text{ mm} \qquad 20 \text{ mm} < L_{slot} < 60 \text{ mm} \\ &10 \text{ mm} < L_{stub} < 30 \text{ mm} \end{aligned} \tag{5.1}$$

The cost functions for $|S_{11}|$, gain and AR are defined as follows, in the frequency bands 1.16 - 1.3 GHz and 1.54 - 1.61 GHz:

$$cost_{|S_{11}|} = max(|S_{11}(f)|) \tag{5.2}$$

$$cost_{gain} = -min(gain(f)) \tag{5.3}$$

$$cost_{AR} = max(AR(f)) \tag{5.4}$$

These cost functions were minimized by means of an SBO using radial basis functions (RBF) using only 200 simulations. The initial design space consisted of a 50 point latin hypercube complemented with the edge points of the design space, resulting in 82 points. The Pareto-front resulting from this SBO is constrained using the following constraints:

$$constraint_{|S_{11}|} : |S_{11}(f)| < -10 \tag{5.5}$$

$$constraint_{gain} : gain(f) > 3 \tag{5.6}$$

$$constraint_{AR} : AR(f) < 3 \tag{5.7}$$

The resulting constrained Pareto-front is depicted in Fig. 5.6.

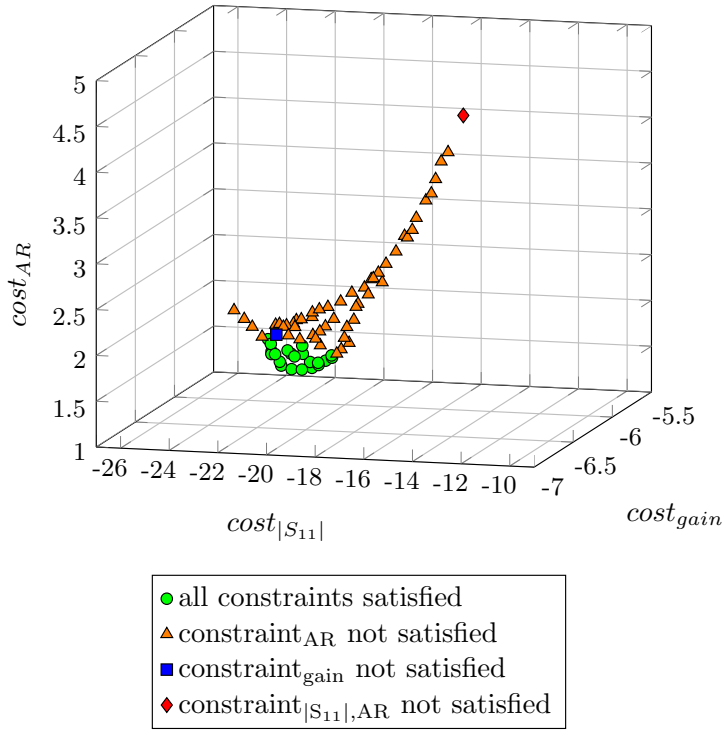

Figure 5.6: Pareto-front resulting from the SBO of the stacked patch antenna.

From the solutions satisfying all constraints, three points were selected to take a more detailed look at the resulting antenna performance. In Figs. 5.7 to 5.10, the simulated $|S_{11}|$, gain, AR and efficiency of these three Pareto-optimal solutions is depicted. The antenna dimensions corresponding to these points are listed in Table 5.2. From the simulated antenna performance plots, it is clearly seen that the Pareto-optimal designs meet all design requirements, even showing a margin on the frequency range in which these requirements are met. This indicates the design will have a certain robustness towards potential resonant frequency shifts due to antenna bending, on the one hand, and tolerances on the used antenna substrate materials, on the other hand.

After this optimization step, antenna prototypes will be fabricated and subjected to measurements, in order to validate the presented optimization strategy and demonstrate the performance of the proposed wearable textile multi-GNSS antenna.

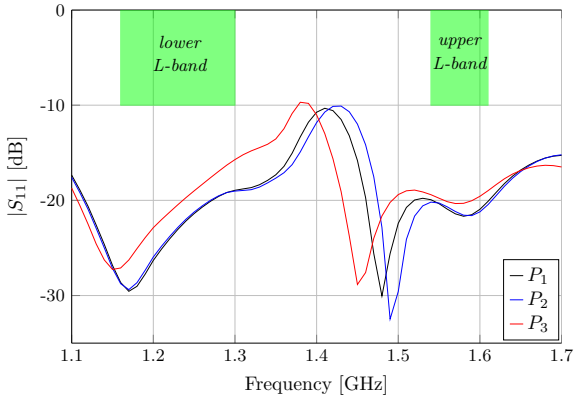

Figure 5.7: Simulated $|S_{11}|$ of the three selected Pareto-optimal designs.

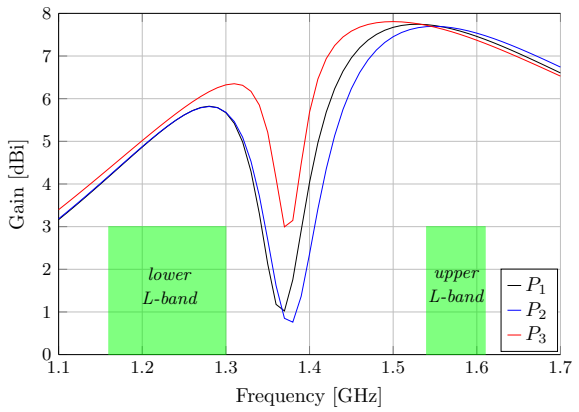

Figure 5.8: Simulated gain of the three selected Pareto-optimal designs.

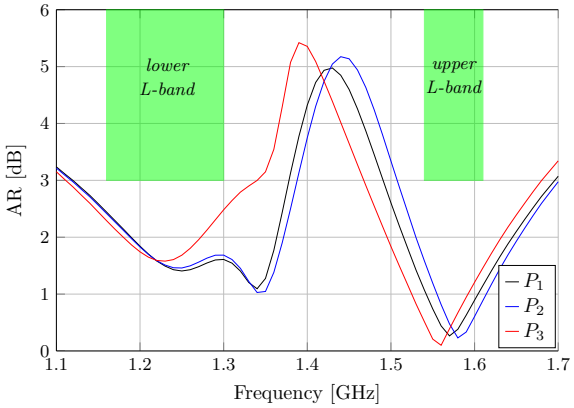

Figure 5.9: Simulated AR of the three selected Pareto-optimal designs.

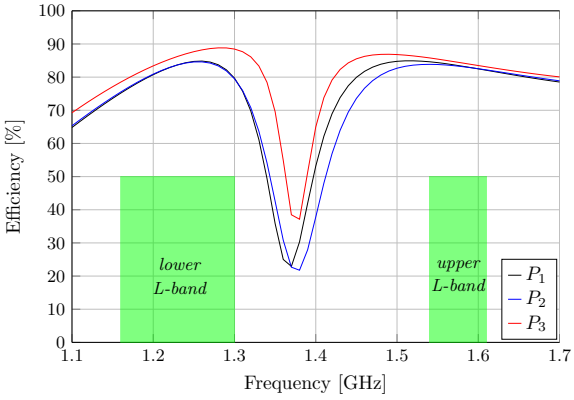

Figure 5.10: Simulated efficiency of the three selected Pareto-optimal designs.

Table 5.2: Dimensions of the three selected Pareto-optimal designs.

Selected design	$L_t(mm)$	$L_b(mm)$	$L_{slot}(mm)$	$W_{slot}(mm)$	$L_{stub}(mm)$
P_1	82.018	82.097	41.210	6.415	26.341
P_2	82.264	80.903	41.586	6.317	26.288
P_3	79.537	84.838	43.688	6.6257	23.100

5.4 Conclusion

Designing robust, wearable antennas for rescue worker systems requires a design strategy that is able to produce antennas that are optimized over a wide bandwidth for often conflicting characteristics such as impedance matching, axial ratio, efficiency and gain. Advanced antenna topologies can be used to incorporate more functionalities into a single wearable antenna. These advanced topologies increase simulation times compared to simpler designs. Therefore, in this chapter, a strategy is presented that performs a multi-objective constrained Pareto-optimization by means of surrogate models for reducing the computational cost caused by more complex antenna designs. This strategy is applied to the design of a wearable stacked patch antenna, intended for GNSS reception in the lower and upper L-band. Currently, the simulation flow is implemented, and a surrogate model based constrained multi-objective optimization has been performed, resulting in several Pareto-optimal designs meeting the specifications. The next step is to validate the presented optimization strategy and the performance of the proposed wearable textile multi-GNSS antenna by means of measurements on antenna prototypes.

Acknowledgment

This work was co-funded by the European Commission in the context of the EC-FP7 Galileo.2011.3.1- 2: Collaborative Project, Grant agreement no.: 287166.

References

[1] A. Dierck, H. Rogier, and F. Declercq, “A wearable active antenna for global positioning system and satellite phone”, *IEEE Trans. Antennas Propag.*, vol. 61, no. 2, pp. 532–538, 2013.

[2] A. Dierck, S. Agneessens, F. Declercq, B. Spinnewyn, G.-J. Stockman, P. Van Torre, L. Vallozzi, D. Vande Ginste, T. Vervust, J. Vanfleteren, *et al.*, “Active textile antennas in professional garments for sensing, localisation and communication”, *International Journal of Microwave and Wireless Technologies*, pp. 1–11,

[3] S. Agneessens, P. Van Torre, F. Declercq, B. Spinnewyn, G.-J. Stockman, H. Rogier, and D. Vande Ginste, “Design of a wearable, low-cost, through-wall doppler radar system”, *International Journal of Antennas and Propagation*, vol. 2012, p. 9, 2012.

[4] J. Lilja, P. Salonen, T. Kaija, and P. de Maagt, “Design and manufacturing of robust textile antennas for harsh environments”, *IEEE Trans. Antennas Propag.*, vol. 60, no. 9, pp. 4130–4140, 2012.

[5] J. Lilja, V. Pynttari, T. Kaija, R. Makinen, E. Halonen, H. Sillanpaa, J. Heikkinen, M. Mantysalo, P. Salonen, and P. de Maagt, “Body-worn antennas making a splash: lifejacket-integrated antennas for global search and rescue satellite system”, *IEEE Antennas Propag. Mag.*, vol. 55, no. 2, pp. 324–341, 2013.

[6] E. Kaivanto, M. Berg, E. Salonen, and P. de Maagt, “Wearable circularly polarized antenna for personal satellite communication and navigation”, *IEEE Trans. Antennas Propag.*, vol. 59, no. 12, pp. 4490 –4496, 2011.

[7] G. Orecchini, L. Yang, M. Tentzeris, and L. Roselli, “"Smart shoe": an autonomous inkjet-printed RFID system scavenging walking energy”, in *2011 IEEE Int. Symp. on Antennas and Propagation (APSURSI)*, 2011, pp. 1417 –1420.

[8] A. Serra, P. Nepa, and G. Manara, “A wearable multi antenna system on a life jacket for Cospas Sarsat rescue applications”, in *2011 IEEE Int. Symp. on Antennas and Propagation (APSURSI)*, 2011, pp. 1319 –1322.

[9] Q. Bai and R. Langley, “Crumpling of PIFA textile antenna”, *IEEE Trans. Antennas Propag.*, vol. 60, no. 1, pp. 63 –70, Jan. 2012.

[10] F. Boeykens, H. Rogier, and L. Vallozzi, “An efficient technique based on polynomial chaos to model the uncertainty in the resonance frequency of textile antennas due to bending”, *IEEE Trans. Antennas Propag.*, vol. 62, no. 3, pp. 1253–1260, 2014.

[11] D. M. Pozar and S. Duffy, “A dual-band circularly polarized aperture-coupled stacked microstrip antenna for global positioning satellite”, *IEEE Trans. Antennas Propag.*, vol. 45, no. 11, pp. 1618–1625, 1997.

[12] M. Ali, A. T. M. Sayem, and V. Kunda, “A reconfigurable stacked microstrip patch antenna for satellite and terrestrial links”, *IEEE Trans. Veh. Technol.*, vol. 56, no. 2, pp. 426–435, 2007.

[13] J. Li, H. Shi, H. Li, and A. Zhang, “Quad-band probe-fed stacked annular patch antenna for gnss applications”, *IEEE Antennas Wireless Propag. Lett.*, vol. 13, pp. 372–375, 2014.

[14] J. Wang, “Antennas for Global Navigation Satellite System (GNSS)”, *Proceedings of the IEEE*, vol. 100, no. 7, pp. 2349–2355, 2012.

[15] D. Gorissen, I. Couckuyt, P. Demeester, T. Dhaene, and K. Crombecq, “A surrogate modeling and adaptive sampling toolbox for computer based design”, *The Journal of Machine Learning Research*, vol. 11, pp. 2051–2055, 2010.

[16] (2014). SUMO - SUrrogate MOdeling Lab, [Online]. Available: `http://www.sumo.intec.ugent.be/`.

[17] I. Couckuyt, D. Deschrijver, and T. Dhaene, “Fast calculation of multiobjective probability of improvement and expected improvement criteria for pareto optimization”, English, *Journal of Global Optimization*, pp. 1–20, 2013.

[18] P. Singh, I. Couckuyt, F. Ferranti, and T. Dhaene, “A constrained multi-objective surrogate-based optimization algorithm”, in *Evolutionary Computation (CEC), 2014 IEEE Congress on*, 2014, pp. 3080–3087.

6

Highly flexible, low loss feed structure for active wearable aperture-coupled antennas with radically trimmed substrate

Arnaut Dierck, Frederick Declercq, Thomas Vervust, and Hendrik Rogier

Ongoing research

★★★

In an effort to improve the flexibility of active wearable aperture coupled patch antennas applied in smart textile systems, a laser shaping technique for the antenna feed substrate is presented. The technique consists of the removal of most of the antenna feed substrate, up to very close distances to the microstrip interconnects and in close vicinity to the coupling slots in the antenna ground plane. On the one hand, this changes the effective dielectric constant of the substrate, influencing the performance of the impedance-controlled designed RF circuitry, and the aperture coupling between the feed lines and the radiating structure. On the other hand, the removal of lossy, textile substrate material surrounding the RF interconnections has the potential to reduce losses in the feed circuit. By taking into account the effects of this altered substrate, design guidelines can be defined to produce high performance, light-weight and flexible wearable antenna designs. In particular, for active antennas, this offers the opportunity to integrate an increasing amount of electronics on the antenna's feed substrate, without compromising the wearability of the antenna. The proposed feed substrate trimming technique is validated by means of two antenna prototypes, one with a full feed substrate, and one with a reduced substrate.

6.1 Introduction

Since some time now, increasingly smaller, cheaper and more powerful electronics pave the way towards a true Internet of Things (IoT). Smart fabrics and interactive textiles (SFIT) are a logical part of this IoT, and offer great potential to increase the functionality in a wide gamut of applications at a low cost, as well in terms of price as space. Unobtrusively implementing advanced features into garments can benefit, for example, healthcare, civil and military services. This unobtrusive integration of electronic systems into garments can be achieved by using suitable materials, such as (conductive) textiles, foams and 3D-fabrics, to realize active circuits and antennas [1]–[8]. For rescue workers, having access to services such as positioning, victim localization, vital signs monitoring and environmental hazard sensing can mean the difference between life and death. Replacing the traditional, rigid, hand-held devices by electronics directly integrated into the wearer's garment, however, does not come without specific design challenges. In smart textile systems, an unobtrusive integration of the different components is essential. However, this objective is not straightforward. In the active antenna's fabrication process, the RF circuitry is directly integrated onto the flexible antenna. This offers increased performance by eliminating lossy wearable RF connections between the antenna and the active circuit, and it enables full-wave/circuit co-design and co-optimization, e.g. by matching the antenna impedance directly to the active circuit's optimal input impedance [9]. Moreover, this approach improves robustness by reducing potential weak links between the antenna interconnects and the active circuitry, in the meanwhile making the complete wearable system more compact by eliminating the need for separate antennas and circuits. Copper-on-polyimide films

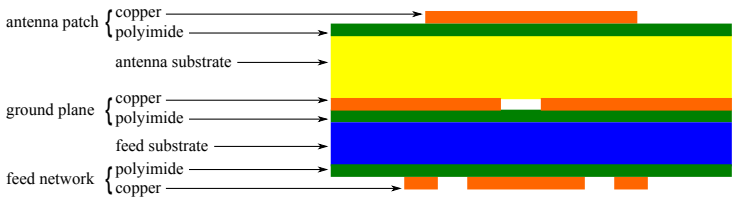

Figure 6.1: Sketch of the material stack used for wearable aperture-coupled patch antennas.

offer an ideal solution for the RF circuit integrated in an active wearable antenna, allowing an accurate fabrication of the flexible RF interconnections. However, when laminated onto a textile substrate, the flexibility is significantly reduced, and the textile substrate introduces dielectric losses. Therefore, we propose a technique involving laser cutting of the textile substrate around the RF circuitry, effectively removing the substrate up to very close distances to the conductive structures. On the one hand, this will influence the behavior of the transmission lines on the feed circuit, including their coupling to the antenna patch through the apertures in the groundplane. On the other hand, this improves significantly the flexibility of the design, by almost completely eliminating a layer from the antenna substrate stack.

This chapter is organized as follows. In section 6.2, the proposed laser trimming technique is detailed. In section 6.3, a proof-of-principle is documented, comparing the performance of a conventional and a radically trimmed design.

6.2 Proposed laser trimming technique

The aperture-coupled microstrip patch antenna topology offers several benefits for wearable antenna realizations. First and foremost, like their probe-fed counterparts, they provide radiation in a semi-hemisphere, shielding the radiating patch from the body by means of a ground plane. Using an adequately large ground plane, this practically eliminates influence of the body on wearable microstrip patch antennas. The aperture-coupled topology, more specifically, exhibits additional interesting properties. From an integration point of view, it eliminates vias through the, often thick, antenna substrate. In wearable applications, such vias present potential failure hotspots when the antenna is exposed to stresses, such as bending or compression. Because the feed structure is integrated behind the ground plane, it is shielded from the antenna radiation, making the aperture-coupled topology very appealing for the integration of active electronics on the antenna's backside. Moreover, the coupling slot, acting as an additional resonator besides the patch, is able to leverage wider bandwidths when compared to probe-fed patch antennas [10].

The material stack that is used here to produce wearable active aperture coupled patch antennas is depicted in Fig. 6.1. Essentially, this is a five-layer structure,

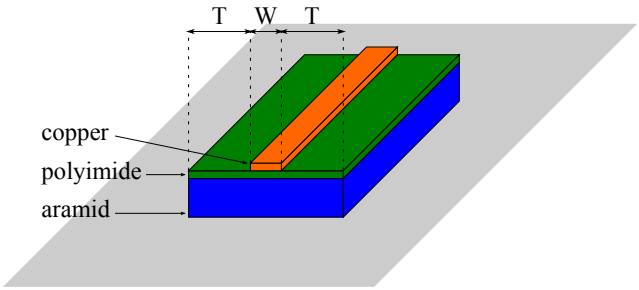

Figure 6.2: Sketch of microstrip feed line on a laser-structured substrate.

consisting of three conductive layers and two dielectric substrates. The conductive layers can be realized by conductive (stretchable) textiles and thin laminates of copper on a polymer carrier, such as polyimide (PI). These copper-on-PI laminates provide excellent flexibility, while allowing accurate definition of intricate patterns by means of photolithographical process. This makes the copper-on-PI laminate an ideal candidate for manufacturing the feed layer conductors. Mechanical tests have pointed out that, after lamination, the assembled five-layer structure, depicted in Fig. 6.1, loses a great deal of the flexibility that is present in the separate materials. However, when the feed conductor layer and the feed substrate are removed, the material stack exhibits a high degree of flexibility, especially when the ground plane and antenna patch conductors are realized using conductive (stretchable) textiles. For wearable applications, the flexibility of the integrated devices is essential, greatly increasing the comfort of the wearer and making the integrated smart textile system less obtrusive. Therefore, we propose a technique wherein the stack consisting of the feed conductor and the feed substrate is radically reduced by means of laser ablation, enabling an accurate patterning. As shown in Fig. 6.2, the feed substrate, together with the polyimide layer, is cut away up to a distance T from the conductors that are defined on the copper-on-PI laminate. In this way, a large part of the redundant feed substrate is removed. Doing this greatly increases the flexibility of the 5-layered stack, because the two layers of the feed flexible circuit board (FCB) are eliminated over a large part of the feed FCB surface. Moreover, removing redundant polyimide from the feed FCB increases the breathability of the wearable antenna. Also, the removal of the redundant aramid reduces the moisture retention of the feed substrate, which can cause additional losses and changes in the effective permittivity [11]. Especially for active wearable antennas, this technique allows to guarantee high flexibility and breathability of the antenna, while permitting electronic circuitry to be integrated on the feed FCB.

Influence of the substrate trimming on the microstrip impedance is expected to be negligible as long as the ratio $T/W > 1$, where T is the width of the substrate on either side of the microstrip with width W [12]. This observation is also supported by a set of simulations performed in CST Microwave Studio, where a microstrip interconnect and an aperture coupled patch antenna (at 1.575 GHz

and at 2.45 GHz) have been simulated with a lossy feed substrate ($\epsilon_r = 2.15$, $tan\ \delta = 0.02$, $h = 400$ µm) with variable width. To increase the flexibility of the wearable antenna design, the limit $T/W > 1$ is not a real restriction, since it enables that the largest part of the feed substrate is cut away, as seen in Fig. 6.7 in section 6.3. Furthermore, from the CST simulations, it is noticed that the influence of the trimmed substrate on the $|S_{11}|$, gain, front-to-back ratio and efficiency of the antenna is very small, even when going below the limit $T/W > 1$. Even for values up to $T/W = 0.6$, the $|S_{11}|$ shifts are limited to a range of 2 MHz around the value for an untrimmed feed substrate. The gain fluctuation stays below 0.1 dB, whereas the front-to-back ratio change is limited to 0.5 dB. This shows that the back-radiation increases slightly for decreasing values of T, however, the change is sufficiently low to retain good antenna functionality. The variations in the antenna efficiency are limited to 1 %. The effects of the trimmed substrate on the antenna's far-field properties are sufficiently small to guarantee a stable high antenna performance, and if measured, the degradation in the far-field performance due to the trimmed feed substrate would fall within the measurement tolerances. Simulations performed on a microstrip interconnect (from 1 to 3 GHz) with a variable substrate width T reveal a decrease of the transmission loss when T decreases. This decrease, however, is only of the order of 0.01 dB for a substrate material with a loss tangent $tan\ \delta = 0.02$, such as aramid. While this decrease is not really significant for the substrate material used in the textile antenna fabrication method discussed here, it shows the potential of the feed substrate structuring technique to lower transmission losses, which can be of more importance when working with lossier substrate materials.

6.3 Comparison between conventional and radically trimmed design

As a proof of principle, we have constructed two prototypes of a wearable Galileo L1-band antenna [2]. The prototypes are fabricated using copper-on-PI conductive layers. To further increase flexibility, geometrically simple shapes, such as the antenna patch and ground plane, can be realized using conductive (stretchable) fabrics. This was not done here, in order to allow the use of antenna patch and ground plane conductors that were fabricated previously, and were readily available. Also, for the purpose of evaluating the performance of the trimmed FCB, this suffices. As depicted in Fig. 6.3, the antenna relies on an aperture-coupled microstrip patch topology. The radiating patch is coupled to the feed lines through two perpendicular slots in the ground plane. In the feed network, a discrete quadrature hybrid coupler provides a 90° phase difference to the two perpendicular modes excited on the antenna patch, generating circular polarization. This antenna is intended for reception of the Galileo E1-band, including the Search-and-Rescue (SAR) downlink. The specifications of this antenna are, in the range of 1.544 to 1.61 GHz, an $|S_{11}| < -10$ dB, a gain > 3 dB, an AR < 3 dB and an efficiency > 50 %. As

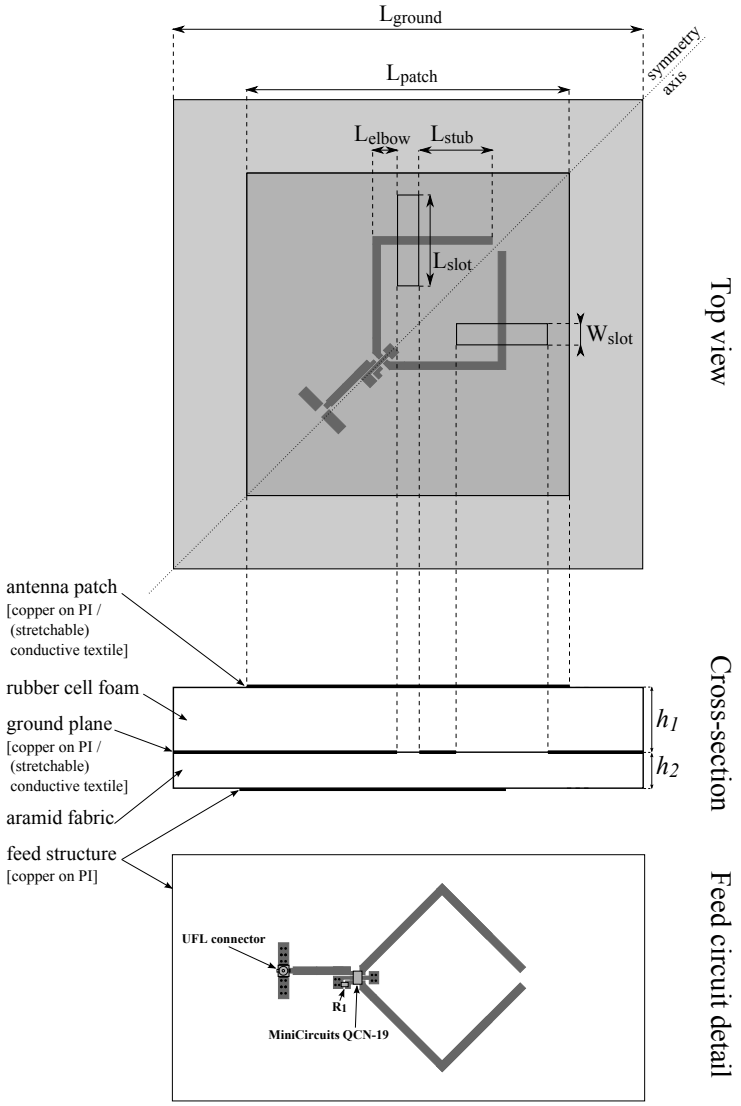

Figure 6.3: Aperture-coupled microstrip patch topology used for the wearable Galileo E1-band antenna.

shown in Fig. 6.7, the one prototype is fabricated using the conventional material stack, whereas the other one is manufactured using the reduced material stack, where the feed substrate is structured by means of laser ablation, with a value of $T/W = 0.6$, to illustrate the lower limit case. Subsequently, the antenna prototype performance is measured in an anechoic room by means of an Agilent N5245A PNA-X Vector Network Analyzer. The measurements are performed between 1.1

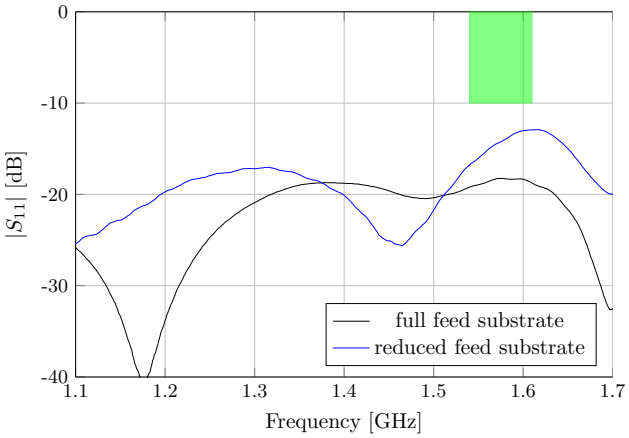

Figure 6.4: Measured $|S_{11}|$ of the Galileo L1-band wearable antenna prototypes.

and 1.7 GHz, which corresponds to the frequency range of the Scientific Atlanta type 1.1 standard gain horn. In Fig. 6.4, the $|S_{11}|$ of the two antenna prototypes is depicted. It is seen that both antenna prototypes fulfill the design requirements. A difference is noticed between the $|S_{11}|$ of the antenna with the conventional feed substrate and the antenna with the trimmed feed substrate. This difference, however, is not attributed to the trimmed feed substrate. The tolerances on the discrete components, such as the hybrid quadrature coupler, and the fact that the components and vias from the feed to the ground plane are hand soldered, contribute to the difference in $|S_{11}|$. In Fig. 6.5, it is seen that, indeed, the different $|S_{11}|$ values of the two prototypes are not related to their antenna performance. The gain of both the conventional and the laser-trimmed prototype show a nice agreement. Also the axial ratios of the two prototypes, depicted in Fig. 6.6, are in good agreement. Differences in the axial ratio are most likely caused by tolerances on the amplitude balance and phase difference of the discrete hybrid coupler. As can be seen from Table 6.1, the efficiencies of the two prototypes exhibit an excellent agreement. The high overall agreement between the two prototypes, shows that the laser-trimming technique offers great potential to increase the flexibility of wearable antennas, without sacrificing performance. However, while this technique has been validated fully (simulations and measurements) for an aperture-coupled patch antenna operating in the vicinity of 1.575 GHz and, with simulations only, for an aperture-coupled patch antenna operating in the vicinity of 2.45 GHz, further simulations and validation by means of measurements should be considered when generalizing the proposed design guideline, for example, taking into account a larger frequency range and different substrate materials.

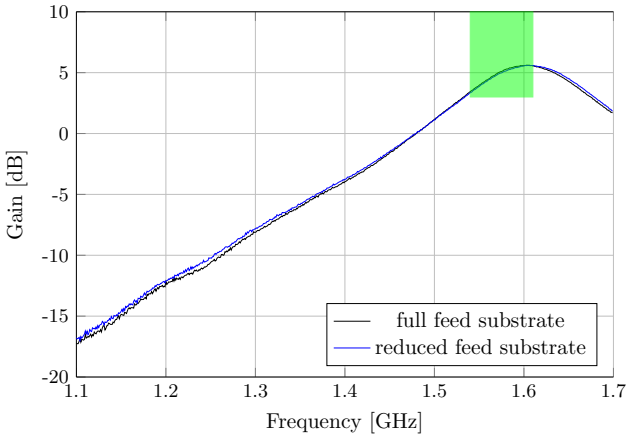

Figure 6.5: Measured gain of the Galileo L1-band wearable antenna prototypes.

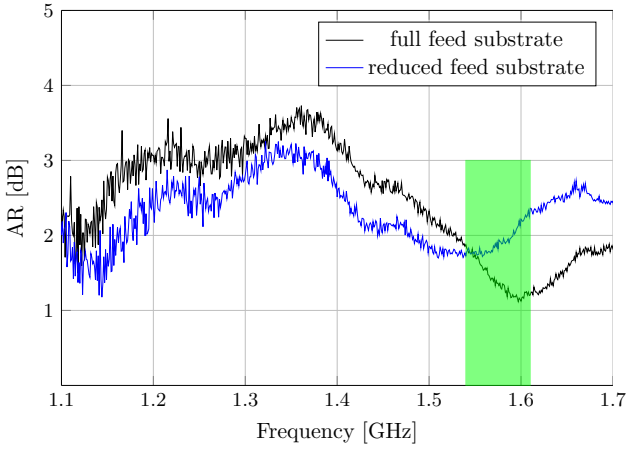

Figure 6.6: Measured AR of the Galileo L1-band wearable antenna prototypes.

Table 6.1: Efficiencies of the conventional and the laser-trimmed wearable Galileo E1 antenna.

Frequency (GHz)	Conventional antenna efficiency (%)	Laser-trimmed antenna efficiency (%)
1.54	54.47	55.22
1.575	77.27	78.72
1.61	87.32	86.2

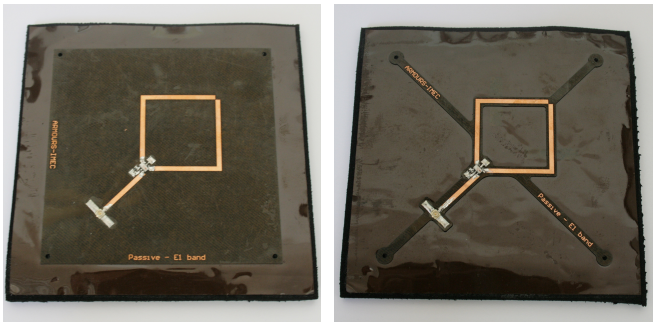

(a) (b)

Figure 6.7: Picture of the antenna prototype with the full feed substrate (a) and the reduced feed substrate (b).

6.4 Conclusion

In an effort to improve the flexibility of active wearable aperture coupled patch antennas applied in smart textile systems, a laser shaping technique for the antenna feed substrate is presented. The technique consists of the removal of most of the antenna feed substrate, up to very close distances to the microstrip interconnects and in close vicinity to the coupling slots in the antenna ground plane. On the one hand, this changes the effective dielectric constant of the substrate, influencing the performance of the impedance-controlled designed RF circuitry, and the aperture coupling between the feed lines and the radiating structure. On the other hand, the removal of lossy, textile substrate material surrounding the RF interconnections has the potential to reduce losses in the feed circuit. A design guideline for the amount of feed substrate reduction is put forward, and validated by means of simulations and measurements. This guideline limits the ratio $T/W > 0.6$, where T is the width of the substrate on either side of the microstrip with width W. Without compromising antenna performance, this allows a high flexibility and breathability for wearable aperture-coupled patch antennas, especially when the antenna ground plane and patch are constructed using conductive (stretchable) textiles. In particular, for active antennas, this offers the opportunity to integrate more and more electronics on the antenna's feed substrate without compromising its wearability. However, while this technique has been validated fully (simulations and measurements) for an aperture-coupled patch antenna operating in the vicinity of 1.575 GHz and, with simulations only, for an aperture-coupled patch antenna operating in the vicinity of 2.45 GHz, further simulations and validation by means of measurements should be considered when generalizing the proposed design guideline.

Acknowledgment

This work was co-funded by the European Commission in the context of the EC-FP7 Galileo.2011.3.1- 2: Collaborative Project, Grant agreement no.: 287166, and was carried out in collaboration with the Centre for MicroSystems Technology (CMST), Technologiepark Zwijnaarde, Belgium.

References

[1] A. Dierck, H. Rogier, and F. Declercq, “A wearable active antenna for global positioning system and satellite phone”, *IEEE Trans. Antennas Propag.*, vol. 61, no. 2, pp. 532–538, 2013.

[2] A. Dierck, S. Agneessens, F. Declercq, B. Spinnewyn, G.-J. Stockman, P. Van Torre, L. Vallozzi, D. Vande Ginste, T. Vervust, J. Vanfleteren, *et al.*, “Active textile antennas in professional garments for sensing, localisation and communication”, *International Journal of Microwave and Wireless Technologies*, pp. 1–11,

[3] S. Agneessens, P. Van Torre, F. Declercq, B. Spinnewyn, G.-J. Stockman, H. Rogier, and D. Vande Ginste, “Design of a wearable, low-cost, through-wall doppler radar system”, *International Journal of Antennas and Propagation*, vol. 2012, p. 9, 2012.

[4] J. Lilja, P. Salonen, T. Kaija, and P. de Maagt, “Design and manufacturing of robust textile antennas for harsh environments”, *IEEE Trans. Antennas Propag.*, vol. 60, no. 9, pp. 4130–4140, 2012.

[5] J. Lilja, V. Pynttari, T. Kaija, R. Makinen, E. Halonen, H. Sillanpaa, J. Heikkinen, M. Mantysalo, P. Salonen, and P. de Maagt, “Body-worn antennas making a splash: lifejacket-integrated antennas for global search and rescue satellite system”, *IEEE Antennas Propag. Mag.*, vol. 55, no. 2, pp. 324–341, 2013.

[6] E. Kaivanto, M. Berg, E. Salonen, and P. de Maagt, “Wearable circularly polarized antenna for personal satellite communication and navigation”, *IEEE Trans. Antennas Propag.*, vol. 59, no. 12, pp. 4490 –4496, 2011.

[7] G. Orecchini, L. Yang, M. Tentzeris, and L. Roselli, “"Smart shoe": an autonomous inkjet-printed RFID system scavenging walking energy”, in *2011 IEEE Int. Symp. on Antennas and Propagation (APSURSI)*, 2011, pp. 1417 –1420.

[8] A. Serra, P. Nepa, and G. Manara, “A wearable multi antenna system on a life jacket for Cospas Sarsat rescue applications”, in *2011 IEEE Int. Symp. on Antennas and Propagation (APSURSI)*, 2011, pp. 1319 –1322.

[9] F. Declercq and H. Rogier, “Active integrated wearable textile antenna with optimized noise characteristics”, *IEEE Trans. Antennas Propag.*, vol. 58, no. 9, pp. 3050–3054, 2010.

[10] F. Croq and A Papiernik, “Large bandwidth aperture-coupled microstrip antenna”, *Electronics Letters*, vol. 26, no. 16, pp. 1293–1294, 1990.

[11] C. Hertleer, A. Van Laere, H. Rogier, and L. Van Langenhove, "Influence of relative humidity on textile antenna performance", *Textile Research Journal*, vol. 80, no. 2, p. 177, 2010.

[12] C. Smith and R.-S. Chang, "Microstrip transmission line with finite-width dielectric", *IEEE Trans. Microw. Theory Tech.*, vol. 28, no. 2, pp. 90–94, 1980.

Conclusions

General conclusions

Throughout this work, design techniques and optimization strategies for the design of robust, high performance wearable textile antennas were presented. These take into account the demanding nature of wearable antennas operating in rescue worker systems. The strict design requirements imposed by GNSS applications further complicated the design process.

First, a hands-on approach illustrated the potential of active wearable textile antennas as robust, high performance modules for localization in rescue worker environments. The integration of an LNA directly onto a wearable GNSS antenna's backside resulted not only in a high performance textile satellite-based localization antenna, but also provides a proof-of-concept for the integration of advanced electronics into wearable antennas. Afterwards, a design paradigm for autonomous active wearable antennas was outlined and validated by means of several design examples, showcasing the wide range of applications that can benefit from these antennas. Next, the focus shifted to the multi-objective optimization of the antenna element itself, taking into account the tolerances of unconventional substrate materials applied in the fabrication process for wearable antennas. This optimization strategy was then further developed to cope with increasingly complex antenna designs, by means of surrogate modeling. Finally, a technique was presented that increases the flexibility of active wearable aperture-coupled patch antennas by laser-structuring the antenna's feed substrate. These strategies and techniques were validated by measurements on fully functional prototypes. Not only does this work present guidelines to design highly optimized wearable antennas, it also shows the potential of these antennas for real-life applications, focusing on GNSS antennas for rescue workers.

Future work

The design strategies presented here were mainly validated by means of measurements on optimized wearable textile GNSS antennas for rescue workers. However, the presented strategies could be employed for the design of increasingly advanced (active) wearable antennas for a wide gamut of applications.

While the prototypes in this work were constructed using copper-on-polyimide conductors, the use of conductive, stretchable textiles has the potential to provide additional flexibility and breathability to the wearable antennas, while reducing

internal stresses that occur when the antennas are bent, increasing their robustness even further. Improving the discussed antennas in this way is very well within reach, as automated laser cutting techniques are able to shape these textiles accurately, and several other antenna prototypes were already shown to exhibit satisfying performance when constructed using conductive fabrics. Screenprinting of conductive inks onto textiles, or embroidering conductive yarns, could produce detailed conductive structures, potentially enabling to realize antenna feed networks, which are often more complicated than a patch or ground-plane, in a more flexible way. The vias present in the antenna designs that are discussed in this work, are realized by manually threading copper wire through the antenna's feed substrate. This offers a reliable way of establishing connections between the feed network and the antenna's ground plane, but makes the fabrication process time-consuming, limiting the usability of this technique to prototype manufacturing. In order to speed up fabrication, new techniques for implementing the vias can be developed, such as automated filling of the via holes with solder paste. The flexibility and robustness of the electronics integrated in the antenna's feed network can also be further increased by means of advanced fabrication techniques. Encapsulation of the discrete components using a suitable material, such as thermoplastic polyurethane (TPU), can provide increased robustness of the mechanical connection of these components to the feed network, as well as protection from moisture. Thinning of silicon chips results in an extremely low integration profile with increased flexibility. In order to rely on the above-listed manufacturing techniques, their effect on the antenna performance should be thoroughly analyzed, by means of simulations and prototype measurements.

The design paradigm for reliable, autonomous textile antennas for professional garments illustrates the successful integration of flexible solar cells onto a wearable antenna. This example can be expanded to a more thorough approach of securing smart textile system autonomy, taking advantage from harvesting different sources besides solar power, and coupling this to the integration of a power management system in combination with flexible batteries, ensuring a continuity in the available power.

Aside from increasing the flexibility, the feed networks could be designed to include even more functionality. The integrated LNAs are a proof-of-principle, showing that it is possible to unobtrusively integrate active electronics directly onto a wearable antenna. But the active electronic components do not have to be limited to amplifiers. Thanks to on-going miniaturization, integration of microcontrollers, RF transceivers, GNSS receivers, electronic compasses, etc. can be considered. Integrating a multi-band GNSS receiver on a wide band textile GNSS antenna would upgrade it to a highly autonomous, compact positioning module. This would also further increase robustness of the complete SFIT system, because the received GNSS signals are processed directly by the active antenna, eliminating a potentially weak link between the antenna and a separate receiver. The presented design strategies and techniques could be used as stepping stones towards truly unobtrusive, autonomous, textile GNSS localization modules that not only tackle

the design requirements needed for rescue worker applications, but also offer a way to integrate reliable localization capabilities into a wide range of smart textile systems.